



FABRICATION AND GAS SENSING PROPERTIES OF PURE AND AU-FUNCTIONALISED W₃ NANONEEDLE-LIKE STRUCTURES, SYNTHESISED VIA AEROSOL ASSISTED CHEMICAL VAPOUR DEPOSITION METHOD
Toni Stoycheva

Dipòsit Legal: T-1803-2011

ADVERTIMENT. La consulta d'aquesta tesi queda condicionada a l'acceptació de les següents condicions d'ús: La difusió d'aquesta tesi per mitjà del servei TDX (www.tesisenxarxa.net) ha estat autoritzada pels titulars dels drets de propietat intel·lectual únicament per a usos privats emmarcats en activitats d'investigació i docència. No s'autoritza la seva reproducció amb finalitats de lucre ni la seva difusió i posada a disposició des d'un lloc aliè al servei TDX. No s'autoritza la presentació del seu contingut en una finestra o marc aliè a TDX (framing). Aquesta reserva de drets afecta tant al resum de presentació de la tesi com als seus continguts. En la utilització o cita de parts de la tesi és obligat indicar el nom de la persona autora.

ADVERTENCIA. La consulta de esta tesis queda condicionada a la aceptación de las siguientes condiciones de uso: La difusión de esta tesis por medio del servicio TDR (www.tesisenred.net) ha sido autorizada por los titulares de los derechos de propiedad intelectual únicamente para usos privados enmarcados en actividades de investigación y docencia. No se autoriza su reproducción con finalidades de lucro ni su difusión y puesta a disposición desde un sitio ajeno al servicio TDR. No se autoriza la presentación de su contenido en una ventana o marco ajeno a TDR (framing). Esta reserva de derechos afecta tanto al resumen de presentación de la tesis como a sus contenidos. En la utilización o cita de partes de la tesis es obligado indicar el nombre de la persona autora.

WARNING. On having consulted this thesis you're accepting the following use conditions: Spreading this thesis by the TDX (www.tesisenxarxa.net) service has been authorized by the titular of the intellectual property rights only for private uses placed in investigation and teaching activities. Reproduction with lucrative aims is not authorized neither its spreading and availability from a site foreign to the TDX service. Introducing its content in a window or frame foreign to the TDX service is not authorized (framing). This rights affect to the presentation summary of the thesis as well as to its contents. In the using or citation of parts of the thesis it's obliged to indicate the name of the author.

Toni T. Stoycheva

**Fabrication and gas sensing properties of pure
and Au-functionalised WO₃ nanoneedle-like
structures, synthesised *via* Aerosol Assisted
Chemical Vapour Deposition method**

DOCTORAL THESIS

Supervised by Prof. Xavier Correig Blanchar
and Dr. Stella Vallejos Vargas

Department of Electronic, Electrical & Automatic Control Engineering



UNIVERSITAT ROVIRA I VIRGILI

Tarragona

2011

UNIVERSITAT ROVIRA I VIRGLI
FABRICATION AND GAS SENSING PROPERTIES OF PURE AND AU-FUNCTIONALISED W03 NANONEEDLE-LIKE STRUCTURES,
SYNTHESISED VIA AEROSOL ASSISTED CHEMICAL VAPOUR DEPOSITION METHOD
Toni Stoycheva
DL:T-1803-2011



UNIVERSITAT
ROVIRA I VIRGILI

ESCOLA TÈCNICA SUPERIOR D'ENGINYERIA
DEPARTAMENT D'ENGINYERIA ELECTRONICA, ELÈCTRICA I AUTOMÀTICA

Avinguda dels Països Catalans, 26
Campus sescelades
43007 Tarragona
Tel. (977) 55 96 10
Fax. (977) 55 96 05
e-mail: secelec@etse.urv.es
<http://www.etse.urv.es/DEEEA/>

I, Xavier Correig, Professor at the Department of Electronic, Electrical & Automatic Control Engineering of the University Rovira i Virgili and I, Stella Vallejos, Postdoctoral researcher at the Department of Chemistry of the University College of London

CERTIFY:

That the present thesis, entitled "Fabrication and gas sensing properties of pure and Au-functionalised WO₃ nanoneedle-like structures, synthesised *via* Aerosol Assisted Chemical Vapour Deposition method", presented by Toni T. Stoycheva for the award of the degree of Doctor of Science, has been carried out under our supervision at the Department of Electronic, Electrical & Automatic Control Engineering of the University Rovira i Virgili, Tarragona, Spain, and that it fulfils all the requirements to be eligible for the European Doctorate Label.

Tarragona, November 2011.

Prof. Xavier Correig
Thesis Supervisor

Dr. Stella Vallejos
Thesis Co-supervisor

UNIVERSITAT ROVIRA I VIRGLI
FABRICATION AND GAS SENSING PROPERTIES OF PURE AND AU-FUNCTIONALISED W03 NANONEEDLE-LIKE STRUCTURES,
SYNTHESISED VIA AEROSOL ASSISTED CHEMICAL VAPOUR DEPOSITION METHOD
Toni Stoycheva
DL:T-1803-2011

I believe that imagination is stronger than knowledge.

That myth is more potent than history.

That dreams are more powerful than facts.

Robert Fulghum

UNIVERSITAT ROVIRA I VIRGLI

FABRICATION AND GAS SENSING PROPERTIES OF PURE AND AU-FUNCTIONALISED W03 NANONEEDLE-LIKE STRUCTURES,
SYNTHESISED VIA AEROSOL ASSISTED CHEMICAL VAPOUR DEPOSITION METHOD

Toni Stoycheva

DL:T-1803-2011

Acknowledgments

This thesis research work would not have been possible without the financial assistance from the University Rovira i Virgili, as well as collaboration and help from a number of people. Herein, I would like to thank all of them.

I would like to express my gratitude to my director of studies, Prof. Xavier Correig Blanchard, whose expertise, understanding and patience, helped my work in this doctoral thesis. I would also like to thank my co-director of studies, Dr. Stella Vallejos Vargas for her guidance, suggestions and support during my research. To the group leaders – Prof. X. Vilanova and Prof. E. Llobet – who were extremely helpful in all questions related to my research work, I am deeply grateful.

My gratitude also goes to all members of research groups Minos and Nephos, for their personal, scientific and technical assistance during our work together: Dr. Mariana Trifonova, Dr. T. Trifonov, R. Calavia, R. M. Vazquez, J. M. Badia, Dr. L. Vojkúvka, D. Shaposhnik, Dr. H. Lahlou, Dr. R. Leghrib, Dr. R. Ingles, and F. Annanouch. Especially, I would like to thank Dr. R. Pavelko for his help, suggestions and advise during my doctoral work.

I must also acknowledge helpfulness of Dr. C. Blackman (Department of Chemistry, University College of London [UCL], UK), his suggestions for this study and ideas presented here. One of the main parts of this research study was achieved through collaboration with his group. I would also like to express my gratitude to S. Moniz for sharing with me his valuable knowledge and helping me during my three months exchange research study in London.

Furthermore, I would like to thank Prof. J. Calderer for his unreserved help and support he has provided in the clean room at the Universitat Politècnica de Catalunya, Barcelona, Spain.

UNIVERSITAT ROVIRA I VIRGLI
FABRICATION AND GAS SENSING PROPERTIES OF PURE AND AU-FUNCTIONALISED W03 NANONEEDLE-LIKE STRUCTURES,
SYNTHESISED VIA AEROSOL ASSISTED CHEMICAL VAPOUR DEPOSITION METHOD
Toni Stoycheva
DL:T-1803-2011

Last but not least, I would like to thank all members of the Technical and Scientific Service, URV Tarragona, for their continuous help and collaboration during my research.

Finally, I am deeply grateful to my parents and my sister for their help and support during my decision making to continue my research work abroad. And of course, big thanks to my fiancé Dejan for his love, faith, endless patience and for being always next to me...

UNIVERSITAT ROVIRA I VIRGLI
FABRICATION AND GAS SENSING PROPERTIES OF PURE AND AU-FUNCTIONALISED W03 NANONEEDLE-LIKE STRUCTURES,
SYNTHESISED VIA AEROSOL ASSISTED CHEMICAL VAPOUR DEPOSITION METHOD
Toni Stoycheva
DL:T-1803-2011

Dedicated to

My dear fiancé Dejan Vilic

&

My dear family

My dear parents Traycho and Tatiana Stoychevi

&

My dear sister Marina Stoycheva

UNIVERSITAT ROVIRA I VIRGLI
FABRICATION AND GAS SENSING PROPERTIES OF PURE AND AU-FUNCTIONALISED W03 NANONEEDLE-LIKE STRUCTURES,
SYNTHESISED VIA AEROSOL ASSISTED CHEMICAL VAPOUR DEPOSITION METHOD
Toni Stoycheva
DL:T-1803-2011

Abstract

In this doctoral thesis, it has been investigated and developed the Aerosol Assisted Chemical Vapour Deposition (AACVD) method for direct in-situ growth of intrinsic and Au-functionalised nanostructured WO₃, as well as SnO₂-based devices for gas sensing applications. The nanostructured material synthesis, device fabrication and their gas sensing properties have been studied.

AACVD method was used for synthesis and direct deposition of sensing films onto classical alumina and microhotplate gas sensor substrates, demonstrating the compatibility between the microhotplate fabrication process and the sensing nanostructured layer deposition. The fabricated devices were based on WO₃ nanoneedles, WO₃ polycrystalline structure and SnO₂ nanostructure with unusual elongated particle shape. Radio frequency (RF) sputtering method was used to obtain Au nanoparticles functionalised WO₃ nanoneedle-like structures. Pure and Au-functionalised WO₃ nanoneedle-like and pure WO₃ polycrystalline structures were studied and compared as the sensing elements. Additionally, SnO₂-based films were fabricated and also studied as the sensing element.

AACVD co-deposition method was used for synthesis and in-situ deposition of Au-functionalised nanoparticles on the surface of the WO₃ nanoneedles. Au-functionalised WO₃ nanoneedle-like films were studied and compared like a sensing element with the structure of a non-functionalised one.

Structural characterization techniques were employed to extract important information of gas sensitive films such as their morphology, chemical composition, crystal structure and orientation. This information helped to better understand the nature of nanostructured material growth and link its characteristics to their gas sensing properties.

UNIVERSITAT ROVIRA I VIRGLI
FABRICATION AND GAS SENSING PROPERTIES OF PURE AND AU-FUNCTIONALISED W03 NANONEEDLE-LIKE STRUCTURES,
SYNTHESISED VIA AEROSOL ASSISTED CHEMICAL VAPOUR DEPOSITION METHOD
Toni Stoycheva
DL:T-1803-2011

Resumen

En esta tesis doctoral, se ha investigado y desarrollado un nuevo método de CVD asistido por aerosol (AACVD), que permite el crecimiento de nanoestructuras de WO₃ intrínsecas y funcionalizadas con Au. Así mismo se han depositado capas policristalinas de SnO₂ para aplicaciones de detección de gases. La síntesis de materiales nanoestructurados, la fabricación de dispositivos y sus propiedades de detección de gases, han sido estudiadas.

El método AACVD fue utilizado para la síntesis y la deposición directa de capas activas encima de sustratos de alúmina y también sobre sustratos micromecanizados (microhotplates), lo que demuestra la compatibilidad entre la tecnología de silicio y la deposición de la capas activas nanoestructuradas.

En la tesis se ha demostrado que las capas nanoestructuradas de WO₃ funcionalizadas con oro tienen una sensibilidad mejor que las intrínsecas frente a algunos gases relevantes y al mismo tiempo se ha producido un cambio de selectividad.

UNIVERSITAT ROVIRA I VIRGLI
FABRICATION AND GAS SENSING PROPERTIES OF PURE AND AU-FUNCTIONALISED W03 NANONEEDLE-LIKE STRUCTURES,
SYNTHESISED VIA AEROSOL ASSISTED CHEMICAL VAPOUR DEPOSITION METHOD
Toni Stoycheva
DL:T-1803-2011

Thesis publications

UNIVERSITAT ROVIRA I VIRGLI
FABRICATION AND GAS SENSING PROPERTIES OF PURE AND AU-FUNCTIONALISED W03 NANONEEDLE-LIKE STRUCTURES,
SYNTHESISED VIA AEROSOL ASSISTED CHEMICAL VAPOUR DEPOSITION METHOD
Toni Stoycheva
DL:T-1803-2011

Thesis publications

The author's work has also resulted in 4 publications and 2 international conference proceedings listed below.

Full papers

1. Stella Vallejos, Toni Stoycheva, Polona Umek, Cristina Navio, Rony Snyders, Carla Bittencourt, Eduard Llobet, Christopher Blackman, Savio Moniz and Xavier Correig "Au nanoparticle-functionalised WO₃ nanoneedles and their application in high sensitivity gas sensor devices", *Chemical Communications The Royal Society of Chemistry*, 47, 565-567, 2011;
2. Toni T. Stoycheva, Stella Vallejos, Roman G. Pavelko, Viktor S. Popov, Vladimir G. Sevastyanov and X.Correig, "Aerosol assisted chemical vapour deposition of SnO₂ thin films for gas sensors application", *Chemical Vapor Deposition*, 17, 247-252, 2011;
3. Cristina Navio, Stella Vallejos, Toni Stoycheva, Eduard Llobet, Xavier Correig, Rony Snyders, Christopher Blackman, Polona Umek, Xiaoxing Ke, Gustaaf Van Tendeloo, Carla Bittencourt, "Gold Clusters on WO₃ Nanoneedles Grown via AACVD: XPS and TEM Studies", *Journal of Physical Chemistry*, in press, 2011;
4. Toni Stoycheva, Stella Vallejos, Christopher Blackman, Josep Calderer, Xavier Correig, "Gas Sensing Properties of Intrinsic and Au Functionalised WO₃ Nanostructures", *Sensors and Actuators B-Chemical*, submitted, 2011;

Conference proceedings

1. Toni Stoycheva, Stella Vallejos, Josep Calderer, Ivan Parkin, Christopher Blackman and Xavier Correig, "Characterization and gas sensing properties of intrinsic and Au-doped WO₃ nanostructures deposited by AACVD technique", *Procedia Engineering EUROSENSORS XXIV*, 5, 131-134, 2010;
2. Muhammad U. Qadria, Toni Stoycheva, Maria Cinta Pujol, Eduard Llobet, Xavier Correig, Josep Ferre Borull, Magdalena Aguiló and Francesc Díaz, "WO₃ nano-needles by Aerosol Assisted CVD for optical sensing", *Procedia Engineering EUROSENSORS XXV*, in press, 2011;

UNIVERSITAT ROVIRA I VIRGLI
FABRICATION AND GAS SENSING PROPERTIES OF PURE AND AU-FUNCTIONALISED W03 NANONEEDLE-LIKE STRUCTURES,
SYNTHESISED VIA AEROSOL ASSISTED CHEMICAL VAPOUR DEPOSITION METHOD
Toni Stoycheva
DL:T-1803-2011

Posters and presentations

1. T. Stoycheva, S. Vallejos, C. Blackman, I. Gràcia, X. Correig, "Fabrication and characterization of intrinsic WO₃ nanoneedles-based layers deposited onto microhotplates gas sensor substrates via AACVD method", *Graduate student meeting on electronic engineering*, poster presentation, University Rovira i Virgili, Tarragona, SPAIN, 2011;
2. T. Stoycheva, S. Vallejos, J. Calderer, I. Parkin, C. Blackman and X. Correig, "Characterization and gas sensing properties of intrinsic and Au-doped WO₃ nanoneedles deposited by AACVD technique", *Eurosensors XXIV*, Poster presentation, Johannes Kepler University, Linz, AUSTRIA, 2010;
3. T. Stoycheva, X. Correig, "Characterization and gas sensing properties of intrinsic and Au-doped WO₃ nanoneedles deposited by AACVD technique", *Graduate student meeting on electronic engineering*, Oral presentation, University Rovira i Virgili, Tarragona, SPAIN, 2010;
4. T. Stoycheva, X. Correig, "Deposition of tungsten oxide nanoneedles by Aerosol Assisted Chemical Vapor Deposition (AACVD) for metal-oxide gas sensors", *Graduate student meeting on electronic engineering*, Poster presentation, University Rovira i Virgili, Tarragona, SPAIN, 2009;
5. T. Stoycheva, X. Correig, "Deposition and characterization of tungsten oxide layers by Aerosol Assisted Chemical Vapour Deposition (AACVD) for metal-oxide gas sensors", *Graduate student meeting on electronic engineering*, Poster presentation, University Rovira i Virgili, Tarragona, SPAIN, 2008;

UNIVERSITAT ROVIRA I VIRGLI
FABRICATION AND GAS SENSING PROPERTIES OF PURE AND AU-FUNCTIONALISED W03 NANONEEDLE-LIKE STRUCTURES,
SYNTHESISED VIA AEROSOL ASSISTED CHEMICAL VAPOUR DEPOSITION METHOD
Toni Stoycheva
DL:T-1803-2011

INDEX

I.	Introduction	3
1.	Motivation	3
2.	Objectives	7
3.	Structure of the thesis	8
II.	State of the art	13
1.	WO_{3-x} gas sensors	13
1.1.	Physical and chemical properties of WO _{3-x}	13
1.2.	WO _{3-x} for gas sensors applications	17
2.	Nanostructured gas sensors	24
2.1.	Nanostructured materials	24
2.2.	Nanostructured metal-oxide in gas sensor applications	25
2.3.	Modified nanostructures	27
2.4.	Deposition methods for nanostructured metal-oxides gas sensors	31
2.4.1.	<i>Film growth mechanism</i>	31
2.4.2.	<i>Methods for nanostructured metal-oxides gas sensors</i>	37

3.	Chemical Vapour Deposition (CVD) techniques for development of active sensing material for gas sensors applications	44
3.1.	CVD basic principles	44
3.2.	CVD methods and their applications for nanostructured gas sensors	48
3.3.	Aerosol-assisted deposition methods – applications for gas sensors.....	52
III.	Experimental methods and material characterization.....	61
1.	Film deposition	61
1.1.	AACVD system.....	61
1.2.	Precursor synthesis - general procedure.....	63
1.2.1.	<i>Tungsten hexaphenoxide [W(OPh)₆]</i>	63
1.2.2.	<i>Synthesis of tin complexes [Sn(18-Cr-6)Cl₄] and [Sn(H₂O)₂Cl₄](18-Cr-6)</i>	65
1.3.	Active sensing layer deposition	67
1.3.1.	<i>General procedure</i>	67
1.3.2.	<i>Liquid precursor solution preparation</i>	69
1.3.3.	<i>Annealing process</i>	71
1.4.	Functionalisation of the deposited layers	71
1.4.1.	<i>R.f. magnetron sputtering (ex-situ)</i>	71
1.4.2.	<i>Co-deposition via AACVD (in-situ)</i>	72

2.	Material (physical) characterization of the active layers	73
2.1.	ESEM - Environmental Scanning Electron Microscopy	74
2.2.	AFM - Atomic Force Microscopy	75
2.3.	TEM - Transmission Electron Microscopy	75
2.4.	XRD - X-ray Diffraction and crystallite size calculations	76
2.5.	The other methods	76
3.	Gas sensor fabrication	78
3.1.	Alumina gas sensors	78
3.1.1.	<i>Electrode and heater printing</i>	<i>78</i>
3.1.2.	<i>Assembling and solder pasting of alumina gas sensors substrates</i>	<i>79</i>
3.2.	Microhotplate gas sensors	80
3.2.1.	<i>Micromachining substrate technology</i>	<i>80</i>
3.2.2.	<i>Assembling of microhotplate gas sensor substrates</i>	<i>81</i>
4.	Gas sensors characterization study	82
4.1.	Measuring set up	82
4.2.	Target gases	84

IV. Fabrication and characterization of intrinsic and gold (Au) functionalised tungsten trioxide (WO₃) nanostructure-based gas sensors deposited via AACVD method	89
1. Introduction	89
2. Nanostructured WO₃ film deposition	89
2.1. Film analysis.....	89
2.1.1. <i>Morphology</i>	91
3. Characterization of gas sensors based on nanostructured WO₃ films	98
3.1. Sensing film analysis.....	98
3.1.1. <i>Morphology</i>	98
3.1.2. <i>XRD analysis</i>	100
3.2. Gas sensing characterization	102
3.2.1. <i>Sensor response - reducing gases</i>	103
3.2.2. <i>Sensor response - oxidizing gases</i>	105
3.2.3. <i>Stability</i>	106

4.	Characterization of gas sensors based on Au-functionalised WO₃ nanoneedle-like films	108
4.1.	Film analysis	109
4.1.1.	<i>Morphology</i>	109
4.1.2.	<i>Chemical composition</i>	111
4.1.3.	<i>XRD analysis</i>	112
4.2.	Gas sensing characterization	113
4.2.1.	<i>Sensor response</i>	113
4.2.2.	<i>Stability</i>	114
5.	Micro-machined gas sensors with nanostructured WO₃ films	115
5.1.	Film analysis	115
5.1.1.	<i>Morphology</i>	115
5.1.2.	<i>XRD analysis</i>	117
5.2.	Gas sensing characterization	118
5.2.1.	<i>Sensor response - reducing gases</i>	118
5.2.2.	<i>Sensor response - oxidizing gases</i>	123
5.2.3.	<i>Stability</i>	124
6.	Summary	125

V.	Fabrication and characterization of intrinsic tin oxide (SnO₂)- based gas sensors deposited <i>via</i> AACVD method.....	131
1.	Introduction	131
2.	Film analysis	132
2.1.	Morphology.....	132
2.2.	XRD analysis.....	135
3.	Gas sensing characterization	136
3.1.	Sensor response	136
3.2.	Stability.....	137
4.	Summary	138
VI.	Conclusions	143
VII.	Bibliography.....	149

UNIVERSITAT ROVIRA I VIRGLI
FABRICATION AND GAS SENSING PROPERTIES OF PURE AND AU-FUNCTIONALISED W03 NANONEEDLE-LIKE STRUCTURES,
SYNTHESISED VIA AEROSOL ASSISTED CHEMICAL VAPOUR DEPOSITION METHOD
Toni Stoycheva
DL:T-1803-2011

UNIVERSITAT ROVIRA I VIRGLI
FABRICATION AND GAS SENSING PROPERTIES OF PURE AND AU-FUNCTIONALISED W03 NANONEEDLE-LIKE STRUCTURES,
SYNTHESISED VIA AEROSOL ASSISTED CHEMICAL VAPOUR DEPOSITION METHOD
Toni Stoycheva
DL:T-1803-2011

Introduction

UNIVERSITAT ROVIRA I VIRGLI
FABRICATION AND GAS SENSING PROPERTIES OF PURE AND AU-FUNCTIONALISED W03 NANONEEDLE-LIKE STRUCTURES,
SYNTHESISED VIA AEROSOL ASSISTED CHEMICAL VAPOUR DEPOSITION METHOD
Toni Stoycheva
DL:T-1803-2011

I. Introduction

This doctoral study comprehends the author's research in the last four years which was focused on the deposition *via* Aerosol Assisted Chemical Vapour Deposition (AACVD) technique of intrinsic and Au-functionalised nanostructured WO₃ active films. These films have been morphologically and structurally characterized and their gas sensing properties have been study.

1. Motivation

In the past few decades, solid state gas sensor devices, mainly based on SnO₂, WO₃, In₂O₃, ZnO, have attracted a lot of attention due to their compact size, reliability and low cost, as well as their higher sensitivity in detecting very low concentrations (at the levels of ppm or even ppb).

Metal-oxide gas sensors show a very good response to a number of gases, both oxidising and reducing. They found application in many industrial and commercial activities: a range of applications from domestic gas alarms and medical diagnostic apparatus to security, health and safety, food quality control and environmental pollution monitoring. Without these sensors, significant advances in industrial and environmental monitoring would not be possible.

Solid state gas sensors have been widely used, but they also suffer from limited sensitivity, selectivity and long-time stability. However, recent advances in nanotechnology produced novel classes of nanostructured materials with enhanced gas sensing properties, providing this way the opportunity to dramatically increase the performances of solid state gas sensors. In order to improve efficiency and sensing selectivity and sensitivity of these gas sensor devices a detailed understanding of the surface and interfacial processes and their relationship with material properties and device performances is required.

A large amount of literature on quasi-one dimensional (1D) nanostructured materials, including nanowires, nanoneedles, nanotubes, nanorods and nanobelts, is published every year. Therefore, the use of nanostructured metal-oxides for gas

sensing application has emerged as one of the most important research topics. Because of the gas detection taking place on the material surface, nanostructured gas sensors will have greater sensitivity, due to their higher surface-to-volume ratio. This favours the adsorption of gases on the sensor's surface and can increase the sensitivity of the device.

Other benefits of these materials are the potentially improved stoichiometry and greater level of crystallinity. For this reason, quasi-one dimensional metal-oxides are very promising materials for gas sensing. From the operative point of view, they have not reached commercial viability due to the time consuming and expensive fabrication processes used (i.e. single nanowires gas sensors). Therefore, because of their high demand, nanostructured gas sensor devices need to be developed using the simple and cost effective manufacturing techniques, such as in-situ deposition of nanostructures.

Various technologies are being employed for the growth of metal-oxide nanostructures at present. The techniques include mainly vapour processing methods such as Chemical Vapour Deposition (CVD), Electrochemical Vapour Deposition (EVD), Metal-Organic CVD (MOCVD), sputtering and plasma spray, etc. These fabrication methods are generally very expensive because they involve the use of sophisticated reactors and vacuum systems. Therefore, these methods are not viable for the large-scale commercial production. Additionally, traditional methods, such as CVD, require relatively high deposition temperatures for metal-oxide nanostructure formation that are not compatible with the microelectronic substrates (i.e. microhotplates) which are widely used in gas sensor production.

On the contrary, the nanostructured metal-oxide gas sensors based on microelectronic substrates are fabricated in two steps. During the first step the nanostructures are grown separately onto the suitable substrate. Subsequently, in the second step the nanostructures are removed from the substrate, mixed with different additives and deposited by the conventional ceramic processing methods. However, the conventional ceramic processing methods, such as tape casting, screen printing, drop coating or sol-gel methods, do not give dense thin films due to the poor density of the obtained layers and are generally used for thick films fabrication.

In addition, much effort was also devoted to developing of new surface modification strategies which would be particularly useful for functionalisation of quasi-one dimensional semiconducting nanoneedles and effectively incorporating noble metal catalyst nanoparticles on nanoneedle's surface, which in turn could modify the gas sensing properties. However, well-known surface modification strategy is a doping technique (i.e. ion implantation), which utilize ex-situ bombardment of the metal-oxide nanostructures with energetic ions (dopants), may create crystal damage and degrade the device's performance.

In this doctoral study it is present one possible solution for these problems by exploiting the deposition *via* AACVD method, which offers following advantages:

- high deposition rate;
- flexibility – possibility to deposit many different metal-oxides, using different precursors with no requirement for volatility, as well as simultaneous deposition of metal-oxide and catalysts/nanoparticles in one single step;
- easy implementation – the deposition temperatures are relatively low (i.e. < 500 °C) and compatible with microelectronic gas sensor substrates;
- inexpensive fabrication process – deposition process without the need of a sophisticated reactor or any vacuum system;
- possibility for low cost industrialization.

The higher deposition rate and synthesis under atmospheric pressure in AACVD make this technique attractive for scaling up of large areas or mass production of thin film metal-oxides.

This thesis is mainly focused on the growth of nanostructured WO₃, a widely used metal-oxide, well known for its effectiveness in detection of NO₂ gas. Moreover, in the last few years, the nanostructures of tungsten oxides have been found to be more effective sensing materials due to their higher surface-to-volume ratio, demonstrating novel sensing properties such as higher sensitivity, faster response time, and lower operation temperature.

Due to the growing interest, WO₃ nanostructures have been widely studied and deposited *via* techniques such as AACVD method, using different precursors. The precursor used for the metal-oxide synthesis *via* AACVD has to be soluble in any solvent from which the aerosol can be generated. Therefore, it requires thorough design of precursor-solvent system with closer partial pressures of the components and their similar chemical and thermal stability, which probably impedes wide application of the technique for other popular metal-oxides such as tin oxide (SnO₂).

SnO₂ was one of the first thoroughly studied and still is the most frequently used material for the gas sensing applications. For these reasons, this study was subsequently focused on the investigation of the possibility to use new tin precursors for SnO₂ nanostructured growth *via* AACVD method. Two new tin precursors were used for the first time with the AACVD method which resulted in the growth of the SnO₂ active films composed of the unusually elongated polycrystalline structure. However, due to the difficulty of finding suitable precursor, nanostructured growth of SnO₂ may require more complex and extended investigation which has not been considered in this doctoral study that was using the two new tin precursors.

On the other hand, the possibility of metal-oxide in-situ deposition and functionalisation of the material in one single step, could easily find implementation in gas sensor fabrication, due to the wide range of the material selection and effective improvements of the gas sensing properties. The one step in-situ deposition of nanostructured WO₃ functionalised with Au-nanoparticles *via* AACVD method, was the main area of investigation in this doctoral study and for the first time it was examined the possibility of application of these structures as a gas sensing materials.

2. Objectives

The study of the deposition conditions and their influence on the WO₃ nanostructured film growth

In order to synthesize quasi-one dimensional WO₃ nanoneedles in-situ *via* AACVD, the various deposition temperatures and solvents will be tested until the optimal deposition conditions for the growth of nanostructured WO₃ films is determined. The AACVD method will be used to obtain either intrinsic WO₃ polycrystalline or nanostructured active films. Finally, the obtained films will be characterized by the standard techniques, such as ESEM, TEM, XRD or the other suitable methods.

Investigation of the AACVD co-deposition of WO₃ nanostructures and Au-nanoparticles

To fulfill this objective the AACVD co-deposition method will be applied as the surface modification strategy. The simultaneous growth of WO₃ nanoneedles and Au catalyst nanoparticles incorporated on the surface of the nanoneedles will also be studied. The purpose would be to modulate the selectivity and sensitivity of the layers by the addition of Au catalyst nanoparticles. In this context, the suitable doping precursor concentration and the optimal deposition conditions for the simultaneous synthesis *via* AACVD co-deposition method will be determined.

Fabrication of gas sensor devices based on intrinsic and Au-functionalised WO₃ nanostructured films

The aim of this objective is to deposit intrinsic and Au-functionalised WO₃ nanostructures as active films directly onto traditional alumina or microhotplate gas sensor substrates. Firstly, the alumina substrates will be used for the preliminary compatibility study between the deposition temperature and the substrate. Subsequently, in order to probe the compatibility of the AACVD method with the silicon technology the fabrication of nanostructured WO₃-based gas sensor onto silicon microhotplate substrates will be explored. Finally, the gas sensing characterization and comparison study of all the sensor devices will be conducted.

Fabrication of gas sensor devices based on SnO₂ films deposited via AACVD method

Herein, the possibility of using the AACVD method with various popular metal-oxides, such as SnO₂, will be investigated. For this reason, it will be studied and determined the optimal deposition conditions for the growth of SnO₂ films *via* AACVD method using the new tin complexes as precursors.. Subsequently, the use of the obtained SnO₂ films, as the gas sensing element will be investigated.

3. Structure of the thesis

This section indicates the overall structure of the thesis and briefly outlines the content of each chapter.

The state of the art review is presented in the second chapter of this thesis. It has been structured around the available deposition techniques used for nanostructured metal-oxide materials and their applications for gas sensor devices. The literature review starts with the metal-oxide materials, and then move on to the nanostructured metal-oxide materials developed in recent years, such as nanoneedles, nanorods, nanowires, nanotubes, etc. Subsequently, the vapour-solid deposition techniques will be discussed, for being widely used for pure nanostructured metal-oxide growth and even functionalised with other compounds to increase their selectivity to particular analytes. The functionalisation of the nanostructures *via* different doping strategies was also discussed in more detail. Finally, the basics of the aerosol assisted deposition method used in this doctoral thesis are explained and the comparison of the literature has been reviewed and summarized.

The third chapter, explains extensively the experimental work performed during this thesis. This consists of the AACVD system and the direct growth deposition conditions used for the different metal-oxide-based gas sensor fabrication. The characterization procedures used for the morphological and structural study of the sensing layers are presented. In continuation, the technological steps involved in the fabrication of the gas sensors are described. Finally, the gas characterization procedure used for studying the properties of the gas sensors is explained.

The fourth chapter, starts with the conducted study that determined the optimal deposition conditions for WO₃ nanoneedle growth. The AACVD synthesis procedure results in the WO₃ nanoneedle-like or polycrystalline structures which are deposited on various gas sensor substrates. Subsequently, the AACVD co-deposition study, in which WO₃ nanoneedles and Au-nanoparticles are simultaneously grown in one single step, is conducted. The structure, the chemical composition and the morphology of the obtained films are characterized. Finally, the gas sensing properties of the WO₃ nanoneedle-like and polycrystalline structures, as well as WO₃ nanoneedles functionalised with Au-nanoparticles, were tested in various oxidizing and reducing environments.

The fifth chapter, presents the study of the optimal AACVD deposition conditions for SnO₂ layers growth when using the two new tin precursors. It was demonstrated that through the optimization of the AACVD deposition conditions the SnO₂ films were directly grown onto alumina gas sensor substrate. Similarly, to the previous chapter, the obtained active layers are morphologically characterized and tested in the gas characterization chamber. Finally, the general conclusions derived from this doctoral thesis are presented.

UNIVERSITAT ROVIRA I VIRGLI
FABRICATION AND GAS SENSING PROPERTIES OF PURE AND AU-FUNCTIONALISED W03 NANONEEDLE-LIKE STRUCTURES,
SYNTHESISED VIA AEROSOL ASSISTED CHEMICAL VAPOUR DEPOSITION METHOD
Toni Stoycheva
DL:T-1803-2011

State of the art

UNIVERSITAT ROVIRA I VIRGLI
FABRICATION AND GAS SENSING PROPERTIES OF PURE AND AU-FUNCTIONALISED W03 NANONEEDLE-LIKE STRUCTURES,
SYNTHESISED VIA AEROSOL ASSISTED CHEMICAL VAPOUR DEPOSITION METHOD
Toni Stoycheva
DL:T-1803-2011

II. State of the art

1. WO_{3-x} gas sensors

Metal-oxide semiconductors such as WO_{3-x} are widely used for gas sensors, due to their higher sensitivity and ability to detect toxic gases. The first work on WO₃ films related to gas sensing application was presented in 1967 by Shaver et al. [1]. They demonstrated that conductivity of Pt-activated WO₃-based gas sensors changed upon exposure to small amounts of hydrogen-containing gas. Since then, for the past few decades, the oxides of transition metal tungsten have attracted constant research interest, due to their wide future applicability as active sensing material for gas sensors.

The sensing mechanism of the WO_{3-x}-based sensor lies in the change of film resistance resulting from processes of interactions (physisorption, chemisorption and catalytic reactions) between different gases with the film surface [2, 3]. At the same time, the changes in the film properties manifest electrical and photochromic effects. Such electronic properties make tungsten oxide commonly used in several technological areas. WO_{3-x} is commonly applied as active sensing material for hazardous gas detection and has shown good sensing properties towards various reducing or oxidizing gases [4, 5].

Moreover, WO_{3-x} has found unique application in electrochromic devices [6] due to their excellent voltage-modulated optical properties. In addition to the above, photo and thermo-chromic [7, 8] properties were investigated for the use in devices, such as information displays and smart windows. Therefore, because of its interesting chemical and physical properties WO_{3-x} has found a wide application in everyday life.

1.1. Physical and chemical properties of WO_{3-x}

Tungsten (W) is a naturally occurring element found in the earth's surface rocks. Tungsten metal typically does not occur as a free element in nature and can exist in many forms in a wide spectrum of tungstic acids and a variety of different compounds such as tungsten trioxide, tungsten carbide, and ammonium paratungstate. Tungsten

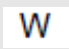

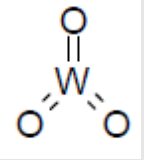
has many common oxidation states (e.g., W[0], W[2+], W[3+], W[4+], W[5+], and W[6+]) and can exist in different WO₃ phases. The most typical forms of tungsten oxides, occur most prominently in states of W[4+] (WO₂, brown), W[5+] (W₂O₅, blue), and W[6+] (WO₃, lemon yellow), where W[6+] its most stable, and therefore its most common valence state. In Table II.1 are presented the chemical and physical properties of the elemental tungsten and tungsten oxides.

It was found that several tungsten suboxides are formed as intermediates during the manufacture of metallic tungsten from tungsten trioxide. The best characterization of these suboxides is a whisker form, W₁₈O₄₉ (WO_{2.72}). Tungsten suboxide whiskers with a nominal composition of WO_{2.72} have been prepared in the laboratory by mixing tungsten trioxide with tungsten dioxide [9]. Another fibrous tungsten oxide is 'blue oxide', with a nominal composition of WO_{2.90} (W₂₀O₅₈). This oxide is formed during the calcination of ammonium paratungstate (APT) and it is a part of the final step in the production of tungsten powder. In Table II.2 one can compare the properties of the oxidation states of tungsten oxides and tungsten suboxides.

Table II.2: Properties of the oxidations states of tungsten oxide [10]

Indicator	WO ₃	WO _{2.90} (W ₂₀ O ₅₈)	W ₁₈ O ₄₉ (WO _{2.72})	WO ₂
Crystal structure	monoclinic	monoclinic	monoclinic	monoclinic
Lattice parameters	0.7285	0.1205	0.1828	0.5650
α β γ, nm	0.7517	0.3767	0.3775	0.4892
	0.3835	0.2359	0.1398	0.5550
Space group	P2 ₁ /n	P2/m	P2/m	P2 ₁
Boiling point, °C	1472	1500	1700	1530
Density, g/cm³ (25 °C)	7.2-7.4	7.15	7.72	10.9-11.1

Table II.1: Chemical identity and physical properties of tungsten and tungsten oxide [11]

Characteristic	Tungsten	Tungsten oxide	Tungsten trioxide
Synonyms	wolfram; VA (tungsten)	tungsten oxide; tungsten dioxide	tungsten blue; tungsten oxide (WO ₃); tungsten trioxide; tungsten(VI) oxide; tungstic acid; tungstic acid anhydride; tungstic anhydride; tungstic oxide; wolframic acid, anhydride
Chemical formula	W	O ₂ W	O ₃ W
Chemical structure			
Molecular weight, g/mol	183.85	215.84	231.85
Colour	steel-gray to tin-white	blue	canary yellow; dark orange when heated
Physical state	solid metal	solid	solid
Melting point, °C	3410	1500–1700 (decomposes)	1472
Density, g/cm³	18.7–19.3	10.82 (theoretical)	7.2

Tungsten oxide is an n-type semiconductor with a reported band gap of about 2.6-2.8 eV [12]. The natural conductivity arises from its non-stoichiometric composition which gives rise to a donor level formed by oxygen vacancy defect in the lattice. Depending on temperature, tungsten oxide can exist in different crystal structures. The elemental tungsten metal has stability in a dry air, at the room temperature, while above 400°C, tungsten is susceptible to oxidation. It was studied [13] that the crystal structure of tungsten trioxide (WO₃) is tetragonal at temperatures above 740°C, orthorhombic from 330 to 740°C, monoclinic from 17 to 330°C, and triclinic from -50 to 17°C. The most common structure of WO₃ is monoclinic with space group P2₁/n. The crystal structures of WO₃ are presented in Table II.3.

Table II.3: The crystal structure of tungsten trioxide depending on temperature [13]

Temperature, °C	Crystal structure	Space group	Lattice constants, Å	Lattice angles, degrees
>740 °C	tetragonal	P4/nmm-D ⁷	a=5.272 c=3.920	-
330 to 740 °C	orthorhombic	Pmnb-D ¹⁶	a=7.340 b=7.546 c=7.728	-
+17 to 330 °C	monoclinic	P2 ₁ /n	a=7.302-7.306 b=7.530-7.541 c=7.690-7.692	β=90.83-90.88°
-50 to +17 °C	triclinic	P1-C ¹	a=7.30 b=7.52 c=7.69	α=80.85° β=90.82° γ=90.95°
-143 to -50 °C	monoclinic	Pc-C ²	a=5.275 b=5.155 c=7.672	β=91.7°

1.2. WO_{3-x} for gas sensors applications

Since Taguchi developed metal-oxide-based gas sensors as an industrial device [14], a lot of effort was invested to further develop those sensors, to optimize their sensing performance, to bring down their costs, and to simplify their use in the real-world environment [15].

The typical semiconductor metal-oxide (SMO) gas sensors are composed of a gas sensing element (deposited active sensing material), gas sensor substrate (substrate with incorporated two electrodes on the front side and the heater track on the back side) and gas sensor support. The operating principle of a such type of SMO gas sensor is well known and it is based on a change in the electrical conductivity due to physicochemical reactions on the surface of the active sensing material [16].

When an n-type metal-oxide crystal such as WO₃ or SnO₂ is heated at a certain high temperature in air, oxygen is adsorbed on the crystal surface with a negative charge. Then, the donor electrons in the crystal surface are transferred to the adsorbed oxygen, resulting in leaving positive charges in a space charge layer. Thus, surface potential is formed to serve as a potential barrier against electron flow (Figure II.1.a). Inside the sensor, electric current flows through the junction parts (grain boundary) of micro crystals. At grain boundaries, adsorbed oxygen forms a potential barrier which prevents carriers from moving freely.

The electrical resistance of the sensor is attributed to this potential barrier. In the presence of reducing gases adsorbed on its surface a density of the negatively charged oxygen decreases. Therefore, the barrier height in the grain boundary is reduced (Figure II.1.b) which leads to an increase in conductance. In the opposite case, under an oxidizing atmosphere, the oxide surface is covered by negatively charged oxygen and the adjacent space charge region is then electron depleted leading to a high film resistance [17, 18].

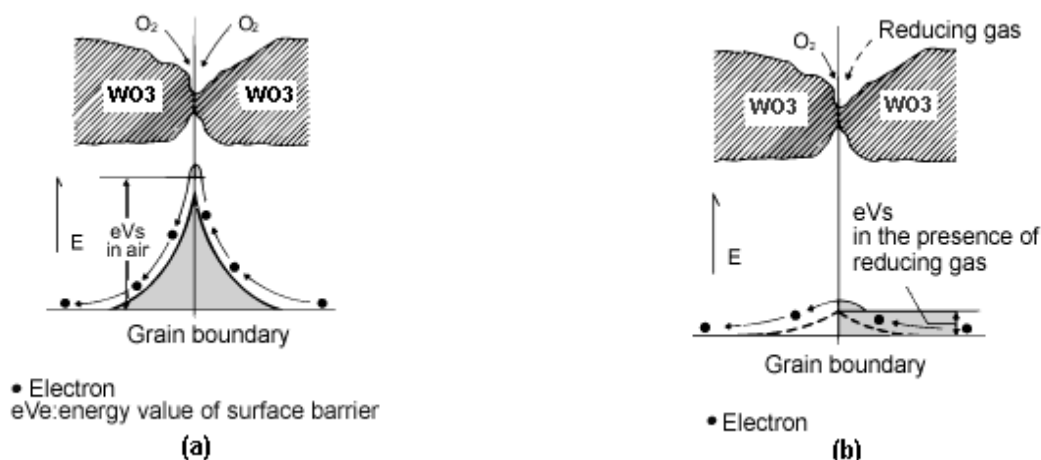


Figure II.1: Model of inter-grain potential barrier (a) in the absence and (b) in the presence of gases [17]

The reduced barrier height decreases sensor resistance. The relationship between sensor resistance and the concentration of a reducing gas can be expressed by the following equation over a certain range of gas concentration:

$$R_s = A[C]^\alpha \quad (II.1)$$

where: R_s is an electrical resistance of the sensor, A – constant, $[C]$ – gas concentration and α is a slope of R_s curve.

Due to the logarithmic relationship between sensor resistance and gas concentration, SMO type gas sensors have an advantage of a high sensitivity to gas even at the low gas concentration. Therefore, SMO gas sensors have shown a huge potential for monitoring the air pollutant emission of many different gases, in comparison with expensive gas analyzers [19]. The SMO type gas sensor devices have several unique properties such as low cost, small size, measurement simplicity, durability, ease of fabrication, and low detection limits (< ppm levels) (Table II.4).

In addition, most SMO-based sensors tend to be long-lived and somewhat resistant to poisoning. For these reasons, they have rapidly grown in popularity, becoming the most widely used gas sensors available these days. Therefore, such systems can have a major impact on the health and safety within domestic and industrial use.

Table II.4: Typical specifications for solid-state sensors [20]

Accuracy	±3% to 10% of full scale
Response time	range from 20 to 90 seconds
Target gases	different gases and ranges, or even the same gas with multiple ranges
Detection range	low ppm levels
Operating temperature range	RT to 400 °C
Humidity	5-90 %
Life expectancy	10+ years
Power consumption	approx. 300 mW

WO_{3-x} is considered to be one of the most interesting active sensing materials in the field of gas sensors based on metal-oxide semiconductors [21, 22]. At present, a tungsten oxide is used in the development of pure and doped WO_{3-x}-based gas sensors and for detection of different reducing or oxidizing gases. It was demonstrated by various authors (Table II.5.) that WO_{3-x}-based thin and thick films were sensitive to nitrogen oxides NO_x (NO₂ and NO), which are few of the most studied toxic gases, considered to be the main culprits of ambient degradation.

Apart from the above, pure and doped WO_{3-x}-based gas sensors have shown promising gas sensing results toward exposure to hydrogen sulphide (H₂S), ethanol (C₂H₅OH), ammonia (NH₃), hydrogen (H₂), ozone (O₂), sulphur dioxide (SO₂) and carbon monoxide (CO) (see Table II.5).

The summary of the successful gas sensor characterization of pure and doped WO_{3-x} active films under exposure of different reducing and oxidizing gases is presented in Table II.5. The WO_{3-x} active sensing films were prepared by the use of various traditional technologies, commonly employed in gas sensors film fabrication.

Table II.5: Summary of successful gas sensor characterization of pure and doped WO_{3-x}-based gas sensors

Active material	Target gases	Reference
WO ₃	Nitrogen oxide - NO _x (NO, NO ₂)	[2, 23-37]
WO ₃ :Au		[25, 27, 30]
WO ₃ :Pt		[25]
WO ₃ :Pd		[30]
WO ₃ :Ru		[25]
W ₁₈ O ₄₉		[38, 39]
WO ₃	Hydrogen sulphide - H ₂ S	[26, 27, 31, 35, 40-44]
WO ₃ :Au		[27, 45]
WO ₃ :Pt		[42]
W ₁₈ O ₄₉ :Pt		[46]
WO _{2.72}		[47]
WO ₃	Ethanol - C ₂ H ₅ OH	[44, 48-51]
WO ₃ :Au		[52]
W ₁₈ O ₄₉		[38]
WO _{2.72}		[53]
WO ₃	Ammonia - NH ₃	[24, 50, 51, 54, 55]
WO ₃ :Pt		[55]
WO ₃ :Cr		[56]
W ₁₈ O ₄₉		[38, 57]
WO ₃	Hydrogen - H ₂	[26]
WO ₃ :Pt		[58, 59]
WO ₃ :Pd		[60]
WO ₃	Ozone - O ₂	[49, 61, 62]
WO ₃	Sulphur dioxide - SO ₂	[31, 42]
WO ₃ :Pt		[42]
WO ₃	Carbone monoxide - CO	[26, 27]
WO ₃ :Au		[27]

The interesting gas sensing properties of WO_{3-x}-based gas sensors have given rise in the exploration of the formation of WO_{3-x} as an active sensing material in the form of thin or thick films as well as nanostructured sensing materials. The first step of the gas sensor fabrication is the synthesis and deposition of the active sensing material. This is the most crucial part in the fabrication of the gas sensor devices, since the processing techniques should be able to provide the desired oxide composition. Moreover, it is well-known, that the sensing behaviour of bulk WO₃ is a function of its chemical and physical properties such as surface area, crystallinity, stoichiometry and phase composition. The sensitivity on the other hand is based on measuring very small changes in the electrical current passing through the active surface layer of the gas sensor. These changes depend on the number of gas molecules which were deposited on the surface. Therefore, the more surface area is in contact with the gas, the higher will be the sensitivity of the gas sensor [63].

Nowadays, scientists have much interest in the development of nanostructure-based thin-film gas sensors as they exhibit more promising properties due to the large surface-to-volume ratio. Therefore, using nanostructures such as nanoneedles, nanowires, nanobelts etc. as active sensing materials is a promising method to improve the response time and the sensitivity of the gas sensors. Both properties are consequently influenced by the synthesis method employed in the development of WO_{3-x} nanostructures and deposition method used for fabrication of thin films. In fact, there are so many deposition techniques available that have led to many studies of the influence on gas sensing properties by varying the processing techniques, substrates used and sensor operating temperatures.

The most simple and common way to fabricate WO_{3-x} layers is by using a WO_{3-x} powder with the aid of the thick film technology, for example screen-printing and drop-coating techniques. Therein, the powder of WO_{3-x} is processed into a paste, which is later printed or dropped onto a gas sensor substrate [64]. Thermal evaporation synthesis and coating procedure are two main deposition techniques, successfully employed for the synthesis of WO_{3-x} nanoneedle structures used for gas sensing thin films. For instance, ultra-thin (diameter less than 5 nm) W₁₈O₄₉ nanowires were prepared by solvothermal technique by dissolving tungsten hexachloride (WCl₆) in cyclohexanol. Subsequently, a layer of tungsten oxide nanowire film was casted onto the substrate by the spin coating procedure [57].

Another example of the thick film technology is a sol-gel process. It is also known as a wet-chemical process, which typically utilizes the synthesis of oxide coating *via* hydrolysis and condensation reactions that start from organometallic compounds or inorganic salts. It is offering an inexpensive way to produce thinner films with nanocrystalline structure and better adhesion [23]. Otherwise, WO_{3-x} active sensing material can be fabricated by depositing individual atoms on a substrate, implementing thin film technology. To create WO₃ thin films with small grain size a special regime of thin film deposition was produced by the r.f. magnetron sputtering of pure tungsten target [65]. Sputtering techniques were used on porous substrate for producing of nanowires-like structures [54]. Furthermore, the reproducibility and controllability of stoichiometry and crystal structure could be improved by techniques like Pulsed Laser Deposition (PLD), where the material is vapourized from the target (in a plasma plume) and deposited as a thin film on a gas sensor substrate [66]. Alternatively, WO_{3-x} thin films could be fabricated by the metal-oxides precursor being vacuum evaporated onto a gas sensor substrate or by vapour processing routes. The tungsten oxide films are so produced with higher instantaneous deposition rate, greater flexibility in the deposition environment and better composition control, which enhance the gas sensing properties.

From the above mentioned vapour processing routes, the liquid phase methods and the wet chemical routes are the most commonly used fabrication methods for processing of nanostructured materials. In Table II.6 are classified the different deposition techniques available for the processing of nanostructured materials. There are atomic and morphological differences between the materials manufactured by the various techniques.

Table II.6: Classification of different deposition techniques available for the processing of nanostructured materials [67]

Processing route	Processing methods	Nanostructured materials
Liquid	Sol-gel	powder/film
	Sonochemistry	powder
	Hydrothermal	powder
	Electrodeposition	powder/film
	Gas Atomization	powder
	Laser Beam Melting	film
Vapour	Chemical Vapour Deposition	powder/film
	Physical Vapour Deposition	powder/film
	Aerosol Processes	powder/film
	Flame-Assisted Deposition	powder

Wet chemical routes, such as so-gel, hydrothermal and electrodeposition methods, require a high number of processing steps, including a pre-treatment, mixing, chemical reactions, filtration, purification, drying and calcination during the fabrication of ultrafine powder. Although, these methods involve relatively simple techniques, they are tedious and time consuming because of the multiple cycles of processing, which are also prone to contamination. Hence, a synthesis route that ensures both successful formation of the product in-situ and active sensing material with well-defined properties is required. For instance, Ashraf and et al. [68] in their work proved that the sensitivity of the sensor heavily depends upon film parameters such as composition, morphology and microstructure. They produced a nanoneedle-like structures by vapour processing routes such as Aerosols Assisted CVD [68] and Atmospheric Pressure CVD [69] techniques using different precursors and fabricated thin films with dramatically

different surface properties dependent on the precursor-solvent solution and temperature of deposition used. Therefore, the synthesis of tungsten oxide active films in the shape of nanoneedles or nanowires has started to be of a great scientific interest. Moreover, the miniaturization and integration of the gas sensors will require processing compatibility with silicon-based technologies.

2. Nanostructured gas sensors

2.1. Nanostructured materials

Nanostructured materials are a new class of materials which provide improved performance and extended capabilities of products in a number of industrial sectors. They are defined as materials whose structural elements - clusters, crystallites or molecules - have dimensions in the range from 1 to 100 nm. These materials can be classified into different categories depending on the number of dimensions that are nanosized such as zero-dimensional (quantum dots), one-dimensional (nanoneedles, nanobelts, nanowires, etc) and two-dimensional (films). Several authors [70, 71], discovered that when decreasing the characteristic parameter of the object (like the crystallite size or film thickness), the electrical properties (e.g. conductivity or impedance) and optical properties (e.g. coefficient of molar absorptivity or refractive index) change and improve generally. For metal-oxide gas sensors, the use of nanostructured active layers increases the sensitivity and decreases the response time.

These materials can be used in a wide range of application areas [72-74] and for production of metal-oxide nanomaterials. These include for example high sensitivity gas sensors, nanoparticulate catalysts, membranes for gas filtration and nanofiltration, harder but also ductile and machinable ceramics, high performance electronics, next generation computer chips, components with an increased fatigue life, etc. As indications suggest there are many other uses yet to be discovered.

A major barrier at this moment is the ability to synthesize nanostructures and films with precisely controlled size, composition and shape in a way that is economical and easy for implementation. Therefore, processing of the nanoscale building blocks

into the real materials suitable for wide range of applications is of crucial importance in order to reveal the high performance and new properties.

2.2. Nanostructured metal-oxide in gas sensor applications

In terms of gas sensor device applications, low dimensional (quasi-one dimensional) nanostructures such as nanowires, nanoneedles, nanofibres, nanorods, nanobelts and nanotubes are in the main focus of intensive research (Figure II.2). Such nanomaterials, especially those of metal-oxides, were widely studied because of their interesting sensing behaviour and possible application in the new types of nanosensing structures. It was reported, that the gas sensors based on various nanostructures found application in a range of detecting elements including biological, electrochemical, gas, optical, pH, orientation, humidity sensors etc [75, 76]. Furthermore, nanostructure-based sensor devices had shown great improvement of their gas sensing properties such as sensitivity, selectivity, response time and recovery time [77].

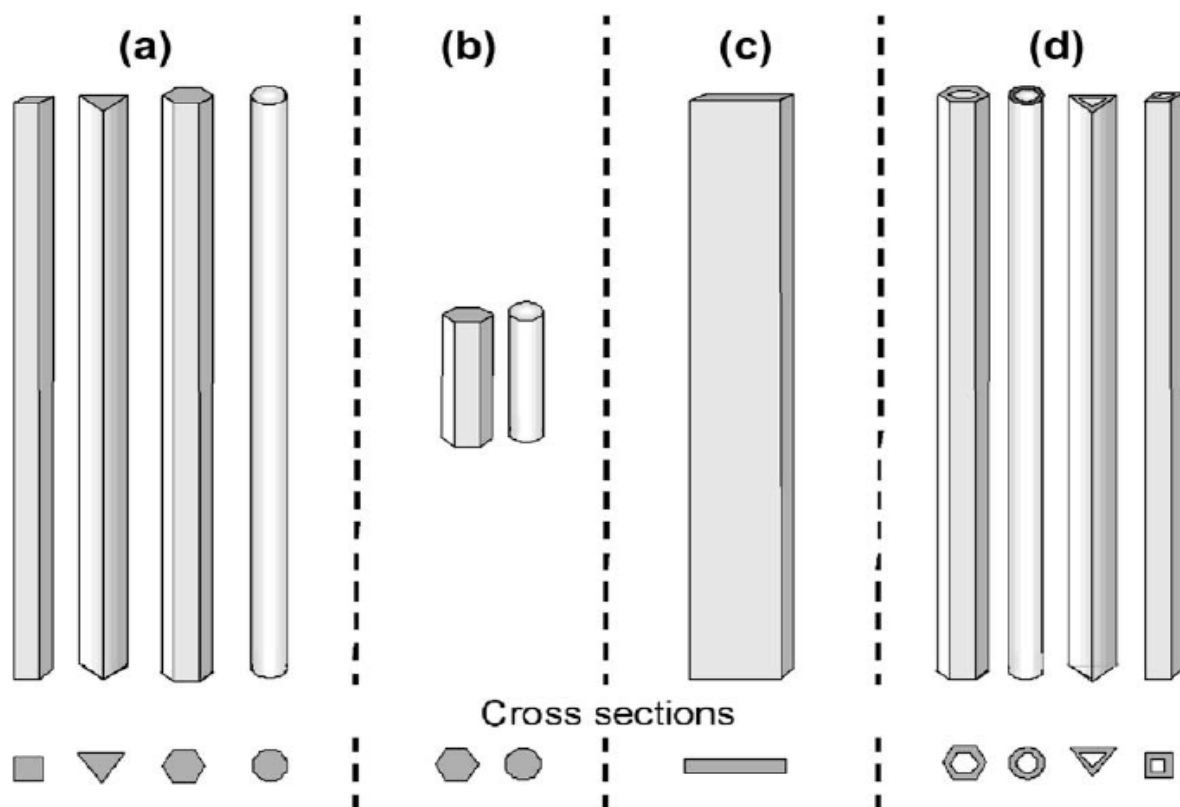


Figure II.2: Schematic illustration of different quasi-one dimensional nanostructure morphologies and the terms typically used to describe them: (a) nanowires (NWs), nanoneedles, nanofibres or whiskers; (b) nanorods (NRs); (c) nanobelts (NBs) or nanoribbons and (d) nanotubes (NTs) [74]

One of the important characteristics of nanostructured materials is their high surface area/volume ratio. Therefore, due to the increase of their specific surface, the surface effects dominate, which leads to the enhancement of the related properties, such as catalytic activity or surface adsorption. Hence, the elevated interaction between the analytes and the sensing area for the same chemical composition can increase the sensitivity of the gas sensor device.

It was found [78], that by controlling the grain size and the depth of the surface space-charge layers, which affect the receptor and transducer functions of the gas sensors, the sensitivity to a particular gas and the long term stability can be enhanced. The smaller the nanomaterials are, the more sensitive the sensor could be. According to the literature review [70], since 2002 the most studied quasi-one dimensional metal-oxide nanostructured material for gas sensors applications are: tin dioxide (SnO₂) and zinc oxide (ZnO). Thirty-two percent of publications are focused on SnO₂ and the same amount for ZnO, followed by (indium (III) oxide) In₂O₃ (10%), (titanium dioxide) TiO₂ (8%) and (tungsten trioxide) WO₃ (5%), presented in Figure II.3.a. Moreover, the quasi-one dimensional metal-oxide nanostructures used for gas sensors are the most widely studied in the form of nanowires (nanoneedles, nanofibres) at 40%, followed by nanorods, nanotubes and nanobelts and nanoribbons at ~ 20% (Figure II.3.b).

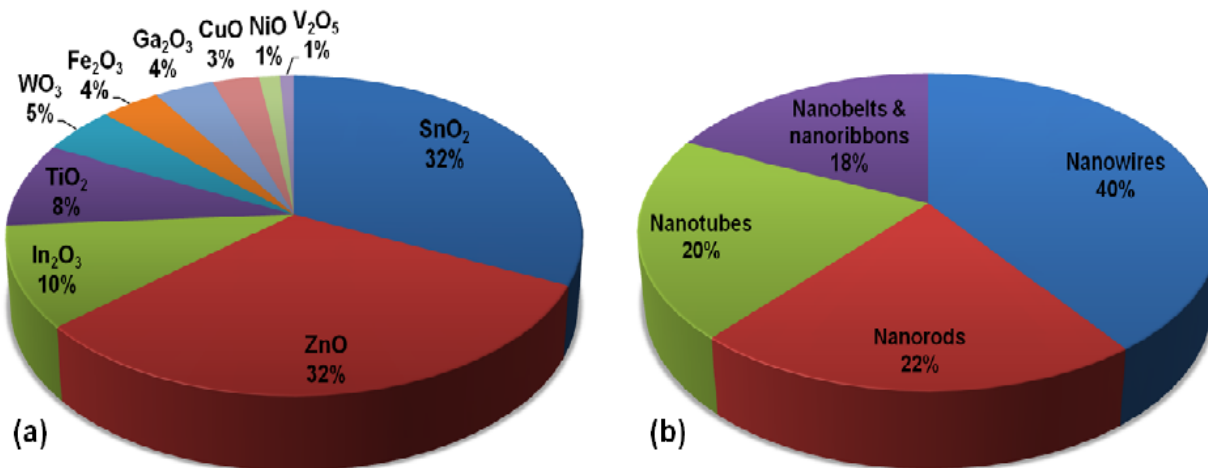


Figure II.3: (a) Top 10 material and (b) forms of quasi-one dimensional metal-oxide nanostructures used for gas sensor applications in publications since 2002 [70]

2.3. Modified nanostructures

The metal-oxide semiconducting nanowires are among the most promising gas sensor systems for the use as chemical detection devices. It is well known, that the presence of noble metal elements (Au, Pt, Pd, etc.) on the surface of a metal-oxide enhances the interaction of reducing gases with the absorbed oxygen on the surface. It was found [79] that gas sensor systems based on metal-oxide nanowires function by converting surface chemical processes, (often catalytic) into observable resistance variations in the nanowire. When such nanostructures are grown from a semiconductor, then their electrical properties can be altered by the addition of small amounts of catalytic metal nanoparticles (dopant) on the nanowire's surface. Hence, modified or functionalised metal-oxide nanowires have also attracted some research attention.

Doping is a technique utilized to improve gas sensing properties of metal-oxides, where the dopant atoms are believed to act as activators for surface reactions. In general, doped semiconductors generate processes that locally change their charge carrier density and conductivity. Well-known conventional doping process for semiconductors is so-called ion implantation process [80]. It is achieved by the bombardment of semiconductors with energetic ions (dopants) followed by the thermal annealing process. In this process external impurity atoms (dopants), with appropriate properties, are incorporated into the host lattice of the semiconductor. Ion implantation process had found application in gas sensor technology in the past few decades. However, every year the minimization of the microelectronics devices required fabrication process with well-defined nanostructures and controllable and reproducible nano-scale doping. Ion implantation is incompatible with nanostructured materials such as quasi-one dimensional nanowires and two dimensional nanosheets, since bombardment of these materials with energetic ions can create crystal damage, thereby degrading the device's performance.

Recently, much effort was devoted to developing new methods which would be particularly useful for modification of quasi-one dimensional semiconducting nanowires and effectively incorporating noble metal catalyst particles into nanostructured semiconductors. Surface functionalisation of nanostructures by attachment of noble nanoparticles is used to modify the gas sensing properties. This is a powerful method which can simultaneously allow modification of the surface chemistry, tailoring of the

electrical properties and optimization of the fabrication process of a device. In 2008, Kolmakov et al. [79], compared the sensing properties of single quasi-one dimensional chemiresistors (i.e., nanowires or nanobelts), before and after the surface functionalisation, with noble metal catalyst particles. It was found that the sensing mechanism can depend dramatically on the degree of metal coverage of the nanowire and it was demonstrated that functionalisation of the nanowires significantly improves the sensitivity towards oxidizing and reducing gases. Functionalisation of nanowire surface can lead to the improvement of the selectivity, sensitivity and operating temperature of nanostructure-based sensing elements.

Palgrave et al. [81] in their publication summarise several strategies for modification of nanostructured semiconductors (Figure II.4). They include: Route 1 - synthesis of the semiconductor matrix followed by the addition of nanoparticles in the second step. Examples of this strategy include spin coating or dip coating a semiconductor film with a nanoparticle solution. The nanoparticles are chemically bound to the surface or become trapped within pores in the semiconductor. Route 2 - synthesis of the semiconductor matrix followed by addition of metal ions in the second step. Techniques like ion implantation and spin coating with a solution of metal ions followed by photocatalytic reduction or heat treatment are examples of this strategy. Route 3 - synthesis of the semiconductor matrix and metal particles in a single step. Examples include sol-gel using a semiconductor and nanoparticle precursor, the related technique of liquid-phase deposition, multitarget magnetron sputtering deposition and chemical vapour deposition using a separate precursor for each phase. Route 4 - layer-by-layer deposition of metal particles and semiconductor material, for example, laser ablation, using alternate metal and semiconductor targets. Route 5 - in-situ surface functionalisation or deposition of metal nanoparticle/semiconductor composite thin films.

The Aerosol Assisted Chemical Vapour Deposition (AACVD) method, which was applied in this doctoral thesis, uses a liquid-gas aerosol to transport soluble precursors to a heated substrate. Unlike conventional atmospheric pressure CVD method, the precursors for AACVD do not have to be non-volatile and thermally stable, which opens new roads for new precursors and films deposition investigations. The authors found that in Routes 2-4, the noble nanoparticles are formed in-situ or concurrently with the matrix. The use of preformed nanoparticles in Route 1 is advantageous because of a

wider range of nanoparticles that could be used. As the semiconductor deposition and nanoparticle formation steps are independent, each can be individually optimized.

Many authors have investigated these routes to produce nanocomposite materials using various noble metal nanoparticles. In (Table II.7) are presented some examples of different routes to produce nanocomposite materials applied to nanostructure metal-oxides and their gas sensing properties.

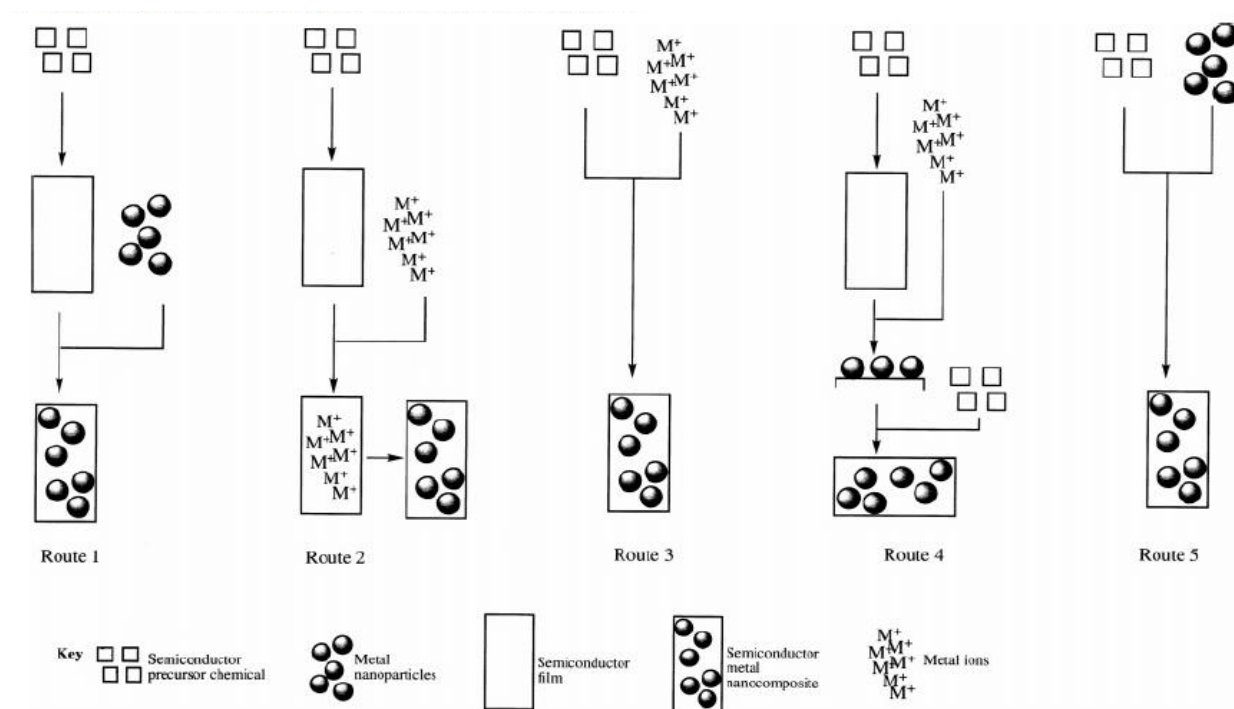


Figure II.4: Routes of metal/semiconductor nanocomposite materials [81]

Table II.7: Examples of materials and routes to produce nanocomposite materials used for fabrication of functionalised nanostructured metal-oxide gas sensors

Active material	Synthesis method and sensors fabrication	Routes for nanocomposite materials and nanoparticles (dopant)	Nanostructure (form)	Target gases and minimum concentration (ppm)	Ref
WO ₃	Ion-exchange method + paste coating	Route 1 (Au)	nanorods	H ₂ (50)	[82]
WO ₃	Conventional solid-state reaction method	Route 3 (Pt)	nanowires	H ₂ (1000)	[58]
WO ₃	Thermal heating procedure + slurry coating	Route 1 (K)	nanosheets	H ₂ S (10) C ₃ H ₆ O (10)	[83]
WO ₃	AACVD – in-situ	Route 5 (Au)	nanoneedles	EtOH (1.5)	[52]
SnO ₂	Thermal evaporation + drop casting	Route 3 (Ru)	nanowires	NO ₂ (50)	[84]
SnO ₂	Thermal evaporation + drop coating	Route 1 (Pd)	nanowires	H ₂ (500)	[85]
SnO ₂	Electrospinning method	Route 1 (Co)	nanofibers	H ₂ (100)	[86]
SnO ₂	Chemical vapour deposition + transferring by direct contact	Route 3 (Pd,Ag)	nanowires	H ₂ (N/A) CO (N/A) C ₂ H ₄ (N/A)	[87]
ZnO	Vapour-liquid-solid method	Route 4 (Au)	nanowires	CO (100)	[88]
ZnO	Hydrothermal method + slurry coating	Route 1 (Au,Pt)	microrods	EtOH (100)	[89]
TiO ₂	Anodization procedure	Route 4 (Pd)	nanotubes	H ₂ (1000)	[90]

2.4. Deposition methods for nanostructured metal-oxides gas sensors

The technology fabrication and proposed growth mechanism of metal-oxide nanostructures in a form of nanowires, nanoneedles, nanofibers, nanorods and nanobelts thin films and their gas sensing properties will be described in this section.

2.4.1. Film growth mechanism

Growth mechanism and deposition process for obtaining thin films were a subject of an intensive study for almost a century, during which many methods were developed. The growth mechanism of thin films includes the processes of nucleation and subsequent growth on the substrate or growth surfaces. The nucleation process plays a very important role in determining the crystallinity and microstructure of the resultant films [91]. For the deposition of thin films with thicknesses in the nanometer region, the initial nucleation process is even more important.

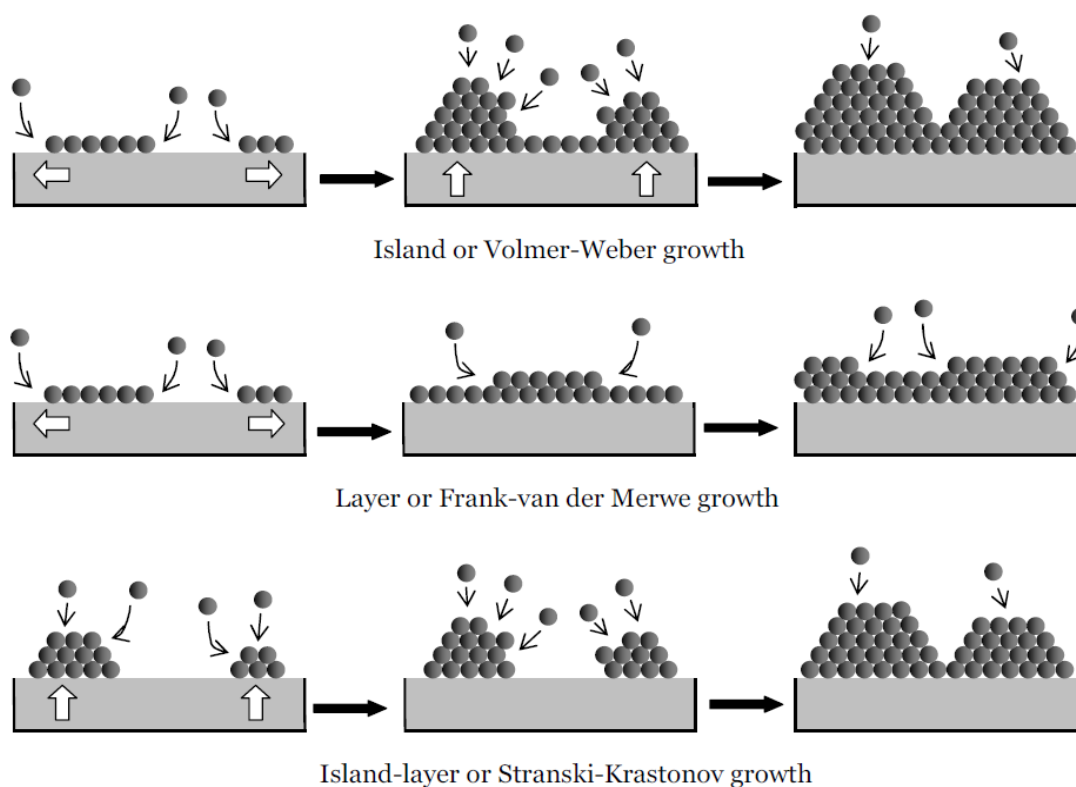


Figure II.5: Schematic illustration of three basic models of initial nucleation in the film growth [91]

The size and the shape of the initial nuclei are assumed to be solely dependent on the change of volume of Gibbs free energy due to super-saturation and the combined effect of surface and interface energies governed by Young's equation [91]. In practice, the interaction between film and substrate plays a very important role in determining the initial nucleation and the film growth. Many experimental observations revealed that there are three basic nucleation modes (Figure II.5):

- Island or Volmer-Weber growth;
- Layer or Frank-van der Merwe growth;
- Island-layer or Stranski-Krastonov growth.

Island growth occurs when the growth species are more strongly bonded to each other than to the substrate. Subsequent growth results in the islands coalescing to form a continuous film. The layer growth is the opposite of the island growth, where growth species are equally bound more strongly to the substrate than to each other. First, a complete monolayer is formed before the deposition of a second layer occurs. The island-layer growth is somewhat in between the layer growth and the island growth. Such a growth mode typically involves stress developed during the formation of the nuclei or films [91].

The essence of 1-D nanostructure formation is crystallisation [92]. Although crystallisation has been studied for hundreds of years, very little is quantitatively known about this process. It is generally accepted that the formation of a perfect nanostructured crystal requires a reversible pathway between the building blocks on the solid surface and those in a fluid phase (i.e. vapour, solution or melt). When developing a synthetic method for growing nanostructures, the most important issue that one needs to address is the simultaneous control over dimensions, morphology (or shape), homogeneity and uniformity [93].

The synthesis and processing of nanomaterials is the first and very important aspect of nanotechnology. There are two different approaches used for the synthesis of nanomaterials and the fabrication of nanostructures: top-down and bottom-up (Figure II.6) [71, 94]. The top-down methods are based on reducing the lateral dimensions of the films to the nanometer scale. These methods consist of a standard micro fabrication processes with deposition, etching and ion beam milling on planar

substrates. Electron beam, focused ion beam, X-ray lithography, nano-imprinting and scanning probe microscopy techniques can be used as the selective removal processes. The advantages are the use of the well developed technology of semiconductor industry and the ability to work on planar surfaces, while disadvantages are their extremely high costs and prolonged preparation times. The bottom-up approach refers to the build-up of a nanostructure from the bottom: atom-by-atom, molecule-by-molecule or cluster-by-cluster. This approach consists of the assembly of molecular building blocks or chemical synthesis by vapour phase transport, electrochemical deposition, solution-based techniques or template growth. The bottom-up methods allow low cost fabrication together with the possibility to easily vary the intentional doping. The main disadvantage is regarding to their integration on planar substrates and difficulty to get nanostructures that are well arranged and patterned.

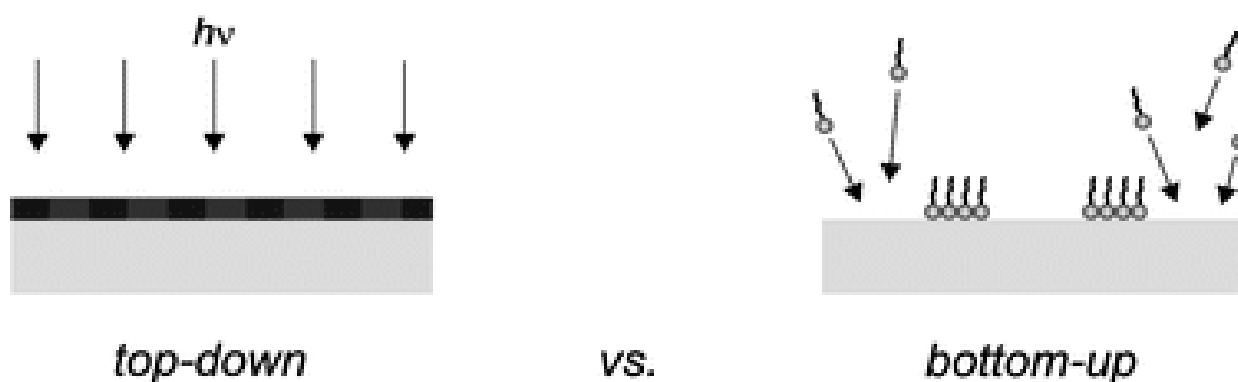


Figure II.6: *Top-down* approaches are based on patterning on a large scale while reducing the lateral dimensions to the nanoscale. *Bottom-up* approaches arrange atoms and molecules in nanostructures [94]

Vapour phase synthesis [Vapour-Liquid-Solid (VLS) and Vapour-Solid (VS)] are probably the most extensively explored bottom-up approaches for the formation of quasi-one dimensional nanostructure such as nanowires, nanoneedles and nanorods. A typical VLS process starts with the dissolution of gaseous reactants into nanosized liquid droplets of a catalyst metal (such as gold, iron, etc.), followed by nucleation and growth of a single crystalline rods and wires. The VLS process was originally developed by Wagner and co-workers in the 1960s, when they reported fabrication of micrometre-sized whiskers [95].

A deeper insight into the potential VLS mechanism was provided by Kolasinski et al. [96] who reported a catalytic growth of a wire (whisker) like structures with diameters ranging from just a few nanometers to the millimetre range. The authors focus on the similarities between the catalytic growth processes, in an attempt to better understand the phenomenon. They found that the nanowires can grow from the top (Figure II.7.b) or the bottom (Figure II.7.a) of the catalyst cluster and a catalyst cluster can give rise to single or multiple nanowires growth. Moreover, it was observed that in a single nanowire growth there is a one-to-one correspondence between the catalyst and nanowires. In the single wire growth control over the nanowire diameter should be obtained by controlling the catalyst radius (Figure II.7.d). While in the multiple nanowires growth the section must be related to other factors such as the curvature of the growth interface and lattice matching between the catalytic particle and the nanowire (Figure II.7.c).

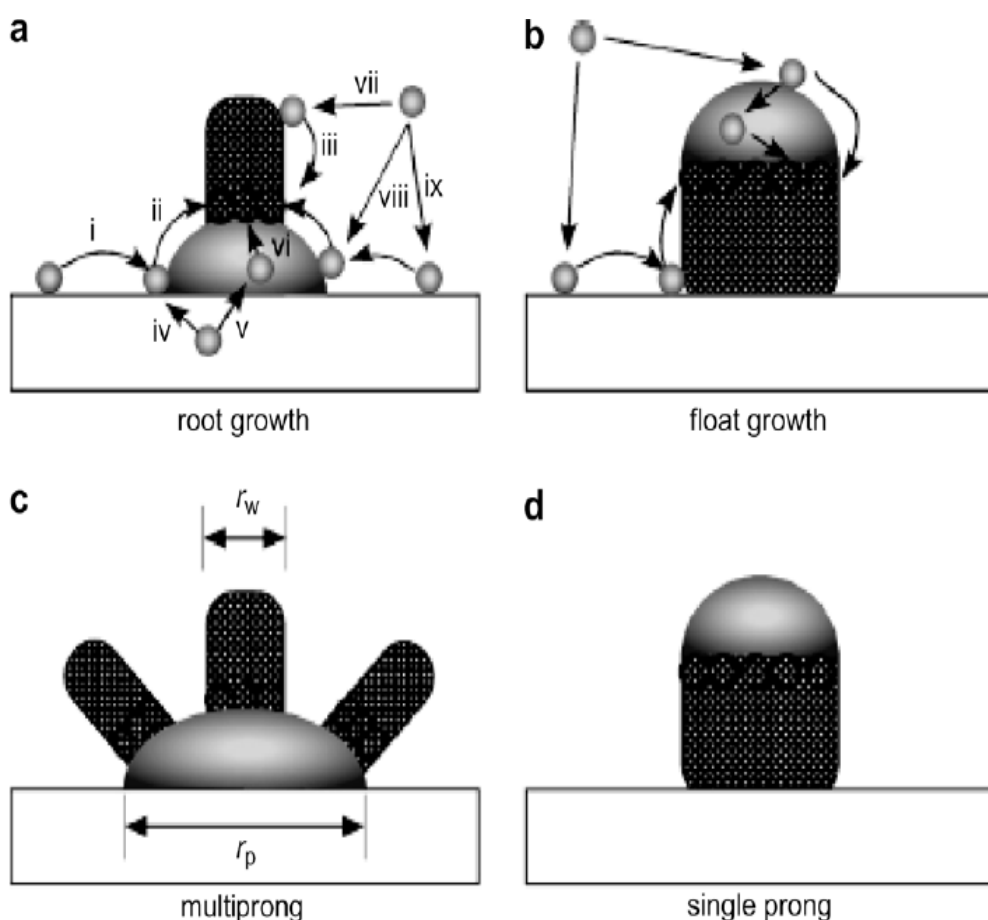


Figure II.7: The processes that occur during catalytic growth. (a) In root growth, the particle stays at the bottom of the nanowire. (b) In float growth, the particle remains at the top of the nanowire. (c) In multiple prong growth, more than one nanowire grows from one particle and the nanowires must necessarily have a smaller radius than the particle. (d) In single-prong growth, one nanowire corresponds to one particle.

One of the surest signs of this mode is that the particle and nanowire have very similar radii [96]

Unlike the VLS method, in VS method nanostructures are formed without introducing metal catalyst. In the absence of metal catalysts, the VS or self-catalytic growth mechanism were mainly used to synthesise metal-oxides and some semiconductor nanomaterials. In a typical VS process, vapour species are first generated by evaporation, chemical reduction, atomization and gaseous reaction. These processes dissolve the gaseous reactants into nanosized liquid droplets, which are then transported and condensed onto the surface of a solid substrate placed in a zone with an elevated temperature. The material morphology of a pure vapour transport synthesis is governed by process parameters, such as substrate temperature, gas-phase composition and overall pressure. This synthetic strategy allows the synthesis of needle-like structures, which show defined side facets with low surface energies. In a perfect crystal, the growth can only proceed if new surface steps are formed and layer-by-layer growth occurs. However, the growth rate of real crystals is much higher due to the presence of defects (kinks, twins, dislocations). The anisotropic growth of nanowires can be promoted by manipulating the differences in crystal surface energies or by defects such as screw-dislocations and self-catalytic formation of a metal wetting layer [74]. The first report dealing with a screw dislocation mediated whisker growth was in 1955 for mercury by Sears et al. [97].

Recently, Calestani et al. [98] reported low temperature (> 500 °C) thermal evaporation deposition of aligned ZnO nanorods. Such VS process, which is catalyst-free thermal evaporation, is generally considered to be a low-cost technology for the growth of metal-oxide nanostructures, that does not require expensive precursors or catalysts. The authors were able to achieve Zn nanocluster formation and a rod growth during a few minutes in a single process, without introducing any foreign element that might produce undesired material contamination and affect the physical properties of these nanostructures. Thanks to the comprehension of the growth mechanism, very uniformed deposition of nanorods was obtained, comparing with the results achieved on different substrates and under different growth conditions. In their work, they observed that if the source temperature and Zn condensation are increased, so that the larger Zn droplets or even a continuous Zn layer are deposited on the ZnO film, not aligned and larger nanorods and crystals are obtained. Similarly, if the ZnO seeding film is not present on the substrate (Si, glass, ITO and alumina were tested), this results in a non-ordered growth of different nanostructures.

Specifically, the underlying nucleation and growth VS mechanisms are not understood in terms of how a slight variation within the Chemical Vapour Deposition (CVD) set up could yield one dimensional crystal growth. In a self-catalysed direct VS mechanism nanostructured films are grown from an initial polycrystalline layer, which provides energetically favourable planes for the nucleation of the quasi-one dimensional end caps. Thangala et al. [99] in their work study the mechanisms responsible for quasi-one dimensional growth of both metal and metal-oxide nanowires using only the vapour–solid schemes. In the case of low-melting-point metal-oxides, the metal itself could provide the medium for either spontaneous nucleation and basal growth [100] or tip-led growth modes [101] for metal-oxides at the synthesis temperatures. However, the metals, such as tungsten, do not melt at the synthesis temperatures. So, the present case of chemical-vapour transport and deposition of metal-oxide species for obtaining both metal and metal-oxide nanowires falls into the category of CVD techniques with only gas–solid interactions and without the use of catalyst particles or templates.

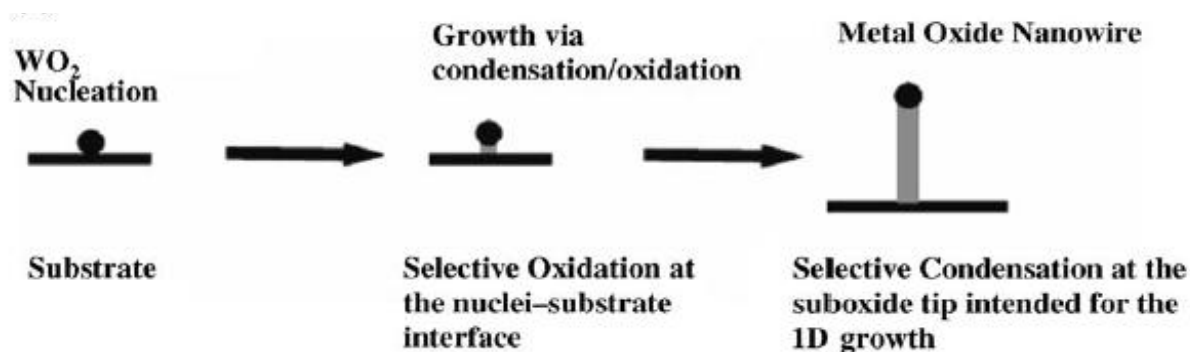


Figure II.8: Schematic image illustrating the mechanism for formation of tungsten oxide nanowires through VS process [99]

In [99] was proposed a growth model, shown in Figure II.8, for the observation of the quasi-one dimensional growth of tungsten oxide nanowires. Firstly, the high supersaturation of WO₂ (gas) leads to condensation into WO₂ (solid) clusters in a nucleation step. Secondly, further oxidation of WO₂ clusters could be favourable at the cluster–substrate interface, which leads to precipitation of WO_{3-x} crystals on the substrate with a tip whose dimensions are considerably less than the crystal. Finally, the enhanced adsorption of WO₂/WO₃ species on the tip relative to the bulk surface, followed by further oxidation at the cluster–crystal interface, leads to quasi-one

dimensional growth of WO_{3-x} nanowires. The enhanced adsorption at the tip was also made possible by the competition between the net condensation reaction and the desorption/oxidation reactions on the WO₂ cluster in comparison to the WO_{3-x} nanowire, and determine the relative rates of axial versus radial growth. In essence, the nanowire nucleation could be achieved through WO₂ cluster nucleation while quasi-one dimensional growth could be led by an amorphous WO_{2+y} cluster (with 2+y less than 3-x) at the tip. The WO_{2+y} tip is not visible in any of the experimental results and it is presumed that the tip will also be oxidized during the experimental shutdown. Hence, there was no tip associated with tungsten oxide nanowires and the entire nanowire was composed of one phase, that is, the oxygen-deficient W₁₈O₄₉ phase. In all experiments, a blue deposit gave an indication of nanowire formation and the yellowish green deposit gave an indication of a nanoparticle formation [99].

2.4.2. Methods for nanostructured metal-oxides gas sensors

Different synthesis processes were employed to fabricate nanostructured materials, such as WO₃ nanowires and In₂O₃ nanorods using sol-gel methods, ZnO nanorods and SnO₂ flower-like nanostructures using hydrothermal methods, TiO₂ nanofibres using electrospinning method, etc. Metal-oxides active films with such structure synthesised in the form of nanowires, nanoneedles, nanobelts and nanotubes are new attractive nanostructures. The formed structures are crystalline with well-defined chemical composition and surface terminations, which seems to be advantageous especially for gas sensor applications (Table II.8). Several strategies were developed for the fabrication of conductometric nanowire metal-oxide gas sensors [102, 103]. The formation of a thin nanostructure layer on top of the predefined contact electrodes is the most commonly employed method for fabrication of sensor device.

The most popular nanowire products are created by techniques like hydrothermal methods or template growth structures. The nanostructures or nanowires are first stripped off from the substrate and then ultrasonically dispersed in solvents such as ethanol or acetone. The resulting material is then dried naturally in air to obtain a paste. Finally, this paste is applied on the substrate with the contact pads either by spin-coating or drop-coating. The sensor material is afterwards subjected to calcinations at temperatures between 300 and 400 °C for 1 to 2 h in air prior to testing. These are so-

called ex-situ techniques, where the process becomes tedious, time-consuming, and overall non-scalable.

Alternatively, nanowire structures can be created by the in-situ techniques or by the direct growth of non aligned nanowire-like structures between electrodes on the sensor substrate [71]. The in-situ techniques have the advantage of fewer processing steps, hence, it is an easier fabrication method, comparing with the existing sensor technology. However, the integration of the quasi-one dimensional nanomaterials *via* in-situ techniques with MEMS microhotplate platforms is still a major challenge, which could offer excellent prospects for advanced gas sensors.

The use of single nanowires bridges between two metal electrodes is another applied strategy. The single nanowire-based chemical sensors have shown great gas sensing properties [104]. However, the ability to fabricate and manipulate such objects in a reliable manner on a large scale is still complicated.

One dimensional ZnO nanorods, nanobelts and nanowire-based gas sensors were studied by the number of researchers. The ZnO nanowires had shown a promising results for applications in alcohol sensors [105]. It was found that sensors based on ZnO nanorods exhibit superior response and stability to ethanol vapour than that of ZnO nanoparticles. Moreover, after working continuously for 50 days, the sensitivity of the ZnO nanorods was still retained, while the sensitivity of the ZnO nanoparticles decreased twice [106]. Similarly, gas sensors based on flower-like ZnO nanostructures were sensitive to both ethanol and ammonia even at room temperature [107]. Furthermore, ZnO nanorod-based sensors had shown a very high sensitivity to lower concentrations (0.05-1 ppm) of nitrogen dioxide (NO₂) gas [108], while the ZnO nanostructures in a form of sphere, flower and star-like, demonstrated higher sensitivity to carbone monoxide (CO) [109].

A conductometric tin oxide nanobelt-based gas sensor was first reported by Comini et al. [110]. It was found that the SnO₂ gas sensors based on different nanostructures (nanobelts, nanowires, flower-like or columnar) were able to detect low concentrations of CO [111, 112], CH₄ [104], NO₂ [110] and ethanol [113]. Furthermore, a number of positive features were demonstrated: easy fabrication, open surface, higher gas sensitivity and long-term stability, which make them prospective material platform for the next generation of durable conductometric gas sensors.

The effect of nanowires dimensions on response of the gas sensors was investigated by comparing two different types of TiO₂-based gas sensors (solid thin film device and nanowire-based) [114]. Subsequently, it was found that between the solid and 100 nm nanowires-based sensors, the response towards different ethanol concentrations (2 to 6%) increased 3 times, while for 200 nm nanowires devices the difference was not so evident. Moreover, gas sensors based on TiO₂ nanofibres were tested towards low NO₂ concentration (0.5 ppm) and had shown huge increase of the sensors resistance [115].

Similarly, in order to examine the influence of the morphology on the gas sensing properties, Li et al. [116] compared gas sensor based on In₂O₃ nanorods and In₂O₃ particles. It was found that the gas response of the sensor based on In₂O₃ nanorods was higher than that of In₂O₃ nanoparticles, when exposed to ethanol vapour. Additionally, it was demonstrated that gas sensors based on In₂O₃ nanostructures had shown superior sensitivity to NH₃ [117] and NO₂ [118] even at the room temperature.

In 2005, Shaw et al. [119] reported the gas sensing properties of tungsten oxide-based nanofibrous films deposited *via* AACVD on alumina substrates. In this work it was found that application of an electric field during deposition encouraged thicker film growth. The gas sensing results for a range of morphologies of a tungsten oxide aligned nanofibres have shown significantly larger responses to NO₂ for concentrations below 300 ppb at 400 °C. In the same year, Sawicka et al. [120] reported gas sensors based on tungsten oxide nanowire and its sensing properties. The gas sensors based on WO₃ nanowire-elements were tested toward NO₂ and it was found an improvement in the gas sensitivity, response time and detection limit, comparing with sol-gel processed conventional films. Moreover, gas sensors based on nanostructured tungsten oxide thin films had shown capability to detected NO₂ even at lower temperatures [121]. The ultra-thin morphology of tungsten oxide WO_{2.72} nanorods and WO₃ nanoplates were considered to be advantageous for effective adsorption and rapid diffusion of the alcohol molecules. They could find application in alcohol sensors for detection of ethanol [122-124], butanol, methanol and isopropanol [125]. Furthermore, gas sensors based on ultra-thin W₁₈O₄₉ nanowires had shown promising results for ammonia detection [126] and it was noted their higher sensitivity to low concentrations of ammonia even at the room temperature [127].

Other nanostructured metal-oxides used for fabrication of gas sensors were reported in 2005 by Comini et al. [128]. They developed MoO₃ nanorod-based gas sensors, which had shown 10 times more sensitivity to CO and ethanol, comparing with the conventional MoO₃ thin film sensors. Similarly, year later Taurino et al. [129] prepared MoO₃ nanorods gas sensors, which had shown good responses to NO₂ and NH₃. Nanostructured IrO₂ in a form of nanoblade, layered-column, incomplete-nanotube and square-nanorod, had shown response to propionic acid gas even at the room temperature [130]. Furthermore, it was found that gallium oxide (Ga₂O₃) nanowire-based gas sensor had shown response to O₂ and CO gas and operated at temperatures much lower than the reported thermal activation temperature for other Ga₂O₃-based gas sensors [131].

Table II.8: Examples of materials and deposition methods used for fabrication of nanostructured metal-oxide gas sensors (part 1)

Active material	Nanostructure (form)	Method and precursor	Gas sensor deposition and substrate	Target gases and minimum concentration (ppm)	Optimal operating temperature (°C)	Ref.
WO ₃	nanofibres	aerosol-assisted CVD – [W(OPh) ₆]	Al ₂ O ₃ sensor substrate	NO ₂ (0.1)	400	[119]
	nanowires	electrospinning technique using metal-oxide sol-gel and polymer solution mixtures	sensor substrate	NO ₂	N/A	[120]
	nanoplatelets	aqueous sol-gel method – [Na ₂ WO ₄]	spin coating onto quartz substrates	NO ₂ (0.6)	175	[121]
	nanoplates	topochemical method	coating procedure onto Al ₂ O ₃ microtube sensor substrate	butanol (2) CH ₃ OH (300) EtOH (200)	300	[125]
	nanorods (WO _{2.72})	colloid-based synthesis method	drop-coating onto sensor Si substrate	N ₂ (2%) EtOH (1000) NH ₃ (10) NO ₂ (3)	RT	[122, 124]
	ultra-thin nanowires (W ₁₈ O ₄₉)	solvothermal method – [WCl ₆]	spin-coating onto sensor glass substrate	NH ₃ (1)	RT	[127]
	nanorods	microwave hydrothermal method – [Na ₂ WO ₄ ·2H ₂ O]	screen-printing onto ceramic tube sensor substrate	EtOH (10)	500	[123]

Table II.8: Examples of materials and deposition methods used for fabrication of nanostructured metal-oxide gas sensors (part 2)

Active material	Nanostructure (form)	Method and precursor	Gas sensor deposition and substrate	Target gases and minimum concentration (ppm)	Optimal operating temperature (°C)	Ref.
SnO ₂	nanobelts	thermal evaporation method [oxide powder]	Al ₂ O ₃ sensor substrate	CO (30) NO ₂ (0.2) EtOH (10)	350	[110]
	nanowires and nanobelts	vapour–solid method – [organo-tin precursor]	spin-coating onto ceramic substrates	2-propanol (0.5)	300	[132]
	single nanowire	vapour–liquid–solid mechanisms or CVD	Si sensor substrate	CO (5)	260	[111]
	nanowires	heating of pure tin powder at 800°C in a quartz tube	Si sensor substrate	CO (50)	250	[112]
	single nanowire	spray pyrolysis method – [SnCl ₄ ·5H ₂ O]	Si sensor substrate	CO (4) CH ₄ (3)	350 200	[104]
	flower-like	hydrothermal method – [SnCl ₂ ·2H ₂ O]	drop-coating onto sensor device	CO (50)	350	[133]
	columnar-like	flame aerosol reactor method [tin (II) 2-ethylhexanoate]	Al ₂ O ₃ sensor substrate	EtOH (100)	250	[113]
ZnO	nanowires	hydrothermal method – [zinc nitrite]	CMOS microhotplate substrate	EtOH (175)	250	[105]
	nanorods	solution procedure	spin-coating procedure onto Si sensor substrate	NO ₂ (0.05)	300	[108]
	nanorods	hydrothermal method – [zinc metal powder]	coating procedure onto Al ₂ O ₃ tube-like substrate	EtOH (50)	330	[106]
	flower-like	electrochemical method – [zinc metal]	glass substrates with Au electrodes	NH ₃ (80) acetone (80) EtOH (80)	RT	[107]
	sphere, flower and star-like	wet chemical method assisted by microwave – [zinc acetate or zinc nitrite]	drop-coating onto Al ₂ O ₃ sensor substrate	CO (200)	300	[109]

Table II.8: Examples of materials and deposition methods used for fabrication of nanostructured metal-oxide gas sensors (part 3)

Active material	Nanostructure (form)	Method and precursor	Gas sensor deposition and substrate	Target gases and minimum concentration (ppm)	Optimal operating temperature (°C)	Ref.
TiO ₂	nanowires array	nanopatterning method	Si sensor substrate	EtOH (2%)	550	[114]
	nanofibres	electrospinning method [titanium(IV) propoxide]	Al ₂ O ₃ sensor substrate	NO ₂ (0.5)	300	[115]
	nanotubes	hydrothermal method [TiO ₂ powder]	screen-printing onto Al ₂ O ₃ sensor substrate	toluene (50)	500	[134]
In ₂ O ₃	nanorods	sol-gel process [InCl ₃ ·4H ₂ O]	coating procedure onto Al ₂ O ₃ tube sensor substrate	EtOH (0.5)	290	[116]
	nanotubes	layer-by-layer assembly on carbon nanotube templates	spin-coating on the top of Au electrodes	NH ₃ (5)	RT	[117]
MoO ₃	nanorods	infrared irradiation heating a Mo foil	Al ₂ O ₃ sensor substrate	CO (30) EtOH (200)	200	[128]
	nanorods	hydrothermal method – [MoO ₃ ·2H ₂ O]	transfer and evaporation onto Al ₂ O ₃ substrate	NO ₂ (1) NH ₃ (10)	240 370	[129]
IrO ₂	nanoblade, layered-column, incomplete-nanotube and square-nanorod	metal-organic CVD – [methylcyclopentadienyl] (1,5-cyclooctadiene) iridium (MeCp)Ir(COD)	gold-coated quartz substrate	propionic acid (1000)	RT	[130]
Ga ₂ O ₃	nanowires	reactive thermal evaporation method – [gallium metal]	Si sensor substrate	O ₂ (1) CO (100)	300 100	[131]
V ₂ O ₅	nanofibres	aqueous suspension depositing method [NH ₄ VO ₃]	Si sensor substrate	1-butylamine (0.15)	RT	[135]

Although some of the methods, like the thermal evaporation method, are simple they are generally achieved in several step processes (ex-situ techniques). In many cases, second procedure like drop-coating or spin-coating is required in order to fabricate the gas sensor. In 2007 Ashraf et al. [68] reported the synthesis of WO₃ nanostructures *via* an AACVD process, in which first was generated solution-precursor vapour in-situ using tungsten hexacarbonyl [W(CO)₆] as a precursor, transported in a reactor to the growth zone with elevated temperature, and finally oxidized to form WO₃ thin film.

Much of our work in recent years was focussed on AACVD-based nanoneedle growth, whereby the growth of one dimensional structures and fabrication of the gas sensor is in-situ using one single step.

3. Chemical Vapour Deposition (CVD) techniques for development of active sensing material for gas sensors applications

3.1. CVD basic principles

CVD is a widely used material-processing technology. The majority of its applications involve applying solid thin-film coatings to the surface, but it is also used to produce high-purity bulk materials and powders, as well as fabricating composite materials. It is an extremely versatile process that can be used to process almost any metallic or ceramic compound. Some of these include: elements, metals and alloys, carbides, nitrides, borides, oxides, intermetallic compounds [136].

CVD methods became popular and useful for deposition of layers in the last twenty years. Nowadays, they are used in a wide range of applications [137, 138]:

- (1) Coatings – coatings for a variety of applications such as wear and corrosion resistance, high temperature and erosion protection and combinations thereof;
- (2) Semiconductors and related devices – integrated circuits, gas sensors and optoelectronic devices;
- (3) Dense structural parts – components that are difficult or uneconomical to produce using conventional fabrication techniques;
- (4) Optical fibres – application for telecommunications;

- (5) Composites – production of ceramic matrix composites;
- (6) Powder production – production of novel powders and fibres;
- (7) Catalysts – coating of fine-porosity carbon;
- (8) Nanomachines – application in silicon microfabrication technology.

In general, the CVD process involves deposition of solid materials from a gaseous phase and consist of the following key steps [137]:

- (1) Generation of active gaseous reactant species;
- (2) Transport of the gaseous species into the reaction chamber;
- (3) Gaseous reactants undergo gas phase reactions forming intermediate species:

(a) homogeneous gas phase reaction can occur at a high temperature above the decomposition temperatures of intermediate species inside the reactor. The intermediate species undergo subsequent decomposition and/or chemical reaction, forming powder and volatile by-products in the gas phase. The powder will be collected on the substrate surface and may act as a crystallisation centre. The deposited film may have poor adhesion;

(b) diffusion/convection of the intermediate species across the boundary layer occurs at temperatures below the dissociation of the intermediate phase. These intermediate species subsequently undergo steps (4)–(7).

(4) Absorption of gaseous reactants onto the heated substrate, and the heterogeneous reaction occurs at the gas–solid interface (i.e. heated substrate) which produces the deposit and by-product species;

(5) The deposits will diffuse along the heated substrate surface forming the crystallisation centre and growth of the film;

(6) Gaseous by-products are removed from the boundary layer through diffusion or convection;

(7) The unreacted gaseous precursors and by-products will be transported away from the deposition chamber.

Figure II.9 represents a schematic illustration of the key CVD steps during deposition. The generated chemical reaction results in a formation of film on a heated substrate surface. For the deposition of denser films and coatings, the process

conditions are tailored to favour the heterogeneous reaction. Whereas a combination of heterogeneous and homogenous gas phase reaction is preferred for the deposition of porous coatings [137].

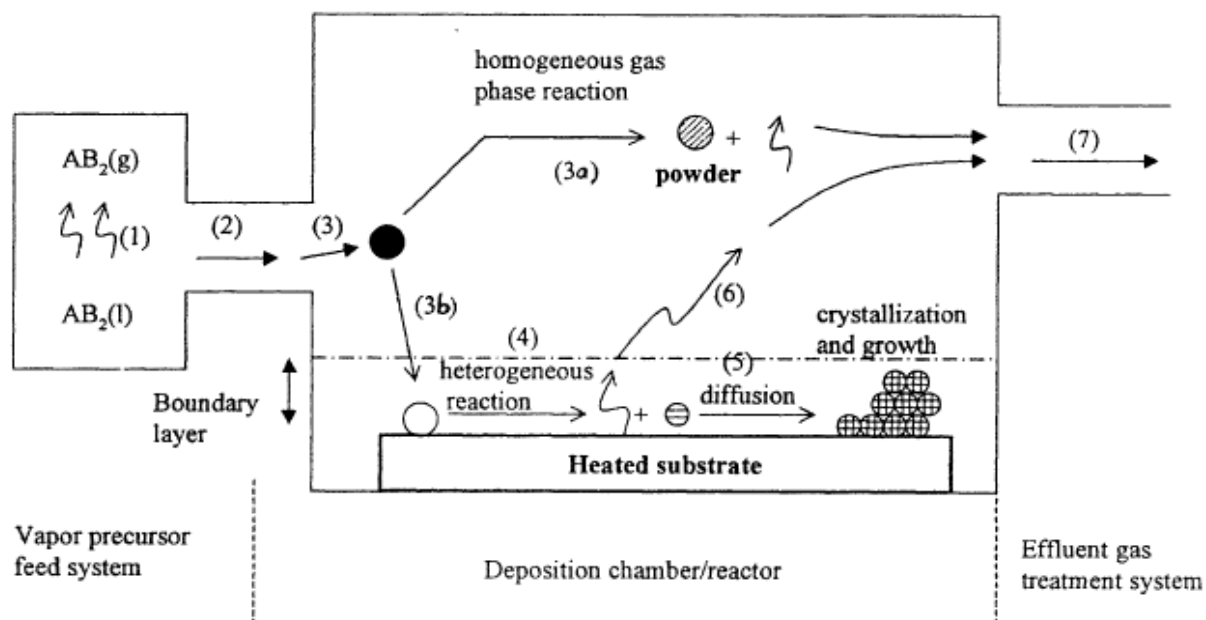


Figure II.9: A schematic illustration of the key CVD steps during deposition [137]

The structures grown by CVD technique are related to deposition conditions used. The efficiency of this complex process primarily depends on appropriate contact between the reactive gas phase and the solid particles. It is possible to control the nature of CVD structure by the deposition parameters such as temperature, pressure, precursor, solvent and the selection of the CVD reaction method. During the CVD, the growth rate of the film is limited by either surface reaction kinetics, mass transport (diffusion) of precursors to the substrate or the feed rate of the precursors [139].

Surface reaction controls the rate when growth occurs at the lower temperatures (where the reaction occurs slowly) and also dominates at lower pressures (where the boundary layer is thin and reactants easily diffused to the surface), see Figure II.10.a. Since reactants easily diffuse through the boundary layer, the amount of reactant at the surface is independent of reactor's pressure. Therefore, it is the reactions and motions of the precursors adsorbed on the surface, which will determine the overall growth rate of the film.

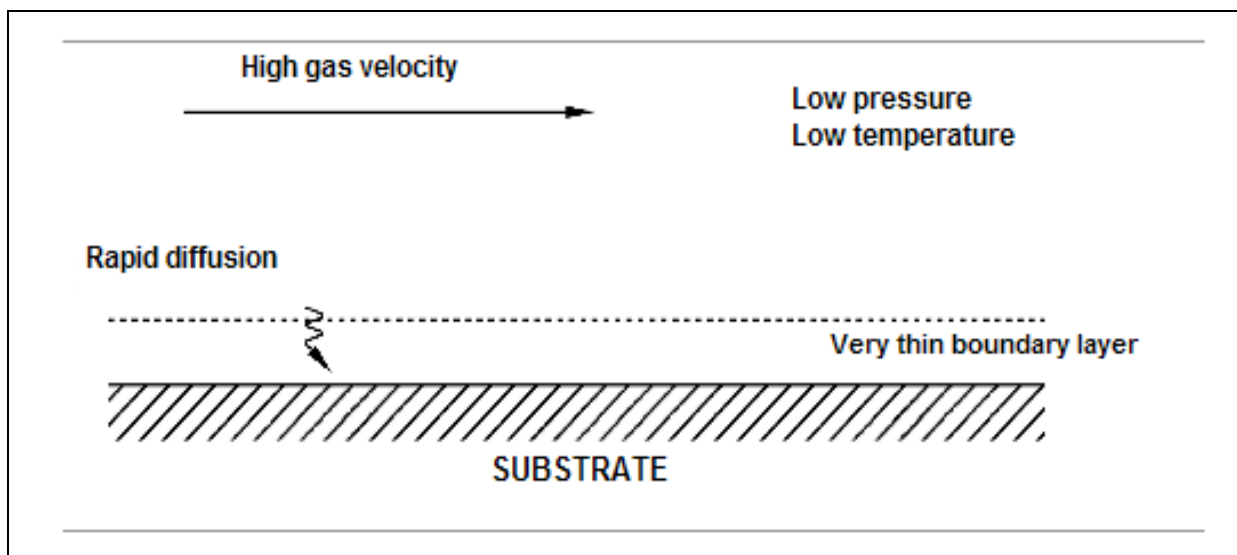


Figure II.10.a: Surface reaction limited growth in CVD [139]

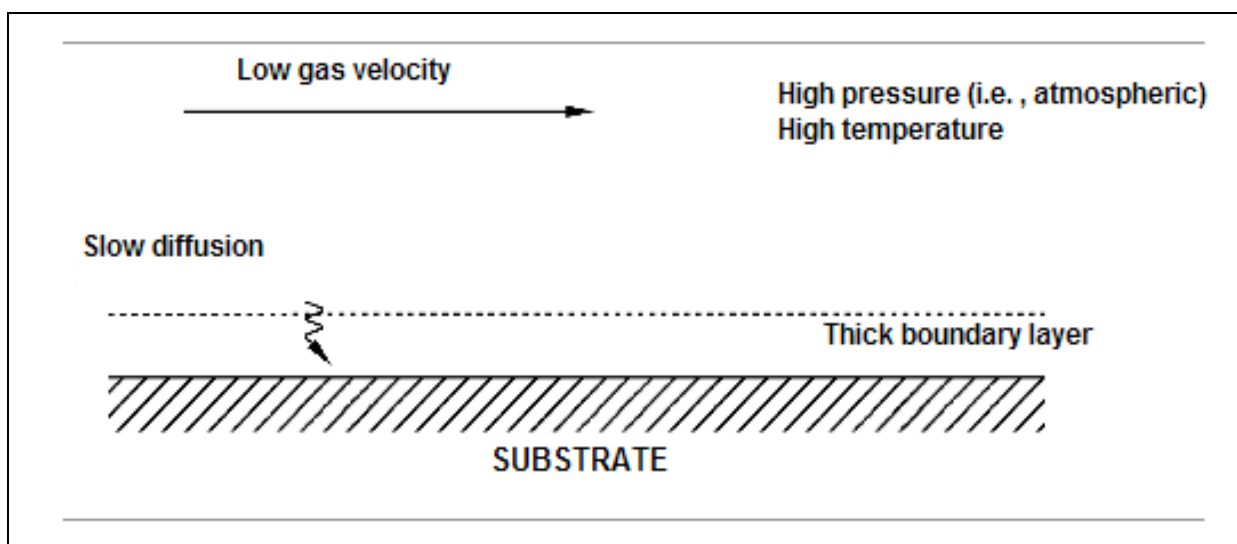


Figure II.10.b: Mass transport limited growth in CVD [139]

A deposition limited by mass transport is controlled by the diffusion of reactants through the boundary layer and diffusion of by-products out of the boundary layer. Mass transport limits reactions when the temperature and pressure are high. These conditions increase the thickness of the boundary layer and make it harder for gases to diffuse through (Figure II.10.b). In addition, decomposition of the reactants is typically quicker since the substrate is at a higher temperature. Mass transport limits reactions at higher temperatures so that growth rate increases with partial pressures of reactants, but is constant with the temperature.

The feed rate limits the deposition when nearly all the reactant is consumed in the chamber. Furthermore, the feed rate is more important for a hot wall reactor since

the heated walls will decompose a large amount of the precursor. Cold wall reactors tend to have higher deposition rates since the reactants are not depleted by the walls. Feed rate limited reactions are independent of the temperature, since it is the rate of gas delivery that is limiting the reaction.

3.2. CVD methods and their applications for nanostructured gas sensors

CVD is a generic name for a group of vapour-processing-based deposition methods. The variants of CVD-based method differ in processes used, architecture of the reactor chamber, heating method, pressure and temperature ranges, type and transport of the precursor-solvent solution. On the other hand, the kinetics of nucleation and growth of the materials and thickness of the films are influenced by the deposition conditions and concentration of reactive species. In general, the right choice of deposition technique can influence the sensing properties of the gas sensors devices. The conventional CVD processes are based on thermally activated CVD, which uses inorganic precursor sources.

The deposition process is initiated by thermal energy and can occur at atmospheric pressure, low pressure or ultrahigh vacuum. The deposition often requires relatively high temperatures (typically 500–1400 °C) depending on the type of inorganic precursor (e.g. halides, hydrides, etc.) used. The other variants of CVD may require special reactor at lower pressure (typically 1.3–1333 Pa) to generate the plasma (PECVD) or the chemical reaction will occur only on the base of the metal-organic precursor (MOCVD). The other variants like Aerosol Assisted CVD (AACVD), Atmospheric Pressure CVD (APCVD) and Low Pressure CVD (LPCVD) are more flexible and can be performed at atmospheric or reduced pressure. Still, the main difference between them is the value of the pressure and the type of the reactor used.

While the sophisticated reactor is required for APCVD and LPCVD, where deposition occurs at atmospheric or low pressure, for AACVD no sophisticated reactor is needed and deposition can occur at atmospheric pressure only. In addition to that, emerging low cost, non-vacuum CVD-based techniques (e.g. AACVD and Flame Assisted CVD) have the potential to be scaled up for large area or mass production [137]. Table II.9 provides a summary of variants of CVD for the deposition of the films and the coatings, their special features and distinctive advantages, which provide the motivation for their development.

Table II.9: Comparison of different variants of CVD [137] (part 1)

Variants of CVD	Special features	Distinctive advantages
Plasma Enhanced CVD (PECVD)	<p>Uses plasma to ionise and dissociate gases as well as to provide a substrate heating source.</p> <p>Requires vacuum and more complex reactor for the generation of plasma.</p>	<p>Lower deposition temperature and enhanced deposition rate.</p> <p>Enables the deposition of a wider choice of films (e.g. diamond, cubic BN, etc.) that are difficult to be synthesised using conventional CVD or PVD techniques.</p>
Photo Assisted CVD (PACVD)	<p>Uses light as a heating source (e.g. arc lamp, CO₂ lasers, Nd-YAG lasers, excimer lasers and argon ion lasers).</p>	<p>Lower deposition temperature and enhanced deposition rate.</p> <p>Enables localised or selected area deposition.</p> <p>Avoids film damage because of the low excitation energies (typically <5 eV).</p>
Atomic Layer Epitaxy (ALE)	<p>Uses thermal/light source.</p>	<p>Controlled growth of epitaxial films.</p> <p>Monoatomic layer deposition.</p>
Electrochemical Vapour Deposition (EVD)	<p>Involves a two-stage process:</p> <ol style="list-style-type: none"> 1. pore closure by CVD, 2. oxide scale growth by EVD, where <p>- metal and oxygen source precursors are introduced to the opposite sides of the porous substrate and separated by the reaction product</p> <p>- deposited materials must possess some ionic and electronic conductivity in order for the growth of the gas tight film to proceed</p>	<p>Enables the deposition of dense ionic or electronic conducting oxide films onto porous substrates that cannot be achieved using conventional CVD and other vapour processing techniques.</p>
Metalorganic CVD (MOCVD)	<p>Uses metal-organic as a precursor source.</p>	<p>Lower deposition temperature.</p>

Table II.9: Comparison of different variants of CVD [137] (part 2)

Variants of CVD	Special features	Distinctive advantages
Pulsed Injection MOCVD (PI MOCVD)	Uses single metal-organic liquid precursor source and a special injector/evaporator for the generation of the vapour precursor.	Fast evaporation of the precursor and a shorter delivery time of the vapour precursor to the reaction zone, and higher growth rate (mm/s). Precise control of the coating thickness, stoichiometry and growth rate for the synthesis of superlattice and multilayer thin films with complex stacking at the nm scale level.
Flame Assisted CVD (e.g. FAVD and CCVD)	Uses flame as the heating source. Performs in an open atmosphere for the oxide deposition.	Low cost. Fast evaporation of the precursor and a shorter delivery time of the vapour precursor to the reaction zone, and the higher growth rate (mm/s).
Aerosol Assisted CVD (AACVD) Pyrosol Ultrasonic generator	Performs in an open atmosphere for the oxide deposition. Generates aerosol precursor using: - ultrasonic generator - electrostatic spraying - electrostatic aerosol generator High deposition efficiency.	Fast evaporation of the precursor and relatively shorter delivery time of the vapour precursor to the reaction zone, and higher deposition rate. Low cost. Thin or thick films.
Chemical Vapour Infiltration (CVI)	Involves the diffusion and infiltration of gaseous reactants through the porous fibre preform where the gaseous reactants undergo decomposition and chemical reaction to deposit the ceramic matrix material on the surface of the fibres in the preform.	Enables the densification of the porous ceramic preform with little thermal, chemical or mechanical damage to the fragile reinforcing fibres as compared to the conventional densification and hot pressing methods. A commercial method for the manufacturing of the ceramic matrix material made of ceramic fibre reinforced composites.

CVD of nanostructured materials in the form of different nanostructures has found technological applications in areas such as electronics, magnetism, optics, energy storage, electrochemistry and biomedical sciences. CVD technique involves chemical decomposition or chemical reactions in the formation of nanostructure materials or in some cases nanostructures are formed by the use of catalyst through the vapour-liquid-solid mechanism. CVD was used to synthesize metal-oxide nanoneedles, nanowires, nanotubes, nanorods, etc. as well for large area arrays of nanostructures by careful control over the supersaturation factor.

In Table II.10 is presented the successful growth of nanostructured metal-oxide materials by the aid of CVD-based methods and their gas sensing properties.

Table II.10: Nanostructured metal-oxide growth *via* CVD-based methods and their gas sensing properties

CVD variant	Active material	Form of the nanostructure	Target gas	Reference
Hot-Wire CVD	WO ₃ MoO ₃	nanorods nanotubes	N/A	[140]
PECVD	SnO ₂	nanorods	NH ₃ CH ₃ OH	[141]
PECVD	SnO ₂	nanocolumn arrays	CO H ₂	[142]
Wet-Assisted CVD	SnO ₂	nanowires	EtOH H ₂ S	[143]
PECVD	SnO ₂ :Pd	nanorods	H ₂ EtOH CO	[144]
CVD	ZnO	nanorods	O ₃	[145]
PECVD	ZnO	nanorods	CH ₂ O	[146]
CVD	ZnO	nanotetrapods	EtOH	[147]
PECVD	ZnO	nano-assemblies	CO H ₂ CH ₄	[148]
CVD	Cu ₂ O	nanostructures	C ₃ H ₆ O EtOH	[149]
CVD	In ₂ O ₃	nanorods, nanowires and nanoneedles	H ₂	[150]
MOCVD	IrO ₂	nanoblades, layered-columns, nanotubes	propionic acid	[130]
LPCVD	Si	nanowires	smoke and humidity	[151]

3.3. Aerosol-assisted deposition methods – applications for gas sensors

The aerosol-assisted deposition method was first proposed in 1999 as a simple technique for the preparation of dense ceramic films at room temperature [152]. Lately, aerosol has been widely used as a material source for the deposition of thin films [153, 154]. The advantages of using aerosols as a delivery system are relatively low equipment costs and wider options for precursor materials. These open atmosphere processing methods offer advantages of a relatively low processing temperature and a simple and flexible technique for preparing coatings without the use of a sophisticated reactor or a vacuum system. Key process parameters such as deposition temperature, properties of the precursor, etc. can be varied to control the microstructure, porosity, grain size and composition of the coatings and deposits.

The simplest way to generate aerosol droplets is by direct spraying towards the heated substrate or by spray pyrolysis. Aerosol Spray Pyrolysis (ASP), is a non-vacuum technique and relatively easy to scale up for a large-area deposition. However, the disadvantage of ASP methods is that the films obtained often have a porous structure and poor adhesion to the substrate. There are several methods of spraying available in order to generate aerosols with droplet size in the micrometer to sub-micrometer range. Pressure nozzles, both hydraulic and pneumatic, are capable of producing aerosols with droplet size of approximately 10 μm [155]. An ultrasonic nozzle can generate aerosols with droplet size $<5 \mu\text{m}$ [154]. However, both techniques require a large volume of carrier gas (normally $>1 \text{ l/min}$) to deliver the aerosol onto the substrate during film deposition. The large flow of carrier gas results in turbulence near the substrate which will adversely affect the efficiency of deposition and the uniformity of the resultant films.

Flame Assisted Vapour Deposition (FAVD) [156] is another example of aerosol-assisted deposition, which combines spray pyrolysis and flame synthesis techniques. The technique is commonly used commercially for the production of micron or sub-micron size powders or for the fabrication of porous films in a single step deposition. However, it is not widely used for the deposition of uniform thin films or adherent thick films, because of the large temperature fluctuation of the flame source during the deposition process.

On the other hand, AACVD-based processes are variants of conventional CVD processes which use aerosol as a delivery system. It involves the atomization of a liquid

precursor solution into the fine sub-micrometer-sized aerosol droplets that are distributed throughout a gaseous medium. In Figure II.11 a simple scheme is presented related to an AACVD-based process.

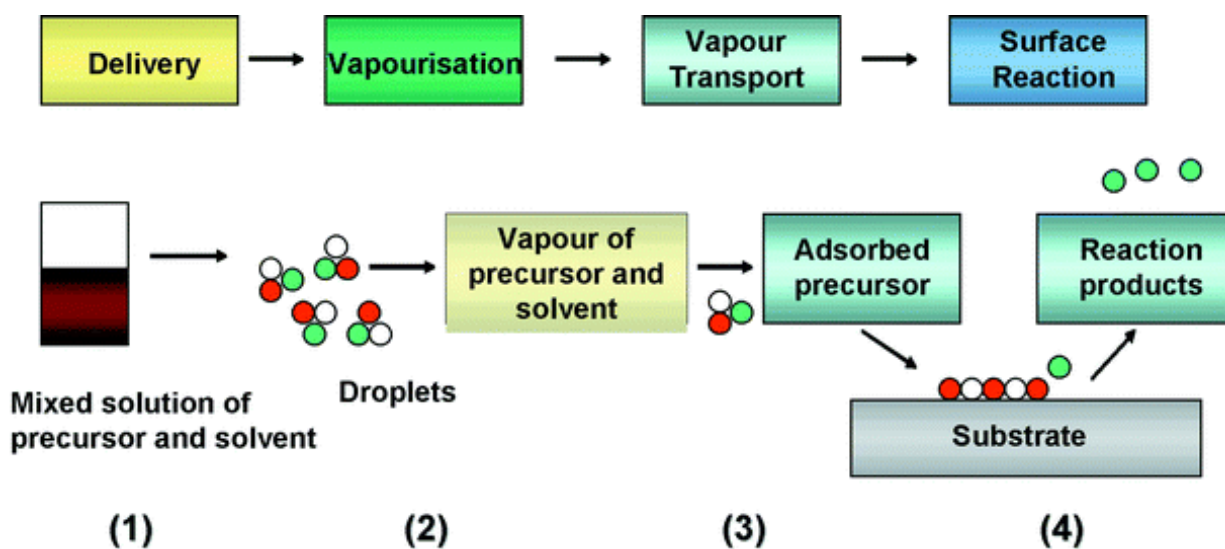


Figure II.11: General schematic representation of the AACVD-based processes

The starting solution (1) can be a pure liquid, single-source precursor or a mixture of several liquid chemicals. Unlike CVD process, in AACVD-based processes, chemical precursors need not necessarily to be volatile or thermally stable for synthesizing the specific materials. On the other hand, the precursors have to be soluble in any solvent from which the aerosol can be generated.

The criteria for the selection of solvents for the atomization process is high solubility of the precursors, low vapour pressure and low viscosity [157]. The atomization or converting into aerosol droplets (2) of the starting precursor solution can be carried out using various types of aerosol generators. Carrier gases are used to assist the generation of aerosol and transport the aerosol to the reaction zone. Argon and nitrogen are the most common inert carrier gases. After atomization, the precursor aerosol is transported to the heated zone (3), where evaporation of solvent and vapourization of precursor take place prior to the major chemical reactions (4). For pure precursor, the vapourization can occur directly from the aerosol droplets. As the vapourization of precursor is the key feature of AACVD, differing from other aerosol processes for material synthesis, the selection of the starting precursor and the control

of processing parameters are very import to ensure the true CVD process. If the aerosol droplets reach the heated substrates before complete evaporation and vapourization, a spray pyrolysis process will take place rather than the true CVD mechanism [158].

In the AACVD-based processes the aerosol can be generated using ultrasonic aerosol generation [159], pneumatic aerosol jet [160], and electrostatic atomization [161, 162]. Ultrasonic aerosol generation is the most common method for the AACVD-based processes. An Ultrasonic Aerosol Assisted CVD (UAACVD) use a piezoelectric transducer placed underneath the precursor solution. When a high-frequency electric field is applied, the transducer vibrates and instigates the formation of a fine droplet with sizes in the range of 1–10 μm . Finer and uniformed droplets are always important for the precise control of processing and synthesis of better quality CVD products.

A pneumatic aerosol jet or Jet Assisted Aerosol CVD (JAACVD) uses the energy of a compressed gas to break up sheets or jets of liquid. Compared to the ultrasonic aerosol generation method, the pneumatic jet normally produces large droplets with a broader distribution.

Electrostatic atomization or Electrostatic Spray Assisted Vapour Deposition (ESAVD) involves spraying atomized precursor droplets across an electric field into a heated substrate. Finer droplet size ($<2 \mu\text{m}$) with mono-dispersed size distribution can be achieved and no carrier gas is needed to transport the aerosol. However, the rate of aerosol generating is very low ($<0.5 \text{ ml/min}$) because of the use of capillary and the process is difficult to scale-up.

The atomized precursor droplets are transported to the heated zone where the evaporation of the solvent and vapourization of the precursor occur. For pure precursor, the vapourization can occur directly from the aerosol droplets. As the vapourization of precursor is the key feature of AACVD, the selection of the starting precursor and the control of processing parameters are very import to ensure a true CVD process.

If the aerosol droplets reach the heated substrates before complete evaporation and vapourization, a spray pyrolysis process will take place rather than the true CVD mechanism. There are four possible deposition mechanisms for fabrication of a film *via* aerosol depending on the deposition/substrate temperature [137]. In Figure II.12 is shown the influence of the temperature on the aerosol-assisted deposition process.

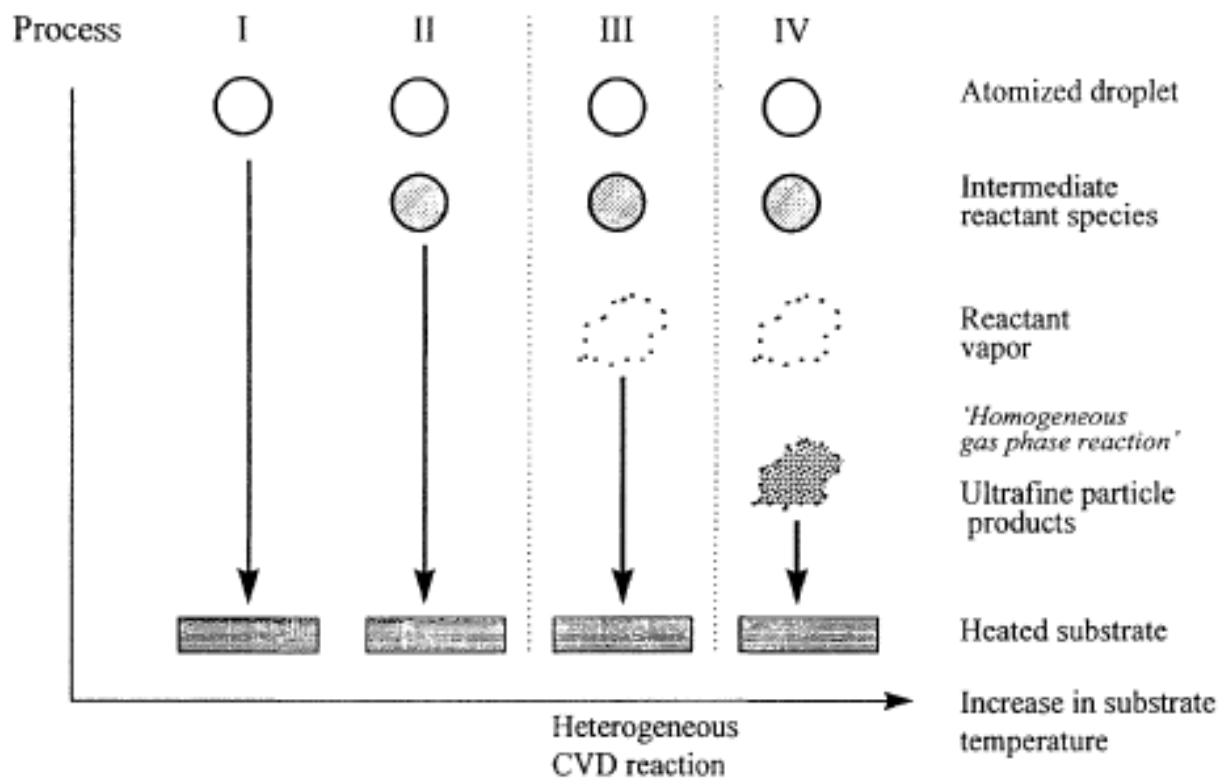


Figure II.12: Influence of the temperature on aerosol-assisted deposition process [137]

Process I: The aerosol precursor droplets are sprayed directly onto the heated substrate, followed by the removal of the solvent through evaporation and decomposition of the precursor to the finished product. Occasionally, the deposited film will require further sintering to achieve a dense crystalline film. Dense thin films (<1 mm) with an ultrafine crystalline structure can be obtained by using this deposition mechanism. In order to obtain a thick film, the process has to be repeated several times, which obviously is a time consuming process. Moreover, as the film thickness increases, the deposited film tends to be porous and cracking of the film can occur because of repeated drying, decomposition and/or sintering procedures. The example of this is Aerosol Spray Pyrolysis (ASP).

Process II: The solvent is evaporated prior to arriving onto the substrate surface, and the precursor precipitate is subsequently deposited onto the heated substrate and decomposed and/or undergoes chemical reactions to yield the desired material. For instance, FACVD method represents this type of a process.

Process III: The solvent is evaporated while approaching the substrate surface. The precursor precipitate formed subsequently undergoes volatilization near the substrate surface and adsorption of the vapour onto the heated substrate surface, followed by the decomposition and/or chemical reaction to yield the desired material. This mechanism is similar to the heterogeneous CVD deposition process, which tends to produce dense film with an excellent coating adhesion.

Process IV: As the deposition/substrate temperature is very high, the decomposition and/or chemical reaction occur in the vapour phase, leading to homogeneous nucleation (similar to the homogeneous CVD reaction). Hence, formation of fine stable particles in the gas phase, which are then deposited onto the heated substrate. The particles are then sintered on the heated substrate, leading to the formation of porous films, with poor adhesion. Alternatively, the powder can be collected in the gas phase for the production of ultrafine powders.

Only processes III and IV are classified as AACVD-based processes. The reason for this is that according to the CVD definition, chemical precursor must be in the form of chemical vapour that undergo chemical reactions (i.e. homogeneous and/or heterogeneous chemical reactions) [137]. Therefore, these factors narrow down various aerosol-assisted-based deposition techniques to a few true chemical vapour deposition processes. Examples of aerosol-assisted chemical vapour deposition for the deposition of high quality films with satisfactory reproducibility are AACVD, JAACVD, and ESAVD.

However, in many aerosol-based processes the evaporation rate of the aerosol droplets has a large influence on the film morphology [163]. Moreover, the difference in the evaporation rates of the aerosol droplets affects the structure and distribution of the nucleation sites in the initial polycrystalline layer [164]. Hence, at higher temperatures the distribution of nucleation sites, which will also depend on the features of the initial polycrystalline layer, could encourage the formation of nanostructured films, as it was demonstrated in this doctoral study.

The recent progress of AACVD-based methods is focused on the deposition and growing of films, coatings, nanowires, nanotubes, etc. Moreover, oxidation can be easily carried out using oxygen from the carrier gas and open air, therefore, the oxide compounds are the most common products of AACVD. This makes the technique well suitable for production of metal-oxide thin films, which find application in gas sensors

fabrication. As it can be noted from the available literature, employment of the aerosol-assisted deposition methods for gas sensors application leads to evenly ordered morphology. In Table II.11 are presented successful synthesizations of a pure and doped metal-oxide active sensing materials by the aid of AACVD-based methods. The obtained active layers mainly consist of spherical particles or in some cases nanofibres or columnar structure. The deposited sensing layers *via* AACVD were tested under the exposure of different oxidizing and reducing gases, and had shown the improvement of their gas sensing properties.

Table II.11: AACVD-based methods of metal-oxide active materials and their gas sensing properties

Aerosol-based method	Active material	Deposited structure (form)	Target gases	Ref.
UAACVD	WO _{3-x}	nanofibres	NO ₂	[119]
UAACVD	WO ₃	spherical grains	NO ₂	[165]
UAACVD	WO ₃	particles	EtOH	[166]
UAACVD	SnO ₂	spherical grains	H ₂ S	[167]
FAVD	SnO ₂	columnar, column-granular granular	EtOH	[113]
FAVD	SnO ₂ :Pd	nanoparticles	CO	[168]
UAACVD	ZnO	granular	EtOH	[169]
UAACVD	ZnO	spherical grains	O _x	[170]
JAACVD	TiO ₂	particles	C ₃ H ₈	[171]
JAACVD	YSZ:CeO ₂	columnar	O ₂	[172]
JAACVD	Fe ₂ O ₃	granular	CH ₄	[173]

Legend: UAACVD – Ultrasonic Aerosol Assisted CVD; FAVD – Flame Assisted Vapour Deposition;
 JAACVD – Jet Assisted Aerosol CVD

AACVD-based method have contributed to a wider use of CVD techniques, and opened up new application areas that might have been previously limited by the cost and the limitations of the conventional CVD technique. Various products, such as oxides, chalcogenides, nitrides, carbons, metals, etc. have been synthesised using AACVD-based processes. AACVD-based methods have good capabilities to produce both simple oxides and multicomponent oxides, which have potential applications in electronics, optics, solid-oxide fuel cells (SOFCs), superconductors, catalysts, biomaterials, etc. As the requirement for volatility and thermal stability of precursors becomes less stringent, new possibilities for production of a high-quality CVD product range by AACVD-based methods will arise.

UNIVERSITAT ROVIRA I VIRGLI
FABRICATION AND GAS SENSING PROPERTIES OF PURE AND AU-FUNCTIONALISED W03 NANONEEDLE-LIKE STRUCTURES,
SYNTHESISED VIA AEROSOL ASSISTED CHEMICAL VAPOUR DEPOSITION METHOD
Toni Stoycheva
DL:T-1803-2011

UNIVERSITAT ROVIRA I VIRGLI
FABRICATION AND GAS SENSING PROPERTIES OF PURE AND AU-FUNCTIONALISED W03 NANONEEDLE-LIKE STRUCTURES,
SYNTHESISED VIA AEROSOL ASSISTED CHEMICAL VAPOUR DEPOSITION METHOD
Toni Stoycheva
DL:T-1803-2011

Experimental methods and material characterization

UNIVERSITAT ROVIRA I VIRGLI

FABRICATION AND GAS SENSING PROPERTIES OF PURE AND AU-FUNCTIONALISED W03 NANONEEDLE-LIKE STRUCTURES,
SYNTHESISED VIA AEROSOL ASSISTED CHEMICAL VAPOUR DEPOSITION METHOD

Toni Stoycheva

DL:T-1803-2011

III. Experimental methods and material characterization

1. Film deposition

In order to fabricate gas sensors, active sensing materials were deposited *via* Aerosol-Assisted Chemical Vapour Deposition (AACVD) on the traditional alumina and microhotplate substrates. Physical characterization of the WO₃ layers deposited onto glass slides or silicon wafer allowed us to establish the optimal deposition conditions for nanoneedle-like structure growth. Subsequently, the active sensing material was deposited onto alumina and microhotplate gas sensor substrates, where the gas sensor characterization study was conducted.

1.1. AACVD system

A cylindrical AACVD reactor chamber was fabricated from stainless steel by our technical services. It consists of two cylindrical pieces, with 95 mm diameter and height of 20 mm each, used as the base (bottom) and the cover (top) of the reactor. A detailed scheme of the reactor chamber is presented in Figure III.1. The bottom part contains a square placement for the substrate with dimensions 10 x 10 mm, two heater cartridges (8mm - diameter, 23,45 W/cm³ WATLOW) parallelly embedded below the substrate placement and a type K thermocouple (1.6 mm - diameter and 152 mm - length, WATLOW) introduced vertically under the substrate placement. The cover was positioned parallel to the substrate and 7 mm above it. The reactor inlet was positioned horizontally, while the exhaust was positioned vertically to the substrate. To control the temperature of the deposition process a PID power controller (EUROTHERM, model 3216) and temperature controller (single-phase thyristor unit, EUROTHERM, model 7100A) were connected to the deposition system. The design of the deposition system was made with the potential to increase the temperature up to 650 °C.

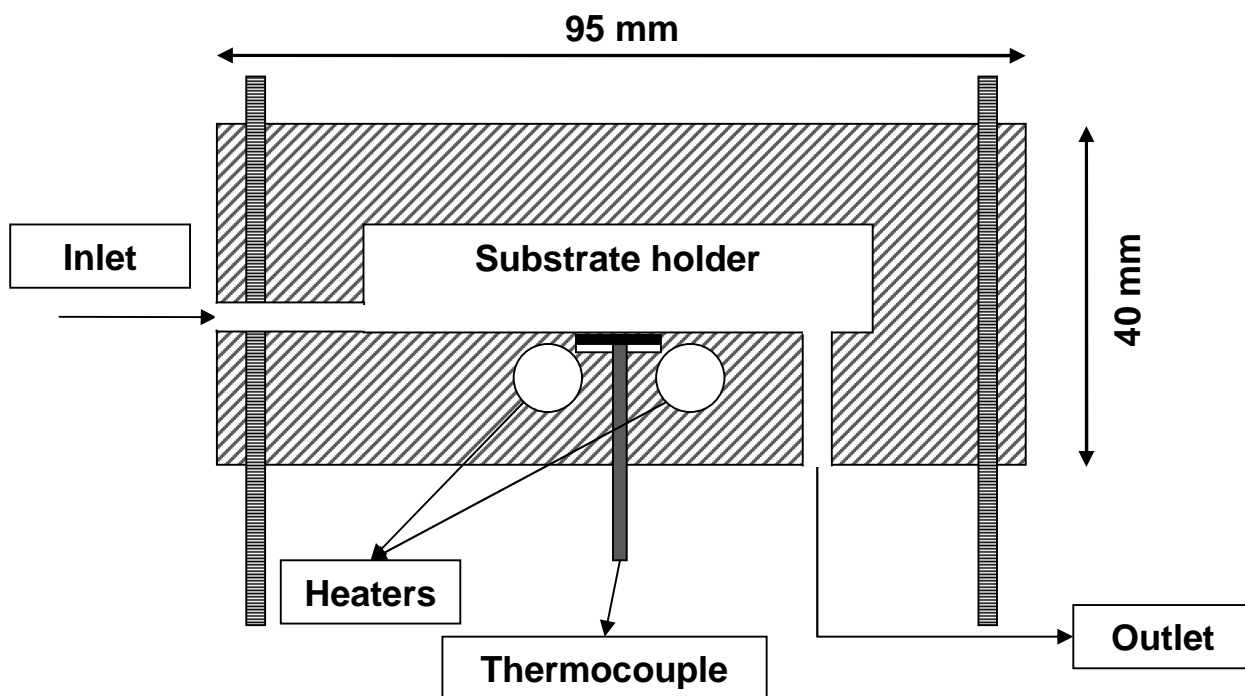


Figure III.1: Detailed schematic drawing of the stainless steel reactor chamber

The generation of the aerosol solution, i.e. a fine mist of liquid droplets, was performed in a commercial piezoelectric ultrasonic atomizer (frequency ~ 1.5 MHz, CHICCO). The formation of an aerosol is required for the delivery process mechanism of a liquid and gas mixture through tube connections. The aerosol mist was formed from a liquid precursor solution contained in a round flask (250 ml capacity, Afora). This flask was immersed in a tank of the ultrasonic atomizer (500 ml capacity), containing water (300 ml).

The bottom of the round flask was placed over the centre of the ultrasonic mist generator, which was the most effective position for the generation of fine aerosols. The produced fine mist was then transported by the aid of the carrier nitrogen gas (N_2 Premier, Carbueros Metálicos) into the heated reactor chamber, which held the sample substrate. The flow-rate (0.5 L/min) of nitrogen gas was controlled by using the needle valve on a gas flow meter (KeyInstruments, model 3A14), with measuring range of up to 5 L/min $\pm 4\%$. All gas-handling lines were made of the PTFE material and have had 3.45 mm internal and 6.35 mm external diameter. All the experiments were performed inside the fume-cupboard. The experimental set up is shown in Figure III.2.

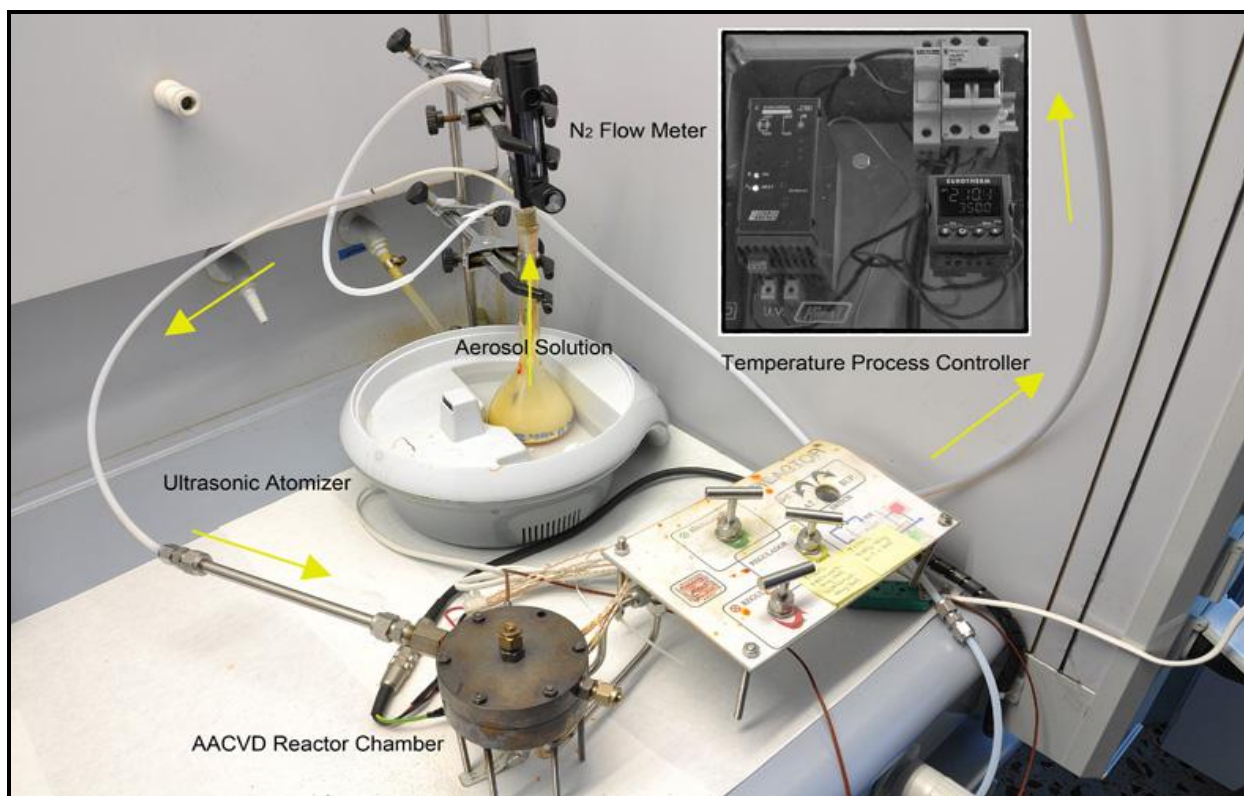


Figure III.2: Experimental set up of the AACVD procedure

1.2. Precursor synthesis - general procedure

1.2.1. Tungsten hexaphenoxide [W(OPh)₆]

Tungsten hexaphenoxide [W(OPh)₆] (Ph = C₆H₅) was synthesised by the reaction of tungsten hexachloride in toluene (250 cm³) and Phenol (14.1 g, 0.150 mmol) under nitrogen atmosphere using standard Schlenk techniques, similar to previously reported [174]. The reaction mixture yielded a dark red solid, which was recrystallised in ether (200 cm³) and washed with ca. 5% NaOH (3x100 cm³) to remove the entire undissolved residue. The ether was then removed in *vacuo* to give a red solid, which was subsequently dissolved in acetonitrile and filtered. Once the reactions were completed, no special handling of the synthesised compounds was required. The detail crystallographic study and element analysis of the precursor was reported in [174, 175]. Crystallographic data for [W(OPh)₆] is given in Table III.1.

The Temperature Gradient Annealing (TGA) method was used for determination of the melting point and the rate of decomposition of the precursor [175]. According to

TGA profile, [W(OPh)₆] undergoes melting at the temperature of approximately 100 °C. The thermal decomposition of the tungsten hexaphenoxide precursor commences at about 150 °C and the rate increases until reaching 325 °C, which corresponds to 90 % of the weight loss. TGA profile for [W(OPh)₆] is presented in Figure III.3.

Table III.1: Crystallographic data parameters [174]

Tungsten hexapheoxide [W(OPh)₆]	
Empirical formula	C ₃₆ H ₃₀ O ₆ W
Formula weight	742.45
Temperature, K	293(2)
Wavelength, Å	0.71069
Crystal system	monoclinic
Space group	P2 ₁ /n
a, Å	13.702(1)
b, Å	16.163(4)
c, Å	13.893(1)
β, °	90.39(1)
Volume, Å ³	3076.7(5)
Z	4
Density (calc), mg/m ³	1.603
Reflections collected	4799
Reflections, <i>I</i> > 2σ (<i>I</i>)	3122
Final R indices [<i>I</i> > 2σ (<i>I</i>)]	R ₁ = 0.0392, wR ₂ = 0.0952

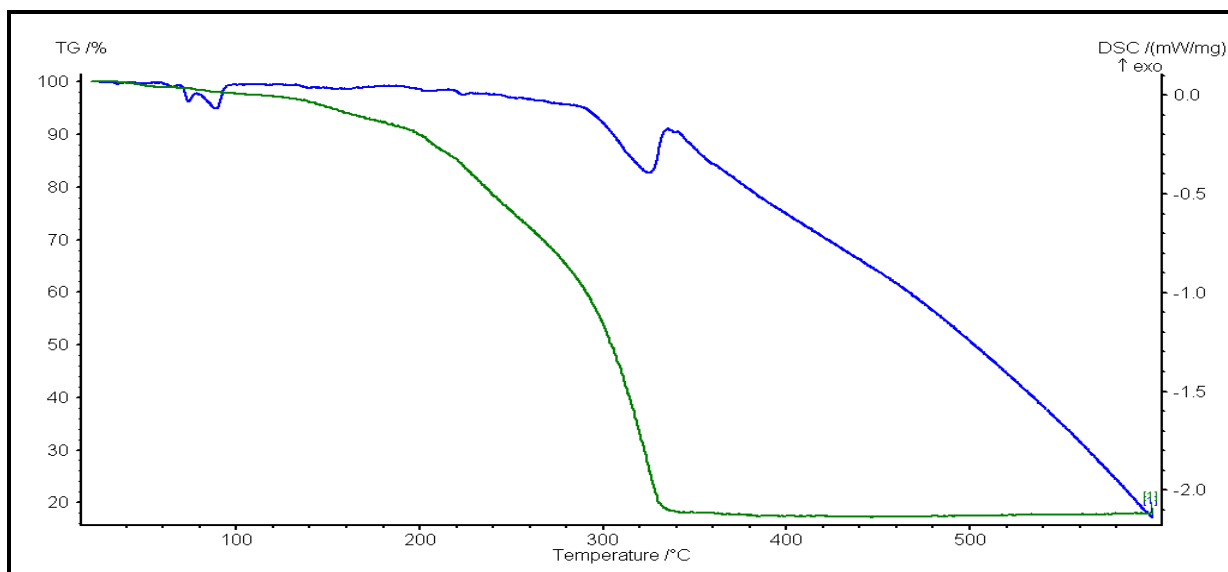


Figure III.3 TGA profile for [W(OPh)₆] [175]

The precursor possessed high solubility in a typical organic solvent such as acetone or toluene, but was not soluble in methanol. This precursor was synthesised in the Department of Chemistry, University College London, UK.

1.2.2. Synthesis of tin complexes [Sn(18-Cr-6)Cl₄] and [Sn(H₂O)₂Cl₄](18-Cr-6)

Tin complex compounds I [Sn(18-Cr-6)Cl₄] and II [Sn(H₂O)₂Cl₄](18-Cr-6) were synthesised from the reaction of 18-Crown-6 (10 % excess) (99 %, Fluka) in a 0.1 M aqueous solution of hydrochloric acid (reagent grade). The successive addition of SnCl₂ · 2H₂O (high-purity grade), acetylacetone (analytical grade) and diethyl ether (analytical grade) to the reaction mixture resulted in a white flaky precipitate. The precipitate was separated by filtration and dried in air. The starting molar ratio of the reactants 18C6 : SnCl₂ · 2H₂O : HC₅H₇O₂ was 1.1 : 1 : 2. The product obtained was a dense white powder that was sublimed under reduced pressure (10 ± 1 Pa) and at temperature of 90 – 100°C. The elemental analysis of the precursors is reported in [176]. The experimental crystallographic data for the tin compounds I and II was determined and the results are presented in Table III.2.

These two tin precursors possessed high solubility in an organic solvent methanol, but they were not soluble in other typical organic solvent used, such as toluene or acetone.

Table III.2: Crystallographic data parameters [176]

	Tin complex I	Tin complex II
Empirical formula	SnCl ₄ O ₈ C ₁₂ H ₂₈	SnCl ₄ O ₁₀ C ₁₂ H ₃₂
Colour	Colourless	colourless
Formula weight	556.8	596.8
Crystal system	Orthorhombic	orthorhombic
Space group	<i>Cmca</i>	<i>Pna21</i>
a, Å	16.871(1)	14.206(2)
b, Å	7.7305(7)	20.376(3)
c, Å	16.939(1)	8.319(1)
Volume, Å ³	2209.2(3)	2408.0(6)
Z	4	4
Density (calc), g/m ³	1.674	1.646
Reflections collected	11756	20508
Final R indices [<i>I</i> >2σ(<i>I</i>)]	R ₁ =0.0453, wR ₂ = 0.1008	R ₁ =0.0276, wR ₂ = 0.0515

The TGA method was used for determination of the melting point and rate of the decomposition of the two tin complexes. According to TGA profile, sublimation onset of [Sn(H₂O)2Cl₄](18-Cr-6) was observed without melting at 150 °C and reached its maximum at 195 °C. On the other hand, [Sn(18-Cr-6)Cl₄] underwent melting at the temperature of 136°C and its evaporation started at 163 °C with a maximum point at 182°C. It was found that the thermal decomposition of the two tin precursors commences at about 190 °C. The rate increases until reaching 280 °C, which corresponds to 72 % of the weight loss. At higher temperatures the decomposition rate slowly decreases until 400 °C, yielding 95 % weight loss. TGA profiles for [Sn(H₂O)2Cl₄](18-Cr-6) and [Sn(18-Cr-6)Cl₄] are presented in Figure III.4.

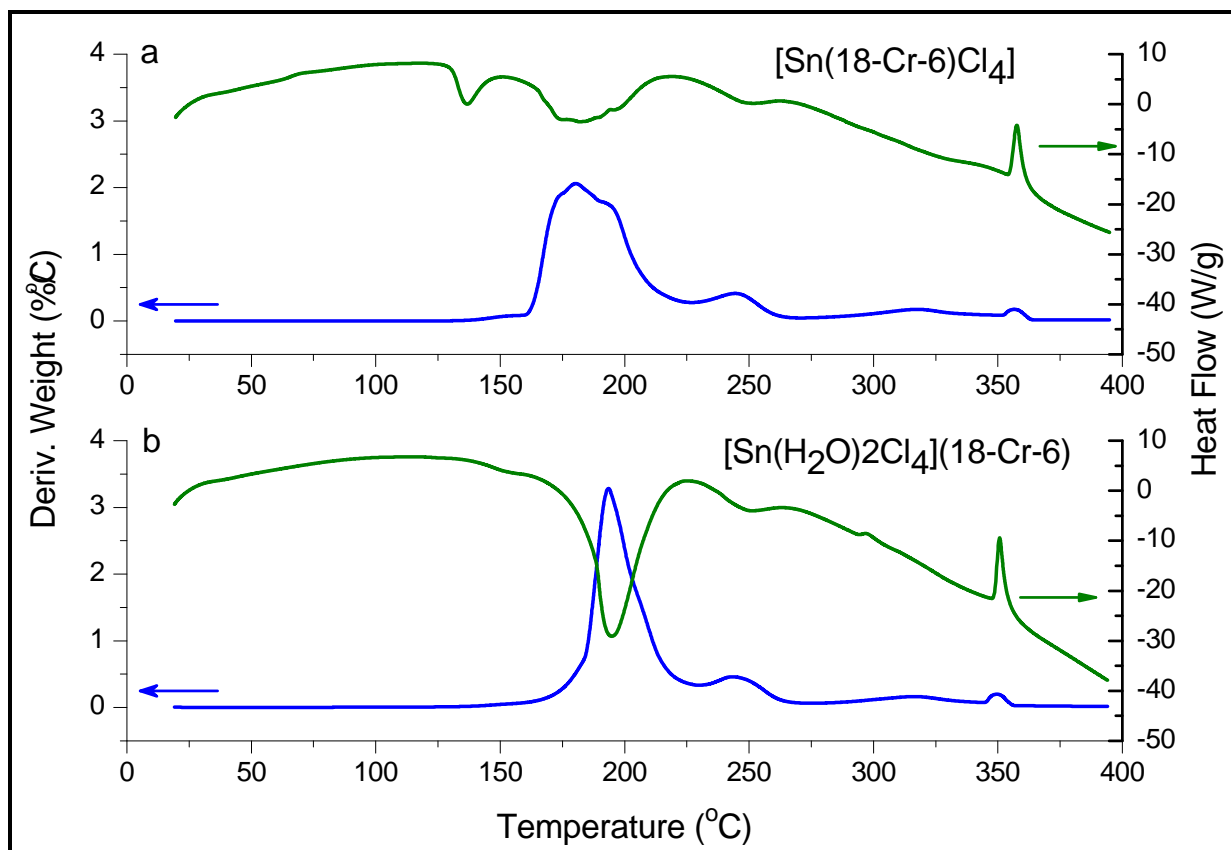


Figure III.4: (a) TGA profile for [Sn(18-Cr-6)Cl₄], (b) TGA profile for [Sn(H₂O)₂Cl₄](18-Cr-6)

These two precursors were synthesised in Kurnakov Institute of General and Inorganic Chemistry, Russian Academy of Sciences, Moscow, Russia and synthesis procedure is described in details in [176].

1.3. Active sensing layer deposition

1.3.1. General procedure

At the beginning of every deposition the substrate was cleaned with ethanol (99.5 %, Scharlau) and then dried with synthetic air (99.99%, Premier). Subsequently, it was placed in the substrate holder into the reactor chamber, which was later securely closed. The deposition process was started after the reactor had reached the adjusted temperature. The nitrogen flow was introduced and then the atomizer was switched on.

The aerosol was generated ultrasonically and nitrogen flow at constant rate of 0.5 l/min was used as a carrier gas. The intensity of the oscillations of the ultrasonic atomizer was set up only once and kept constant for all the depositions.

By introducing nitrogen carrier gas to the atomized precursor solution the aerosol droplets were transported to the heated reaction zone, where the solution underwent evaporation and/or decomposition. The deposition of the active layer continued until all the precursor solution had passed through the reactor. After turning off the atomizer and the temperature process controller, the nitrogen carrier gas was allowed to flow until the deposited layer was cooled down to the room temperature and then the reactor chamber lid was taken off. The substrate was stored and handled in air before it was taken out for further analysis.

The effectiveness of the deposition was tested under various conditions and changes in the solvents used, volume of the liquid precursor solution, deposition temperatures, rate of nitrogen flow and deposition time were investigated. The glass substrate (0.5 mm thick microscopic slide) was used for preliminary study.

The Table III.3 shows the set up values for the AACVD processes running in the cylindrical reactor chamber. Three types of organic solvents were tested as well as some of their mixtures in order to perform nanoneedle-like deposition.

In order to determine the optimal operating conditions for deposition, the influence of the different parameters involved (reactor temperature, gas flow, solvent, etc.) was systematically investigated. Therefore, one parameter was varied while keeping the other factors constant. This approach was repeated with all the parameters, until the optimal conditions for the deposition were found. As a result, homogeneous and nanoneedle-like structured films were deposited.

Table III.3: Tested set up values for an AACVD process running in the cylindrical reactor

Parameter	Value	Units
Temperature of the deposition	250-650	°C
Precursor	50-150	mg
Solvent	10-30	mL
Liquid precursor solution concentration	0.67	Mmol
Carrier gas flow rate	0.5-1	L/min
Deposition time	30-90	min
Atomizer frequency	1.5	MHz

1.3.2. Liquid precursor solution preparation

All chemicals were used as received without further purification. For the preparation of the liquid precursor solution, the solid precursor was dispersed in the solvent or the mixture of solvents. In Table III.4 are presented the organic solvents used for AACVD and some of their properties. The solid precursor was previously weighed by the analytical balances (resolution 0.1 mg, A&D Instruments, model GR-120-EC). The solvent was weighed in a graduated cylinder (graduation 1 mL, Duran). The mixing of the two components was performed in a round volumetric flask.

Table III.4: Properties of the organic solvents used for AACVD deposition of metal-oxide

Solvent	acetone	toluene	methanol
Provider	Sigma-Aldrich	Sigma-Aldrich	Sigma-Aldrich
Purity, %	99,8 %	99,9 %	99,6 %
Molecular formula	C ₃ H ₆ O	C ₇ H ₈	CH ₃ OH
Molar mass	58.08 g/mol	92.14 g/mol	65 g/mol
Boiling point	56 °C (329 K)	110.6 °C (383.8 K)	32.04 °C (338 K)

Tungsten hexaphenoxide [W(OPh)₆] was used as a precursor and dissolved in an organic solvent. The liquid precursor solution concentration was kept equal (0.67 mM) and the solution was prepared before each deposition. The dissolution in any solvent gives a red liquid solution. This set of conditions was used as the basis for the investigation of the effects of varying the substrate temperature.

In Table III.5 are given the deposition conditions and precursor/solvent solution values adjusted for each experiment conducted during this thesis work.

Table III.5: Deposition conditions and precursor/solvent solution values used in each experiment

Deposition, T, °C	Main precursor/solvent mixture		Doping precursor/solvent mixture		Substrate	Deposition time, min
	Precursor, mg	Solvent, mL	HAuCl ₄ 3H ₂ O, mg	methanol, mL		
350	W(OPh) ₆ , 150	A; T; A+T, 30	–	–	glass	30-100
400						
450						
500						
550						
350	W(OPh) ₆ , 100	A+T, 20	–	–	alumina	40-65
500						
350	W(OPh) ₆ , 150	A, 25	10	5	alumina	35-45
350	W(OPh) ₆ , 100	A+T, 20	–	–	microhotplate	30-70
450						
500						
250	tin complex I, 60	M+T, 20	–	–	silicon	20-35
400						
550						
250	tin complex II, 78	M+T, 20	–	–	alumina	45-55
400						
550						
400	tin complex I, 89	M+T, 30	–	–	alumina	45-55
400	tin complex II, 117					

Legend: A – acetone, T – toluene, A+T – (50:50 volume) mixture of acetone and toluene,
 M+T – (50:50 volume) mixture of methanol and toluene, – – not tested

1.3.3. Annealing process

All the as-deposited metal-oxide layers on sensor substrates (alumina and microhotplates) went through the annealing procedure. The full annealing process was performed into a horizontal tube furnace (Carbolite model GHA, max.temp.1200 °C). The temperature of the annealing process was slowly raising with a rate of 20 °C/min until it reached the annealing temperature of 500 °C. This temperature was held for 2 h in order to complete the oxidation process. It was then slowly cooled down until reaching the room temperature with natural convection. The annealing process aims to stabilize the structure and electrical properties.

1.4. Functionalisation of the deposited layers

One way to improve the gas sensor properties is to modify the surface with catalytic metal nanoparticles. Usually, these metal nanoparticles are deposited by sputtering or the thermal evaporation process. In this work, the WO₃ layers deposited onto alumina and microhotplate gas sensor substrates were functionalised by introducing gold nanoparticles, either ex-situ (*via* r.f. magnetron sputtering) or in-situ (co-deposition *via* AACVD) by two types of processing.

1.4.1. R.f. magnetron sputtering (ex-situ)

The sputter deposition is a physical vapour deposition process where surface atoms are physically ejected by momentum transfer from an energetic bombarding particle which is usually a gaseous ion accelerated from plasma. The atomic size particles are ejected from the surface, which is called the "sputtering target". Some examples of the sputtering targets include gold, aluminium, nickel, cobalt, titanium, etc. Sputter deposition is performed in a vacuum and starts when a negative charge is applied to the target material placed in a chamber with the sputtering gas such as argon or oxygen, causing plasma or glow discharge. Positively charged argon or oxygen ions generated in the plasma region are attracted to the negatively biased target plate at a very high speed. The sputtered atoms can ballistically fly from the

target in straight lines and impact energetically on the substrates. This collision creates a momentum transfer and ejects atomic size particles from the target and the nanoparticles are deposited onto the surface of the substrates.

In this work, the modification of the nanostructured WO₃ deposited onto alumina gas sensor substrate was performed in an ESM100 Edwards r.f. magnetron sputtering system with a planar magnetron cathode and a rotatable substrate holder. This surface modification process consisted in introducing of metal nanoparticles is related to the Route 3 of doping strategies described in point 2.3 of the state of the art. The modification of alumina gas sensors was performed in a sputter chamber, where the pressure was pumped down to prescribed process pressure. The air was evacuated from the chamber and 10 sccm of argon (Ar) sputter inert gas was introduced, controlled by the gas flow meter.

The gold nanoparticles were ejected from a planar gold sputtering target with a purity of 99.99 %. The deposition was carried out under the pressure conditions of 5×10^{-3} mbar and the r.f. sputtering power of 10 W. The sputtering time for each doping process was adjusted at 3 min. The substrate temperature was kept constant during the sputtering process. The sputtering conditions were chosen in a manner to avoid the coalescence of gold nanoparticles and the formation of a continuous film on the WO₃ nanostructure.

The sputtering process of the alumina gas sensors was performed by UPC (Technical University of Catalonia), Barcelona, Spain.

1.4.2. Co-deposition *via* AACVD (in-situ)

By using the in-situ AACVD co-deposition technique the synthesis and functionalisation of a WO₃ nanostructured active material was performed in one single step. Surface modification process of this type is related to the Route 5 of doping strategies described in point 2.3 of the state of the art. Similarly to the main active layer deposition process, the kinetics of nucleation and growth of the modified nanostructures are influenced by the deposition temperature and the concentration of reactive species. Thus, affecting the microstructure and the properties of the coatings. By combining the two syntheses together in a single AACVD process the

functionalisation of the metal-oxide structures by co-deposition with metal nanoparticles have been achieved.

The co-deposition process was carried out in the AACVD reactor described previously. Herein, composite films were deposited from a solution of noble metal precursors (gold (III) chloride trihydrate, [HAuCl₄.3H₂O], Sigma-Aldrich, 99.9 %) (0.67 mM) dissolved in methanol (5 mL) mixed with a solution of main precursor [W(OPh)₆] (0.67 mM) dissolved in acetone (25 mL).

2. Material (physical) characterization of the active layers

In this section are presented the material characterization methods used to analyse the surface morphology (needles or grains distribution and size), crystallographic structure, chemical composition and thicknesses of the deposited layers. Each technique is explained in the individual subheading below. The technical characteristics of the techniques used for morphology characterization of the samples are summarised in Table III.5. All the measurements have been gathered at the Scientific Resources Service, University Rovira i Virgili, Tarragona, Spain.

Table III.5: Technical properties of the equipment used for morphology characterization of the samples

Equipment type	ESEM	AFM	TEM
Model	FEI Company, Quanta 600	Agilent Techn. 5500, PicoScan controller	Jeol JEM 1011
Resolution	3.0 nm at 30 kV	atomic	0.5 nm
Magnification	x 20 – 1,500,000	-	x1,200-1,000,000
Accelerating voltage	200 V to 30 kV	-	40 - 100 kV
Sample rotation	360°	-	-
Sample inclination	-15° to +75°	-	-
Microanalysis	EDAX EDS detector	-	-
Type of the Si tip	-	Micromash Inc.	-
Freq. of the Si tip	-	90 KHz	-
Z Range	-	7.5 μm	-

The estimation of the mean diameter of the grains and needles as well as the length of needles was achieved by using iTEM software version 5.1. For all the samples, the estimation of the mean diameter was calculated for a population of fifty measurements. The standard error of the mean diameter of grains and needles (SEM) was calculated using the following expression:

$$SEM = \frac{SD}{\sqrt{n}}, \quad (III.1)$$

where SD is the standard deviation and n the number of elements.

2.1. ESEM – Environmental Scanning Electron Microscopy

ESEM with built-in energy-dispersive X-ray spectroscopy (EDS) analysis capability was used for morphological characterization of the deposited WO₃ layers. The most important parameters for this technique are summarised in Table III.5.

The images were recorded with a large-field gaseous secondary electron detector with enhanced gain preamplifier using 20 kV accelerating voltage at high vacuum mode. The deposited films were evaluated in terms of morphology identification (nanoneedle-like or polycrystalline morphology), concentration and homogeneity across the substrate, upon varying the different experimental conditions in the deposition protocol. It was important to confirm that the active layer is continuous and covers the electrodes well to ensure the correct function of the gas sensors.

Using the same instrument, a measurement of the films thicknesses was conducted. For this purpose, a cross-section of the sensor device was observed. The images were recorded with the 2-segment solid-state backscattered electron detector. Finally, elemental analysis using the Energy Dispersive X-ray (EDX) technique was used for chemical characterization of the deposited nanostructures on the substrate.

2.2. AFM - Atomic Force Microscopy

The AFM is a technique [177] where a sharp tip (probe) is used to scan the specimen surface by measuring forces between the tip (<10 nm) and the surface at a very short distance (0.2-10 nm tip-sample separation). Variations in the tip height above the surface are recorded while the tip is scanned repeatedly across the sample, producing a topographic image of the surface.

The AFM study was performed for the SnO₂ layers deposited onto silicon wafer. The AFM was operated in dynamic (ac) mode, also known as the intermittent contact (tapping mode), where the tip-surface separation is around 0.5-2 nm. The films were scanned by the silicon tip with a nominal radius of curvature up to 10 nm and a frequency up to 90 KHz. The most important AFM parameters are summarised in Table III.5. The estimation of the mean grain size and image processing were achieved by using MetaMorph 6.1 and WSxM 5.0 software respectively.

2.3. TEM - Transmission Electron Microscopy

The TEM is a microscopy technique whereby a beam of electrons is transmitted through an ultra-thin grid with the specimen. The image is formed by the interaction of the electrons transmitted through the specimen and detected by sensor. The introduction of this microscopy technique is presented in [178].

The TEM microscopy technique was used to estimate the needle morphology in the terms of needle thickness and length depending on deposition temperature. The most important TEM parameters are summarised in Table III.5. To prepare the TEM samples, the following procedure was applied. A specimen of the needles deposited on the glass substrate was dispersed in the absolute methanol (99.6 %, Sigma-Aldrich) using ultrasound bath for 30 min. Then, a drop of the needle's suspension was deposited on a ultra-thin copper grid for TEM analysis and left for 20-30 min in air at the room temperature in order to evaporate the solvent. Subsequently, the support was placed into the holder and inserted into the TEM chamber.

2.4. XRD - X-ray Diffraction and crystallite size calculations

The XRD technique is a non-destructive analytical technique which gives us information about the properties of material and the deposited film [179]. By observing the scattered intensity of an X-ray beam hitting a sample as a function of incident angle the information about the crystallographic structure, chemical composition and physical properties was obtained.

The XRD measurements were made using the Bruker-AXS D8-Discover diffractometer equipped with Bragg-Brentano parafocusing geometry and vertical θ -goniometer. The X-ray diffractometer was operated at 40 kV and 40 mA in order to generate CuK α radiation. The General Area Detector Diffraction System (GADDS) detector was 30x30 cm with a 1024x1024 pixel CCD sensor. The X-ray diffraction patterns covering 16-85° 2θ from three different detector positions at a distance of 15 cm from the sample were collected. The exposition time was 120 s per frame and it was chi-integrated to generate the conventional 2θ vs. intensity diffractogram. Identification of the patterns was achieved by comparison of the XRD diffractogram with the ICDD data base (release 2007) using Diffracplus Evaluation software (Bruker 2007).

The crystallite size calculations were performed using Scherrer equation [180]. The study of the preferred orientation was made by Rietveld analysis [181] of the X-ray diffractograms with the aid of software TOPAS [182]. The preferred orientation was corrected with the March-Dollase model [183].

2.5. The other methods

Furthermore, X-ray Photoelectron Spectroscopy (XPS) analysis and High-Resolution Transmission Electron Microscopy (HRTEM) were used for the study of the chemical changes induced at the WO₃ nanoneedle's surface due to the functionalisation with gold metal nanoparticles.

The XPS is a quantitative spectroscopic technique that measures the elemental composition, empirical formula, chemical state and electronic state of the elements that exist within a material. The XPS can be applied to all elements and used to make a

quantitative analysis of solid surfaces, including monolayers. It is employed extensively to study oxidation, adsorption, catalysis, corrosion, diffusion and also thin films and coatings [184]. The fundamental phenomenon underlying the XPS is the photoelectric effect that describes the ejection of electrons from a surface when photons impinge upon it. The kinetic energy (or binding energy) of the ejected electron is characteristic of each element and its chemical state.

The XPS (VERSAPROBE PHI 5000, Physical Electronics), equipped with a Monochromatic Al K X-Ray was used to investigate the chemical composition of the WO₃ nanoneedle samples. The energy resolution was 0.6 eV. In order to compensate the built up charge on the sample surface during the measurements, a dual beam charge neutralization, composed of an electron gun (~1 eV) and the Argon Ion gun (10 eV) was used. All binding energies were calibrated to the C 1s peak at 284.5 eV. To support the interpretation of the XPS spectra, three standard samples (Tungsten (IV) oxide 99.9 %, Tungsten (VI) oxide 99.8 % and Au foil) were purchased from Alfa Aesar and analyzed.

The HRTEM is an imaging mode in which at least two beams pass through the objective lens aperture. The image produced in this way shows the periodicity of the crystal and, for this reason, is often referred to as a *lattice image* [185]. To observe the microstructure of the WO₃ nanoneedles and to investigate the structure of the hybrid Au/WO₃ materials HRTEM (JEOL JEM-2100 F) was used.

The XPS measurements were performed in the Laboratory of the Plasma-Surface Interaction Chemistry, University of Mons, Mons, Belgium, while the HRTEM study was performed in Solid State Physics Department Jožef Stefan Institute, Ljubljana, Slovenia.

3. Gas sensor fabrication

The design and fabrication of the gas sensor substrates consist of several steps: choosing the gas sensors substrate, designing the electrodes and the heater and finally the assembling procedure. Active sensing material deposition for all the samples was conducted before the final assembling procedure.

3.1. Alumina gas sensors

3.1.1. Electrode and heater printing

The traditional alumina gas sensors were made by screen printing technology (Figure III.4). The alumina tile substrate was made from Rubalit 710 (99.6 % Al₂O₃). Each alumina tile had dimension 10x10x0.635 mm and active area for deposition of approximately 0.3 cm². The process of fabrication began with screen printing of inter-digitated Pt electrodes using a Pt ink (platinum conductor paste, Heraeus) onto a blank alumina tiles. The alumina substrates were then fired at high temperature (900 °C) for 2 h. On the backside of the alumina tile, a platinum heater track with gold contacts was added. The alumina substrates are then fired again at high temperature (900 °C) for 2 h to provide Pt heaters. Alumina sensor substrates, ready for active layer deposition, were composed of inter-digitated Pt electrodes on the topside and Pt heater on the backside with ~200 µm inter-electrode gap [186].

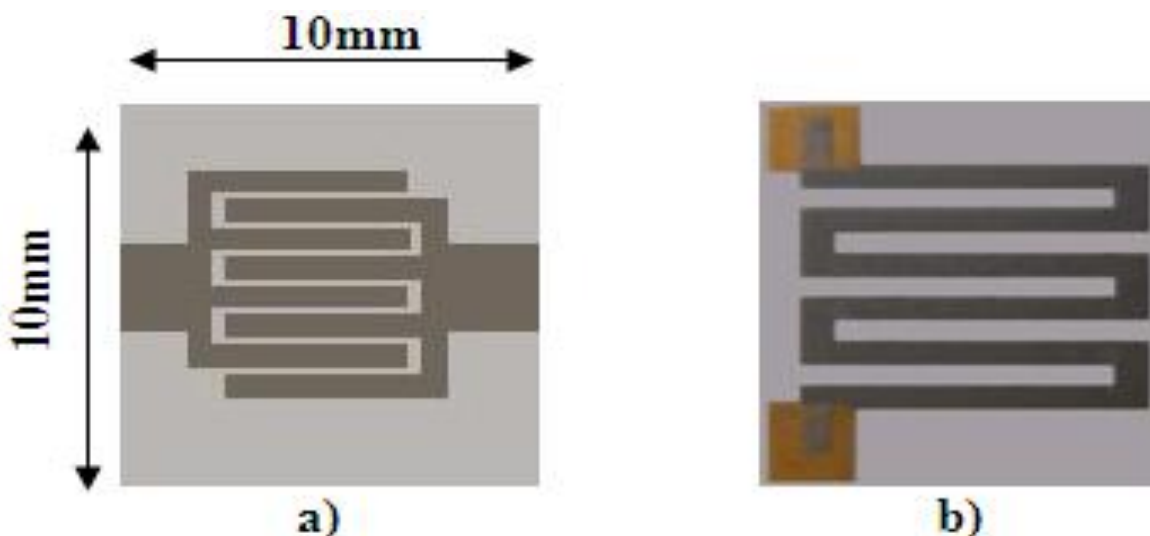


Figure III.4: Front view images of the traditional alumina substrate with screen-printed inter-digitated Pt electrodes on the topside (a) and Pt heater on the backside (b)

3.1.2. Assembling and solder pasting of alumina gas sensors substrates

To assemble alumina gas sensors the printed circuit board (PCB) was used as a holder. Each individual PCB was soldered with one alumina gas sensor substrate that had an active layer previously deposited on it. The image of alumina gas sensor soldered on the PCB holder is shown on Figure III.5. The first step in assembling the gas sensor was to solder two long silver (Ag) leads (0.5 mm, diameter) for the electrodes and two for the heater contacts. Next, to prepare the PCB holder through pins were added to both sides of the holder. With the aid of Ag solder pasting (68%±1%, Heraeus) the pins were connected to the PCB. Finally, the sensor with four long Ag leads was positioned in the centre, holding flat against the PCB and soldered. The excess leads were cut leaving only the solder cone. The solder pasting procedure used in each of the 3 steps consequently was as follow. The Ag liquid solder paste was taken out of the refrigerator and stirred up to make it homogenous. Next, the paste was spread across the contact using a dosimeter. Each place of the connection was covered with a single drop of the Ag solder paste. The drying stove (Memmert) was heated up to 150 °C before placing the gas sensors board in it. The drying procedure continued for 15 min, after that the solder paste turned from dull grey to shiny silver. The solder solidified in few seconds and the gas sensor board was cooled off in the ambient atmosphere. Finally, it was important to ensure that the drying procedure provided a good ohmic contact between the gas sensor and the PCB holder.

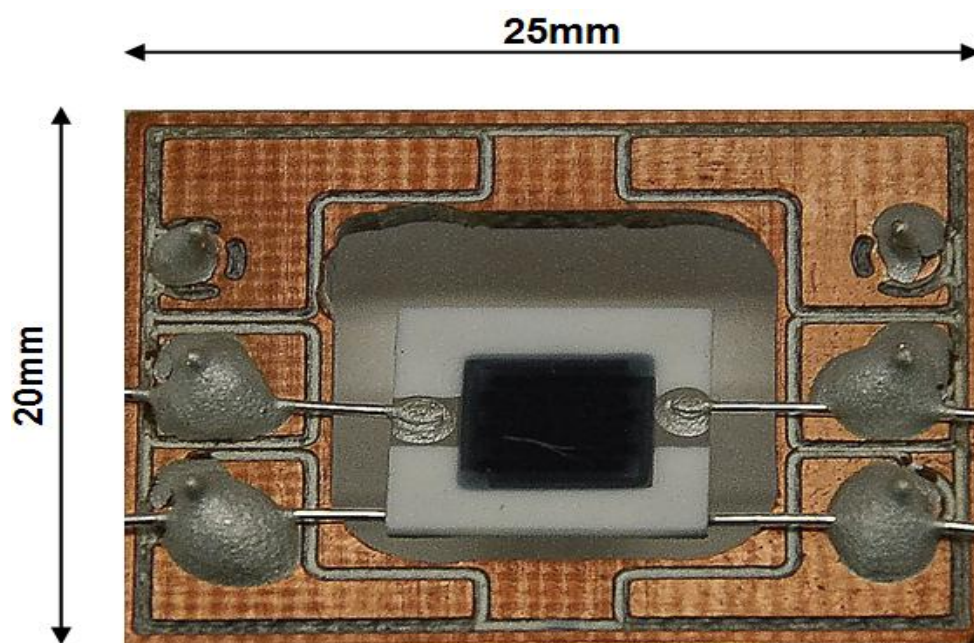


Figure III.5: The front view image of alumina gas sensor soldered onto the PCB holder

3.2. Microhotplate gas sensors

3.2.1. Micromachining substrate technology

The second type of gas sensor substrate used in this doctoral study was realized by using micromachining silicon technology [187]. To fabricate gas sensor substrate, the materials and functional elements have been chosen and designed by CNM (National Center of Microelectronics), Barcelona, Spain. The microhotplate gas sensor substrates were used after checking the deposition conditions onto the glass, silicon and alumina substrates. Microhotplate substrates were used to verify the applicability of the deposition method in micromachined gas sensors and to improve the power consumption properties.

The designed substrates were with low power consumption [$0.20 \text{ mW}/(\text{mm}^2\text{°C})$], well-controlled temperature distribution across the sensing layer and a high mechanical strength. For this purpose, a large membrane area of 6.25 mm^2 , with one microsensor was designed [188, 189]. The devices were fabricated on the double-side polished p-type $\langle 100 \rangle$ silicon substrate $300 \text{ }\mu\text{m}$ thick. First, the membrane layer was deposited and each chip had one membrane. In this work, the closed-membrane-type gas sensor, silicon dioxide and silicon nitride [$\text{SiO}_2/\text{Si}_3\text{N}_4$] were used as a membrane with typical thickness of around $1.2 \text{ }\mu\text{m}$ growth by LPCVD. The heater, deposited on top of the formed membranes, is needed to raise the sensor operation temperature. It was integrated by the vertical approach, where the heater is formed on a different layer. This approach also guarantees appropriate resistance measurements and temperature distributions over the active area.

The heater was made of platinum in an area of 4.5 mm^2 (Figure III.6.b). Next, the SiO_2 layer was deposited to insulate the heater from the electrodes and the active sensing material. Metal electrodes were deposited on the so-called active area and made the measurement of the gas sensitive layer resistance possible. The electrode material used was platinum and the electrode area was 0.25 mm^2 . The dimension of the chip was $8 \text{ mm} \times 8 \text{ mm}$ and membrane area $3 \text{ mm} \times 3 \text{ mm}$ (Figure III.6.a). The sensor had $\sim 50 \text{ }\mu\text{m}$ inter-electrode gap (Figure III.6.c). Finally, the active layer of metal-oxide was deposited onto the thin dielectric membrane with Pt electrodes. The front view images of the microhotplate gas sensor substrate are presented in Figure III.6.

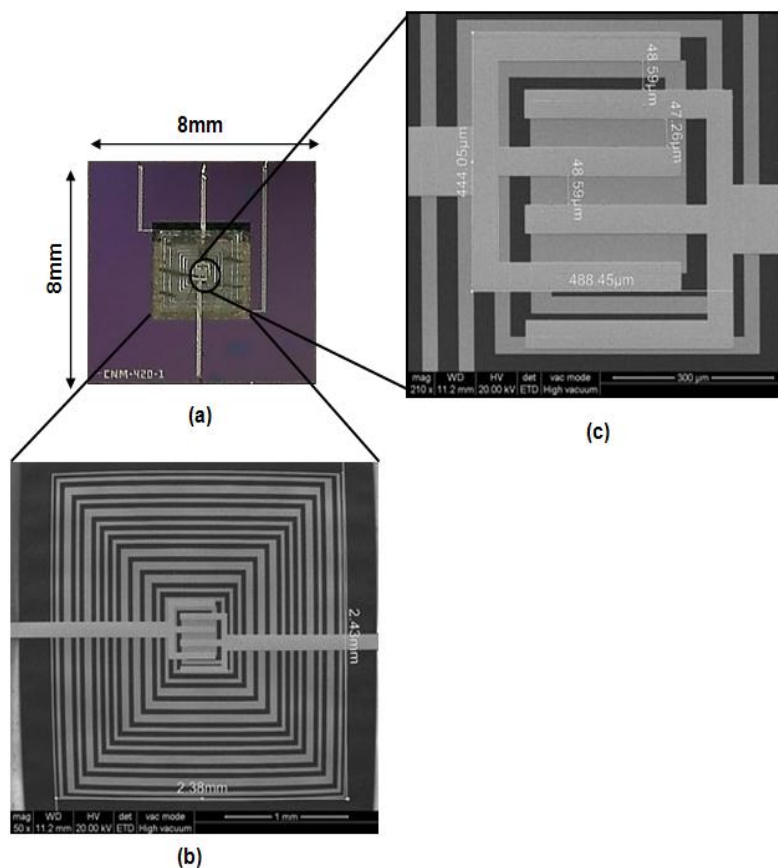


Figure III.6: The front view images of microhotplate gas sensor substrate: microhotplate chip (a), Pt heater (b) and Pt electrodes (c)

3.2.2. Assembling of microhotplate gas sensor substrates

Wire bonding and packaging of the microhotplate gas sensor substrate, was produced by the CNM (National Center of Microelectronics), Barcelona, Spain. Each chip was mounted on a TO-8 package with active layer previously deposited. Aluminium wires, with a diameter of 25 µm, were used for a standard ultrasonic wire bonding. To prevent the membranes from breaking due to air expansion in the cavity below the membranes when the device is heated, the chips were not glued directly to the surface of the metallic package but kept elevated by using two lateral silicon spacers. After this, each microhotplate gas sensor was soldered onto the PCB holder by the procedure described previous in point 3.1.2. The Figure III.7 shows the front view image of microhotplate gas sensor soldered onto the PCB holder.

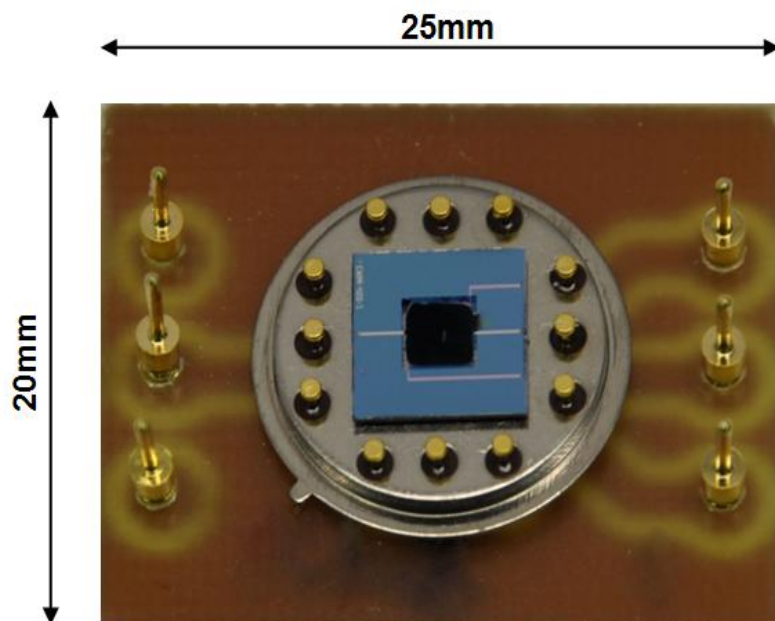


Figure III.7: The front view image of the packed microhotplate gas sensor soldered onto the PCB holder

4. Gas sensors characterization study

The gas sensor characterization was achieved by measuring the change of the electrical resistance of the active layer when the gas sensor was exposed to various concentrations of the test gases and at the different operating temperatures.

4.1. Measuring set up

The computer-controlled characterization system consists of a custom-made gas sensors test chamber, a gas delivery system, an electronic measurement controller and a data acquisition system for sensor response. Each of the components is described in detail below:

1) The test chamber was made from the PTFE material in which the sensor reacts with the gas mixture (toxic gas in dry air). The volume of the test chamber was approximately 280 cm³. The gas stream, coming from the gas mixing set up was led through to a test chamber where 4 samples were located and contacted. The gas was continuously flowing through the chamber with a flow rate of 100 sccm.

2) The gas delivery system included pressure regulators, mass flow controller and required electronics in order to control gas flow inside the test chamber. It was used to control and measure the gas flow and a stream of gas generated with the gas mixing set up. Dry air was chosen as the main gas stream. The variable concentrations of the each gaseous analyte from commercially available bottles (NO₂, EtOH, H₂, CO, H₂S, NH₃, C₆H₆) were obtained by injection of a calibrated concentration into the main gas flow. The concentration was adjusted to desirable levels by a PC using the mass flow controller (Bronkhorst High-Tech V 6.32.0.4).

3) The electronic measurement system, (Keithley Instruments Inc electrometer, model 6517A) with an applied voltage of 5 V, measured the sensor responses while the data acquisition system (A/D converter controlled by a PC) recorded the current changes.

4) The sensor working temperature (up to 400 °C max.) was adjusted by changing the voltage across the sensor heater side by the controlled power supply (Agilent, model N5700). In Table III.6 is presented the range of voltages applied in order to set up the operating temperature. The schematic view of the test set up for the gas sensor characterization is shown in Figure III.8.

Table III.6: Dependence of the operating temperatures on applied voltage for alumina and microhotplate gas sensor substrates

T, °C	Alumina substrate		Microhotplate substrate	
	Voltage, V	Power, mW	Voltage, V	Power, mW
100	2.13	648	13.7	70.3
150	3.15	1249	20.6	152
200	4.17	1956	27.5	255
250	5.19	2739	34.4	375
300	6.20	3566	41.2	509

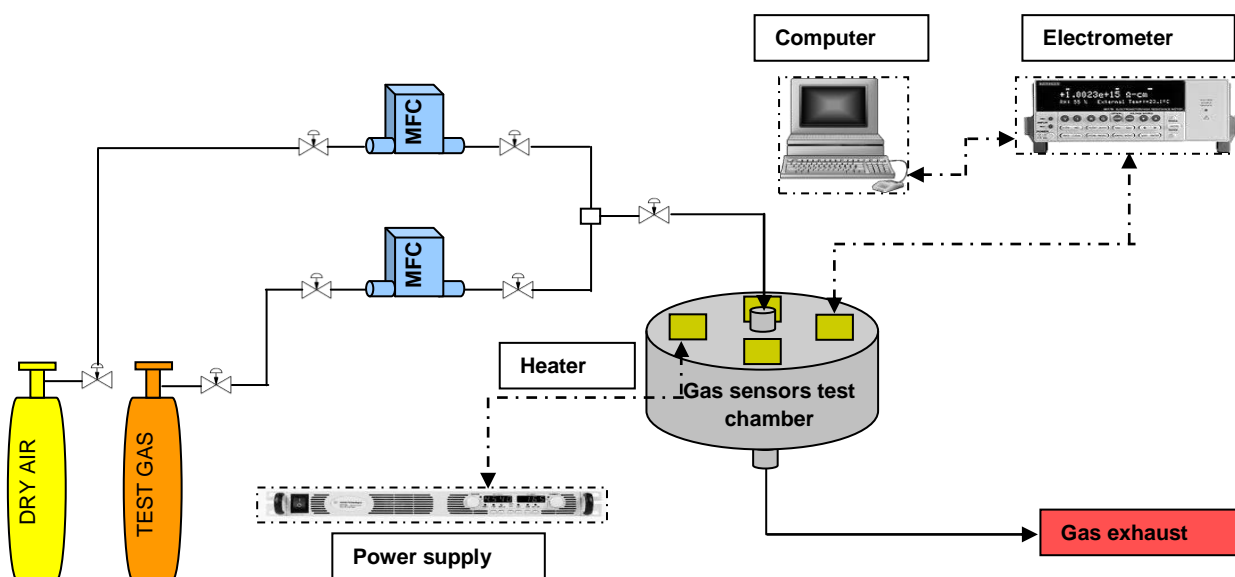


Figure III.8: Measurement gas characterization set up. The electronic measurement system is described for the set of 4 gas sensors

4.2. Target gases

The measurements were performed for pure and Au-functionalised WO₃ active layers deposited onto alumina and microhotplate gas sensor substrates as well as for pure SnO₂ active layers deposited onto alumina gas sensor substrates. In Table III.7 are shown target gases and all concentrations used in this work to test gas sensors. For each experiment, a set of the particular gases and concentrations were chosen according to the sensors to be characterized.

Table III.7: Target gases and their concentrations

Tested gas	Concentration, ppm
Nitrogen dioxide (NO ₂)	1
Ethanol (EtOH)	1.5, 20
Hydrogen (H ₂)	1000
Carbon monoxide (CO)	20, 100
Hydrogen sulfide (H ₂ S)	3
Benzene (C ₆ H ₆)	10

For each gas and concentration the operating temperature was varying from 100 °C to 350 °C with an increment step of 50 °C. The each sensor type was studied and every measurement was repeated 10 times. The gas response magnitude of the sensor S , was determined using one of the following formulas:

$$S = \frac{R_{air}}{R_{gas}} \text{ for oxidizing gases} \quad (\text{III.2})$$

$$S = \frac{R_{gas}}{R_{air}} \text{ for reducing gases} \quad (\text{III.3})$$

The R_{air} is the resistance of the active layer of the measured sensor in dry air and R_{gas} is the resistance of the active layer of the measured sensor in the different concentration of contaminated gas.

UNIVERSITAT ROVIRA I VIRGLI
FABRICATION AND GAS SENSING PROPERTIES OF PURE AND AU-FUNCTIONALISED W03 NANONEEDLE-LIKE STRUCTURES,
SYNTHESISED VIA AEROSOL ASSISTED CHEMICAL VAPOUR DEPOSITION METHOD
Toni Stoycheva
DL:T-1803-2011

**Fabrication and characterization of
intrinsic and gold (Au) functionalised tungsten
trioxide (WO₃) nanostructure-based gas
sensors deposited *via* AACVD method**

UNIVERSITAT ROVIRA I VIRGLI
FABRICATION AND GAS SENSING PROPERTIES OF PURE AND AU-FUNCTIONALISED W03 NANONEEDLE-LIKE STRUCTURES,
SYNTHESISED VIA AEROSOL ASSISTED CHEMICAL VAPOUR DEPOSITION METHOD
Toni Stoycheva
DL:T-1803-2011

IV. Fabrication and characterization of intrinsic and gold (Au) functionalised tungsten trioxide (WO₃) nanostructure-based gas sensors deposited *via* AACVD method

1. Introduction

In this chapter it is discussed the results of the film analysis, sensor fabrication and gas sensing characterization for the intrinsic and Au-functionalised WO₃ sensing active films. In the first stage, it is described the study of optimum deposition conditions used for intrinsic WO₃ nanoneedle growth. After determination of the morphology, two types of alumina gas sensor were fabricated, based on polycrystalline films, with the grain size of ~200-300 nm and on nanostructured films, with non-aligned nanoneedles. Subsequently, Au surface functionalisation study was conducted for the obtained WO₃ nanoneedles ex-situ (*via* r.f. magnetron sputtering) or in-situ (*via* AACVD co-deposition) method. Finally, intrinsic WO₃ nanoneedles and nanoparticles were grown at three different deposition temperatures on microhotplate gas sensor substrates. The experimental conditions used to fabricate and study the gas sensing properties of the films are described in point 4 of the experimental part.

2. Nanostructured WO₃ film deposition

2.1. Film analysis

Depending on the solvent used, a typical deposition lasted between 20 and 110 min. It was found that the solvent used affected the time of the deposition, as well as the adhesion and colour of the deposited WO₃ layers. Table IV.1 summarises some of the results obtained for each solvent. In this doctoral study two types of tungsten precursor were investigated: tungsten hexaperoxide [W(OPh)₆] and tungsten hexacarbonyl [W(CO)₆] (97%, Sigma-Aldrich). Similarly, during the experiments it was found that AACVD reaction of [W(CO)₆] in different solvents results in the formation of polycrystalline films or nanoneedle-like structures, depending on the solvent and the temperature of the deposition as reported in [68]. However, the obtained layers were

less uniformed compared with the layers obtained from the [W(OPh)₆] and the former precursor was not soluble in toluene as the solvent. According to these results, in the following the [W(OPh)₆] was used as the precursor.

Table IV.1: Results obtained with the organic solvents used for AACVD deposition of WO₃ films

Precursor	Solvent	Deposition time for 30 ml of solvent, min	Adhesion properties	Deposition temperature, °C	Colour
[W(OPh) ₆]	acetone	20-30	very good	350	yellow
			good	500	blue
	toluene	90-110	poor	450	black
			poor	500	black
	acetone+toluene (50:50 volume)	50-60	very good	350	yellow
			good	500	blue
	methanol	Not soluble			

The AACVD reaction of [W(OPh)₆] with acetone or mixture of acetone and toluene resulted in the deposition of the adherent films that varied in colour from yellow to dark blue, depending on the deposition temperature. Blue films were grown at the higher temperatures and yellow at the lower temperatures. WO₃ layers deposited from the AACVD reaction of [W(OPh)₆] with toluene needed longer deposition time and showed weaker adherence and darker colour. Previously, it was reported [164] that the yellow WO₃ films are characterized by dense polycrystalline morphology, whereas blue films are characterized by the formation of quasi-one-dimensional structure. Moreover, the decomposition of [W(OPh)₆] at 500 °C in a nitrogen gas stream under AACVD has shown that dark blue films are indicative of reduced tungsten trioxide stoichiometry (WO_{3-x}, x = 0–0.3) and pale yellow films (after annealing at 500 °C in air) are indicative of fully oxidised WO₃, as it was reported in [190].

2.1.1. Morphology

In order to find appropriate conditions for growing nanoneedle-like films *via* AACVD method, variations in the experimental conditions (deposition temperatures and solvents used) have been tested and their effects on the deposited layers have been studied. In Figure IV.1 is shown the effect of varying the deposition temperature of the reaction (in the range from 350 °C to 550 °C with an incremental step of 50 °C) and the solvent used (acetone, toluene or mixture of acetone and toluene), while the other parameters of the deposition were kept constant. It was found, that the increase of the deposition temperature affects the morphology (Table IV.2). These results are in agreement with other reports [68, 159], in which changes were observed in the growth mechanism of WO₃ from different precursors as the function of the lower or the higher temperature. This further suggests that the temperature modulates the type of reaction that precursor undergoes during deposition and thus the growth mechanism and the morphology of the obtained layers.

Thus, when using acetone as the solvent, the formation of the polycrystalline structure was observed at 400 °C and 450 °C, while flower-like nanoneedle structure, similar to [191, 192], was presented at 550 °C (Figure IV.1.a). When using toluene as the solvent, compact agglomerations of nanoneedle-like structures were observed at 450 °C, whereas fine nanoneedles were grown at 550 °C (Figure IV.1.b). The mixture of acetone and toluene as the solvent showed that the polycrystalline structure growth appeared at 350 °C and a mixture of nanotube-like and nanoneedle-like structures at 450 °C. Finally, at 500 °C and 550 °C a higher density of non-aligned nanoneedles was observed (Figure IV.1.c).

Table IV.2: AACVD WO₃ morphology at the range of deposition temperatures using different solvents

Deposition temperature, °C	WO ₃ morphology		
	acetone	toluene	acetone + toluene (50:50 volume)
350	-	-	P
400	P	-	P
450	P	A-NN	NT/NN
500	NN	A-NN	NN
550	F-NN	NN	NN

Legend: P-polycrystalline structure, NT-nanotubes, F-NN-flower-like nanoneedles, A-NN-agglomerations of nanoneedles, NN-nanoneedles

(a) acetone

(b) toluene

(c) acetone + toluene

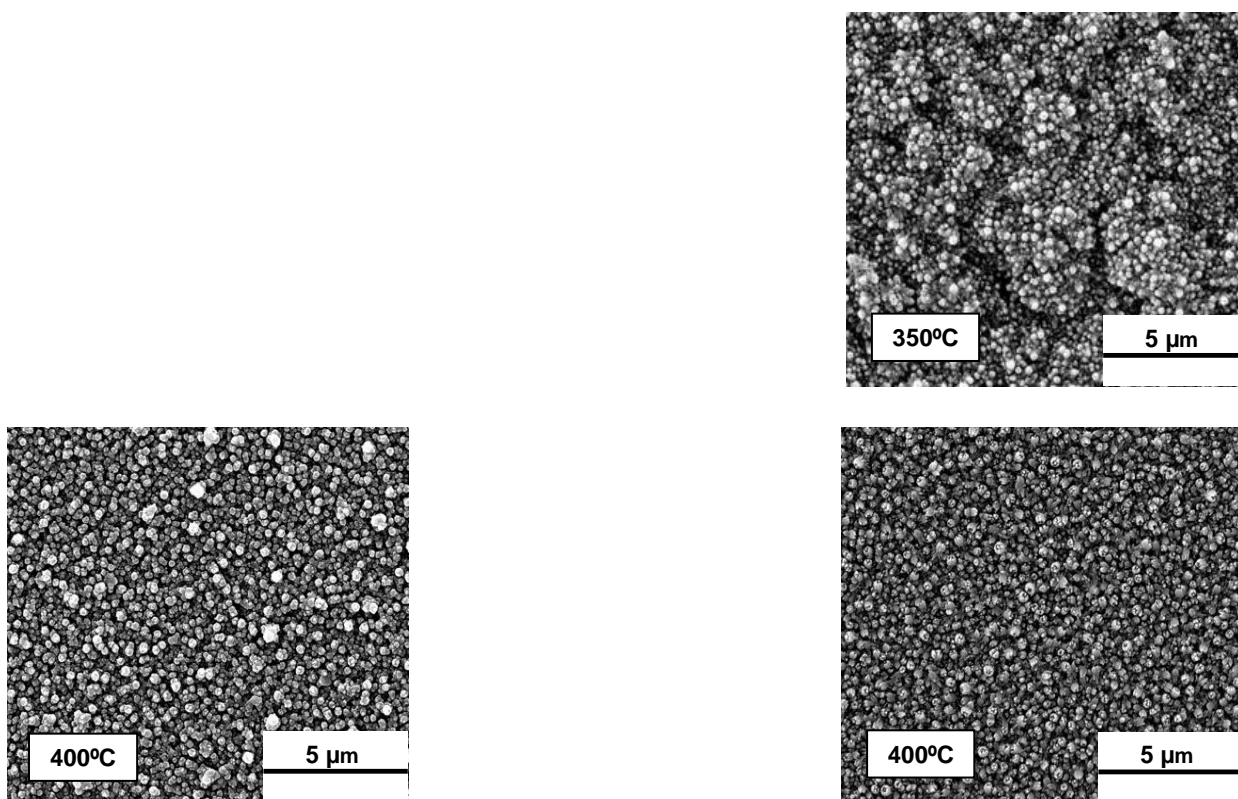


Figure IV.1: ESEM images of WO₃ nanostructures at various deposition temperatures. Depositions were carried out using (a) acetone, (b) toluene and (c) acetone + toluene (50:50 volume) as solvents (part 1)

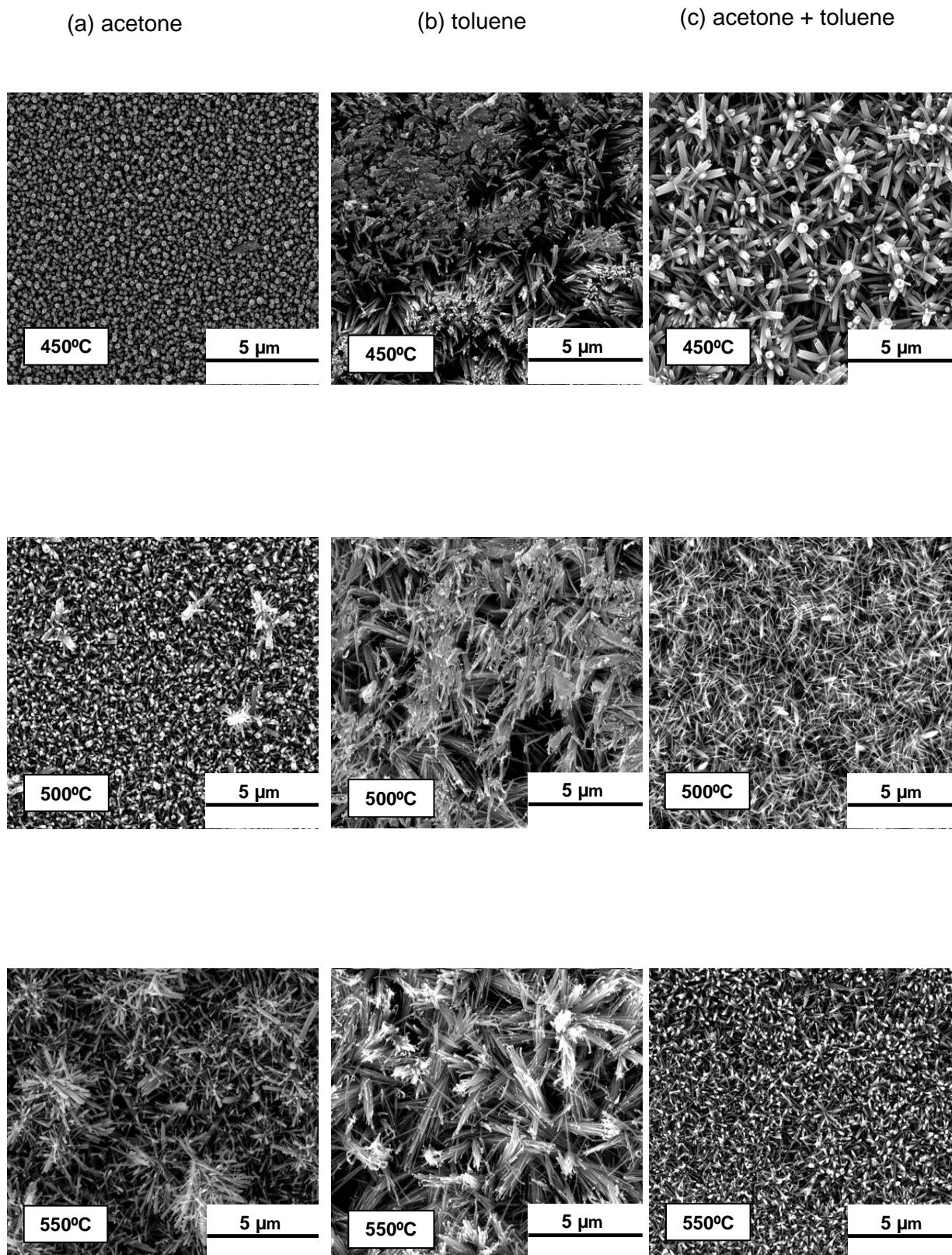


Figure IV.1: ESEM images of WO₃ nanostructures at various deposition temperatures. Depositions were carried out using (a) acetone, (b) toluene and (c) acetone + toluene (50:50 volume) as solvents (part 2)

From our study, it is apparent that the solvent used to dissolve the precursor influences the apparition of the nanoneedle-like structures and the increase of deposition temperature, encourage their formation on the substrate for all tested solvents. At higher temperatures, the distribution of nucleation sites, which will also depend on the features of an initial polycrystalline layer, as stated in [99, 193], can encourage the formation of aligned structures like the nanoneedles that were observed at 500 °C. In some cases their lateral coalescence could form nanotube-like features [194, 195], as observed in films deposited at 450 °C from the mixture of acetone and toluene (Figure IV.1.c). Therefore, it is believed that the growth of different nanostructures could be related to the differences in the initial polycrystalline layer formation mechanism. In [164] it was reported that the difference in the evaporation rates (Figure IV.2) of the aerosol droplets affects the structure and the distribution of nucleation sites in the initial polycrystalline layer. Therefore, the solution evaporation process and its rate could also influence the final morphology [163].

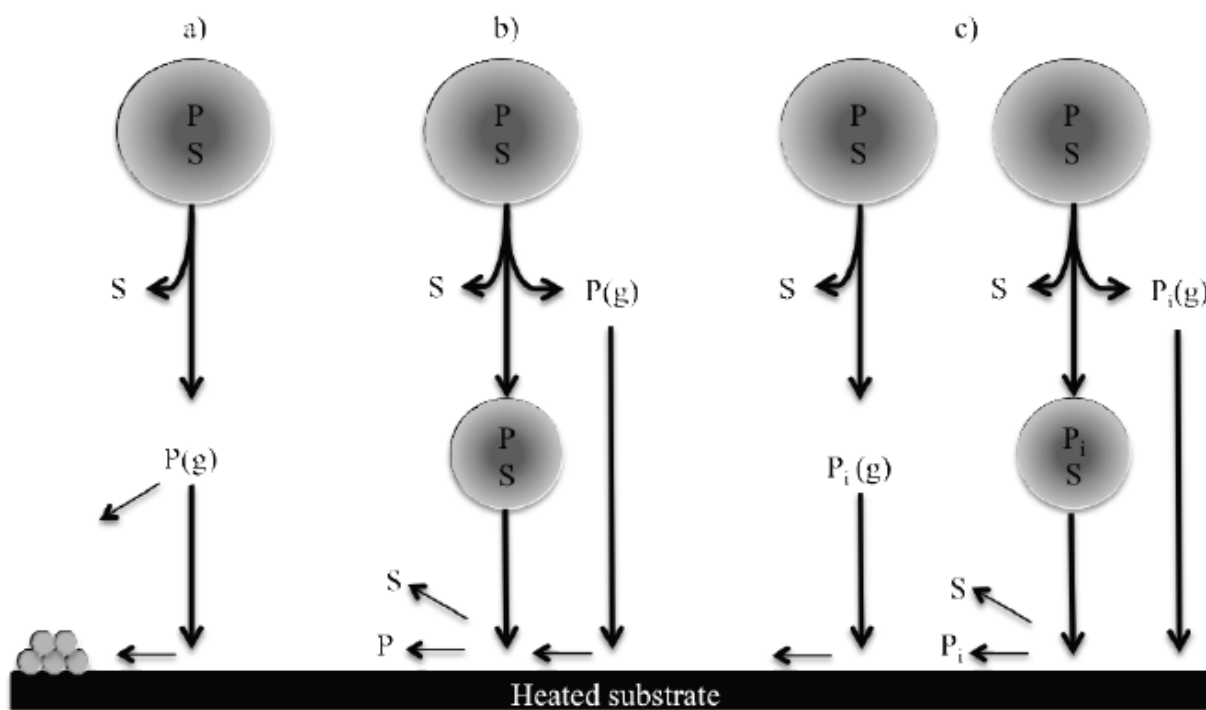


Figure IV.2: Evaporation paths of a droplet in AACVD process: (a) complete, (b) incomplete precursor/solvent evaporation, c) complete and incomplete evaporation with intermediate reactions between solvent and precursor [164]

A further factor, which may also influence the evolution of different nanostructured morphologies from various solvents at the same deposition temperature, is the surface diffusion. It was suggested [164], that the surface diffusion may depend on the characteristics of the initial polycrystalline layer and hence the solvent/precursor evaporation rates, but also on the rate at which the precursor is delivered to the substrate (i.e. deposition time). The deposition time parameter recorded in our experiments showed that the mixture of acetone and toluene solution needed longer deposition time in order to evaporate than the acetone solution, whereas the toluene-based solution needed the longest deposition time. These variations in the deposition time according to the solvent used suggest that this parameter could also play a role in modulation of the resultant film morphology as it was reported in [164].

Cross-section ESEM measurement of the WO₃ nanoneedle-like layers was made for samples deposited onto the glass substrates. The sample deposited at 500 °C using the mixture of acetone and toluene as the solvent had shown that the length of the nanoneedles was approximately 10 μm. As a result it was calculated that the layers deposited at 500 °C for approximately 50 min using mixture of acetone and toluene as the solvent had a growth rate of approximately 180 μm/min. Cross section image of the above described sample is shown in Figure IV.3.

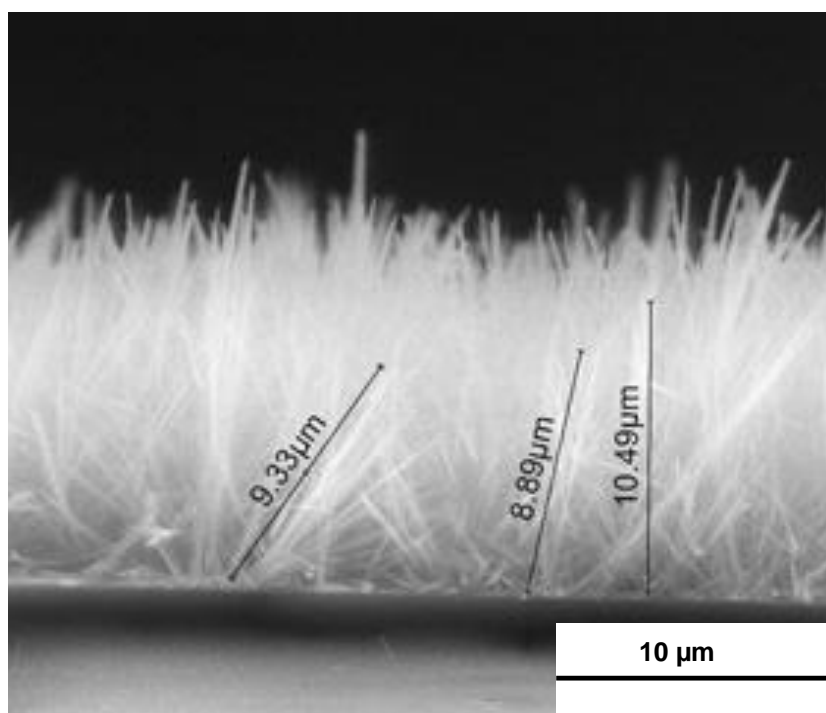


Figure IV.3: Cross-section ESEM image of the WO₃ nanoneedles deposited *via* AACVD at 500 °C using mixture of acetone and toluene as the solvent

The TEM characterization of the WO₃ nanoneedles was used to study the diameter of the nanoneedles. In Figure IV.4 is shown the deposition temperature as the function of the length and the width of the nanoneedles, depending on the solvent used. The maximum value of the measured length and width were taken for each sample. The preparation of the samples was achieved by sonication in methanol of the WO₃ nanoneedles by the procedure described in details in point 2.3 of the experimental part.

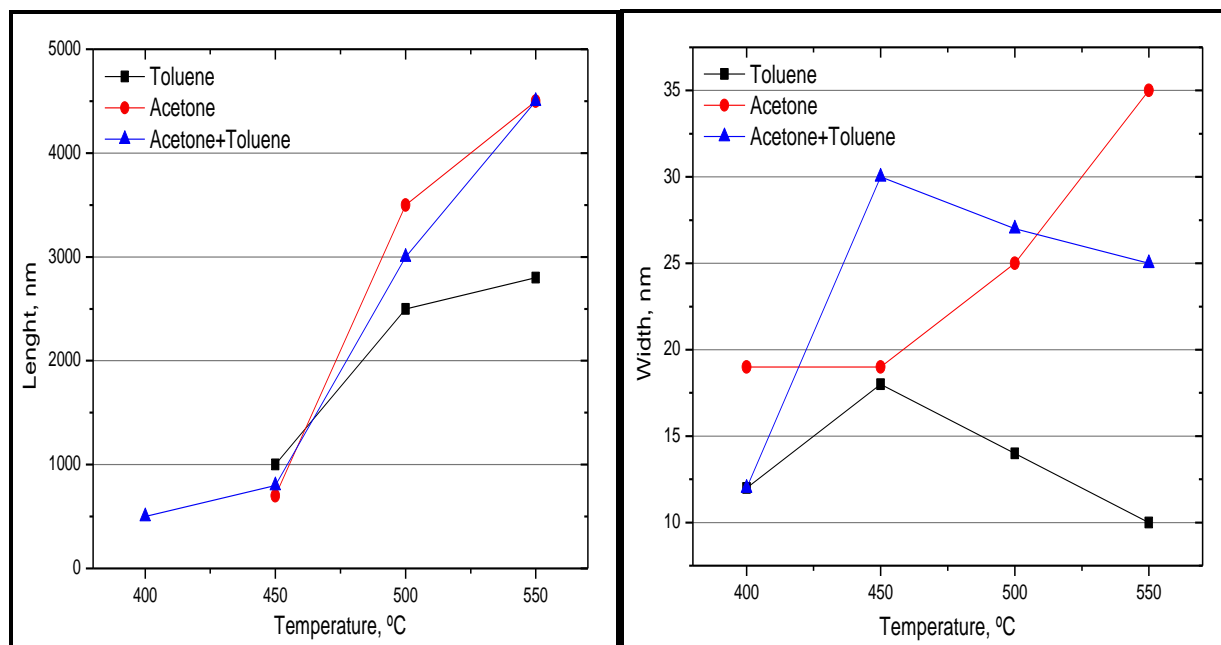


Figure IV.4: Effect of the deposition temperature and the solvent used on the maximum length and width of the nanoneedles

On the basis of the maximum values measured for each sample the following observations were made: The length of the nanoneedles increases with increasing of the deposition temperature and the longest nanoneedles were observed at 550 °C for all the solvents. The width of the nanoneedles, for the depositions made using toluene or mixture of acetone and toluene as the solvent, increase with the increasing of the deposition temperature until reaching 450 °C. After this temperature (i.e. for 500 °C and 550 °C), the nanoneedle's width was observed to decrease. In contrast, by using acetone as the solvent, the nanoneedle's width was observed to increase with the increasing of the temperature in the range from 400 °C to 550 °C.

One can note, that the shorter nanoneedles (Figure IV.4) were observed comparing to the cross-section image results (Figure IV.3). These contradictory results were related to the sonication procedure, in which the deposited nanoneedles were removed and possibly broken from the surface of the substrate (Figure IV.5).

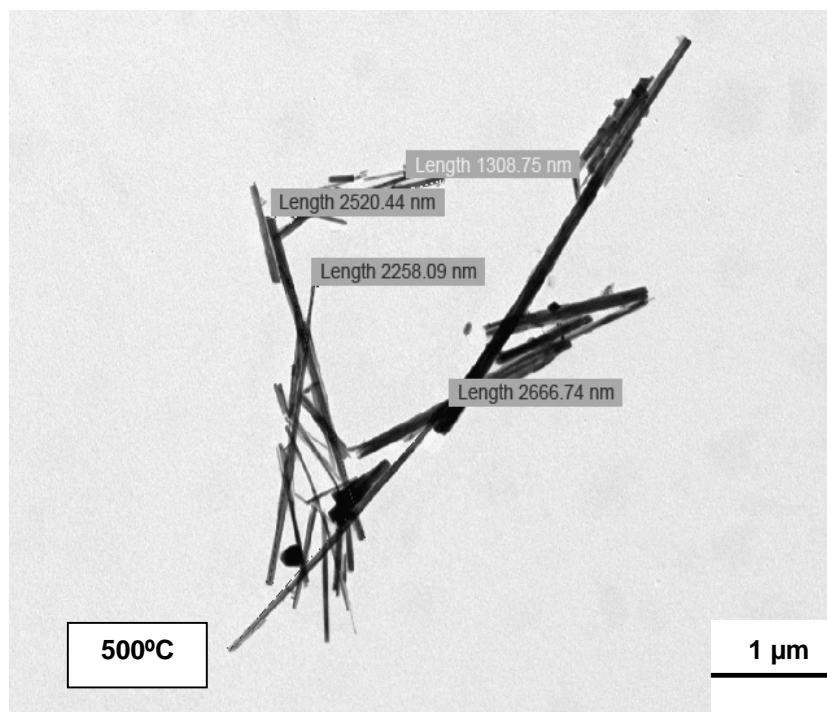


Figure IV.5: TEM image of the WO₃ nanoneedles observed for the samples deposited at 500 °C using the mixture of acetone and toluene as the solvent

In this section it was observed that the use of different solvents for tungsten oxide deposition influences the rates of deposition (deposition time) and potentially the droplet evaporation process, causing changes in the final morphology. The results demonstrated the influence of solvent on the film formation during AACVD process and provided a criteria for the formation of quasi-one-dimensional structures and the modulation of nanostructured morphology. The results from morphology characterization showed that WO₃ polycrystalline and nanoneedle-based structures, deposited using the mixture of acetone and toluene as the solvent, were formed at the slightly lower deposition temperatures (i.e. 350 °C and 500 °C, respectively) comparing with the other solvents, revealing better coverage and adhesion on the gas sensor substrate. Moreover, it was demonstrated that the AACVD method and the lower deposition temperatures required to grow nanostructures, are compatible with

microhotplate gas sensors, which are known to resist thermal shocks for longer periods at around 500 °C [196]. On the basis of these results, the mixture of acetone and toluene was chosen as the solvent for further sensing film deposition on the alumina and microhotplate gas sensor substrates.

3. Characterization of gas sensors based on nanostructured WO₃ films

3.1. Sensing film analysis

3.1.1. Morphology

The surface morphology analysis of the as-deposited WO₃ layers on alumina substrate reveals compact grains, between ~100 and 350 nm and a high density of the non-aligned nanoneedles, for deposition temperatures of 350 °C and 500 °C respectively. These results were similar to the morphology results obtained for samples deposited onto glass substrate from our previous study (section 2). SEM images of the obtained structures are shown in Figure IV.6.

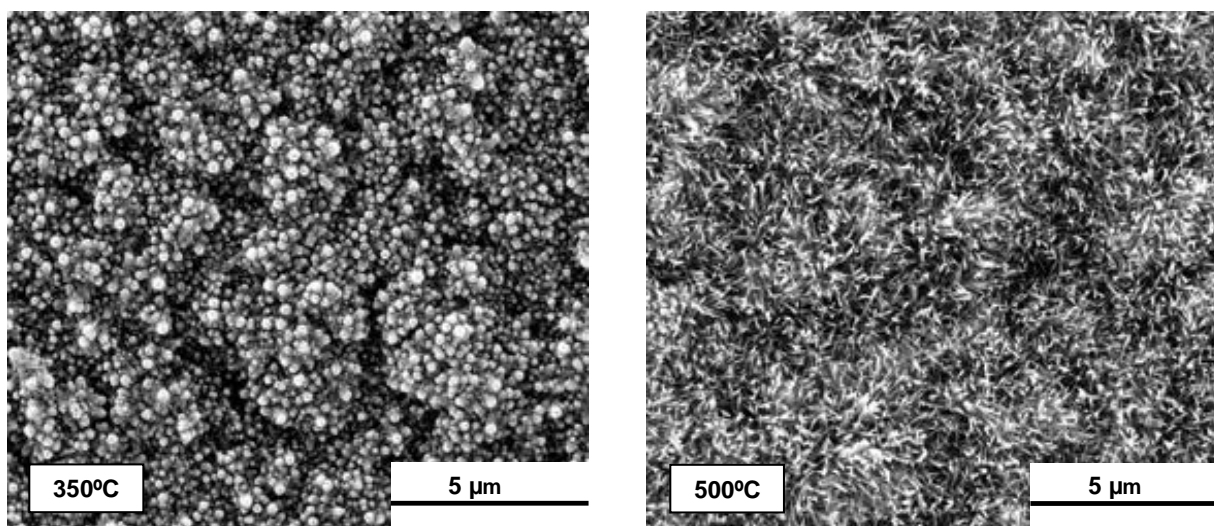


Figure IV.6: ESEM image of WO₃ polycrystalline and nanoneedle-like structures deposited *via* AACVD on alumina gas sensor substrate at 350 °C and 500 °C respectively

Cross-section characterization of the films deposited on alumina gas sensor substrates has shown that the length of the nanoneedles deposited at 500 °C was approximately 7.5 μm, whereas the polycrystalline sample deposited at 350 °C has shown the thickness of the layers of approximately 550 nm. The growth rates for the nanoneedle-like and polycrystalline layers were of approximately 127 and 10 nm/min respectively and a slight decrease was observed for nanoneedle-like structures when comparing with the results obtained for the glass substrate (Figure IV.3).

It is well known that the surface of the alumina substrate has a higher roughness which could influence the formation of nanostructures [197]. When the average surface roughness is large enough, as compared to diffusion length, the atoms will be migrated into craters present on the surface, due to the higher energy barriers for migration. Then, these craters serve as nucleation sites for the growth of the nanoneedle-like structures. Therefore, for a surface with a higher degree of roughness the atoms form the big islands and these islands act as a basis for the growth of wires or needles with larger diameters and shorter lengths [197]. In Figure IV.7 are shown ESEM images of the cross-section of the deposited films onto alumina substrate.

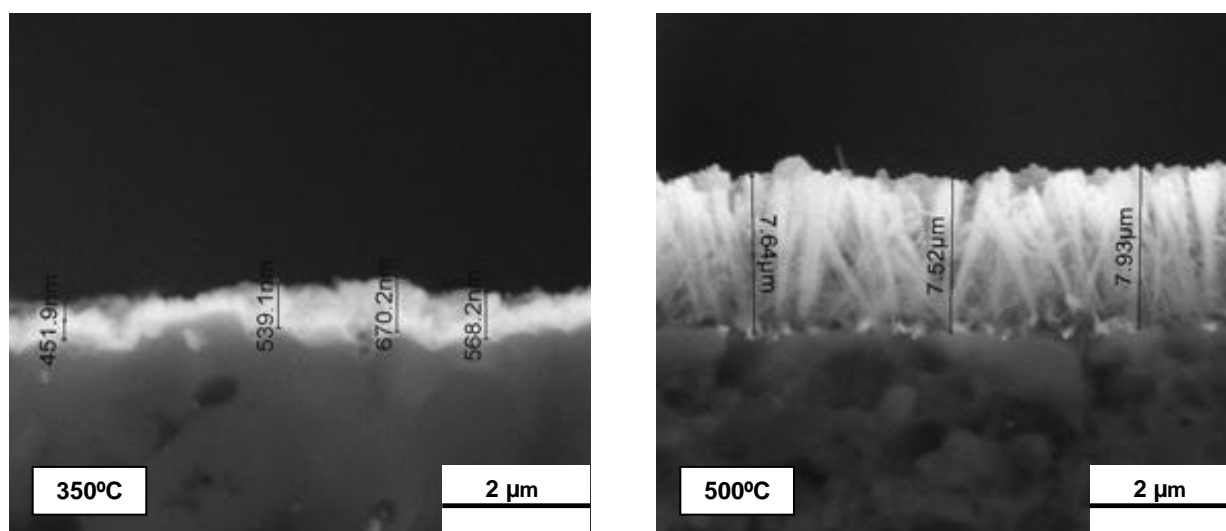


Figure IV.7: Cross-section ESEM image of WO₃ polycrystalline and nanoneedle-like structures deposited via AACVD on alumina gas sensor substrate at 350 °C and 500 °C respectively

The WO₃ nanoneedle samples that proceeded Au-functionalised *via* r.f. magnetron sputtering were also examined by ESEM. The observed samples have

shown no changes in the morphology. Damages in the film or breaking of the nanoneedles were not observed.

The TEM samples were prepared according to the sonication procedure described in point 2.3 of the experimental part. TEM characterization of Au nanoparticles functionalised *via* r.f. magnetron sputtering WO₃ nanoneedles revealed traces of Au nanoparticles with diameters of ~5 nm around the nanoneedle surface (Figure IV.8.a). In the non-functionalised samples, such nanoparticles were not observed (Figure IV.8.b).

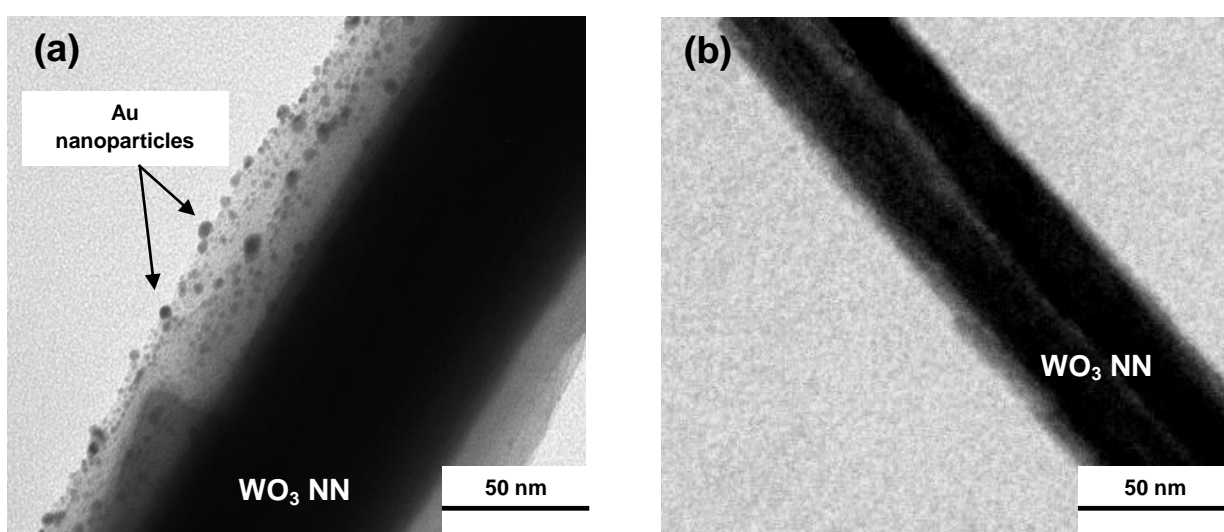


Figure IV.8: TEM images of the (a) Au-functionalised *via* r.f. sputtering and (b) non-functionalised WO₃ nanoneedles

3.1.2. XRD analysis

The phase and crystallinity of the as-deposited tungsten oxide sensing films on alumina substrate were investigated using XRD. The layers were grown from the AACVD reaction of [W(OPh)₆] dissolved in a mixture of acetone and toluene at 350 °C and at 500 °C representing polycrystalline (particles) and nanoneedle morphology respectively.

XRD analysis confirmed the presence of the monoclinic phase of WO₃, described with the P2₁/n space group, ICDD card no. 72-0677 and lattice parameters $a = 7.30600 \text{ \AA}$, $b = 7.54000 \text{ \AA}$, $c = 7.69200 \text{ \AA}$ and $\beta = 90.881^\circ$, in films composed of

polycrystalline and nanoneedle-like structure. The XRD patterns are shown in Figure IV.9. It is important to note, that the characteristic peaks of corundum and spinel found in all XRD analysis are typically found in the alumina substrates used. However, no characteristic peaks due to the Au-functionalisation, were observed in the XRD patterns of the Au-sputtered nanoneedle samples.

The analysis of the XRD patterns found the lattice constants of the WO₃ polycrystalline-based films to be $a = 7.3300(21) \text{ \AA}$, $b = 7.5427(26) \text{ \AA}$, $c = 7.67244(97) \text{ \AA}$ and $\beta = 90.650(31)^\circ$. The WO₃ nanoneedle-based films resulted in a lattice constants with $a = 7.3300(39) \text{ \AA}$, $b = 7.5359(25) \text{ \AA}$, $c = 7.67509(73) \text{ \AA}$ and $\beta = 90.703(29)^\circ$. Crystallite size was determined from the XRD patterns, according to the Scherrer equation, and it was estimated to be about 38.83(1.38) nm in the polycrystalline composed films and 41.58(1.81) nm in the nanoneedle-composed films.

As it was mentioned already in point 2.4 of the experimental part the preferred orientation in both samples was corrected with the March-Dollase model [183]. The best agreement indexes were obtained combining the two directions of orientation: [001] and [100] with different degrees of contribution. The WO₃ polycrystalline-based films revealed less preferred orientation compared to the WO₃ nanoneedle-based films. It should be noted that the intensity of the diffraction from the (200) plane is more defined for the polycrystalline-based films.

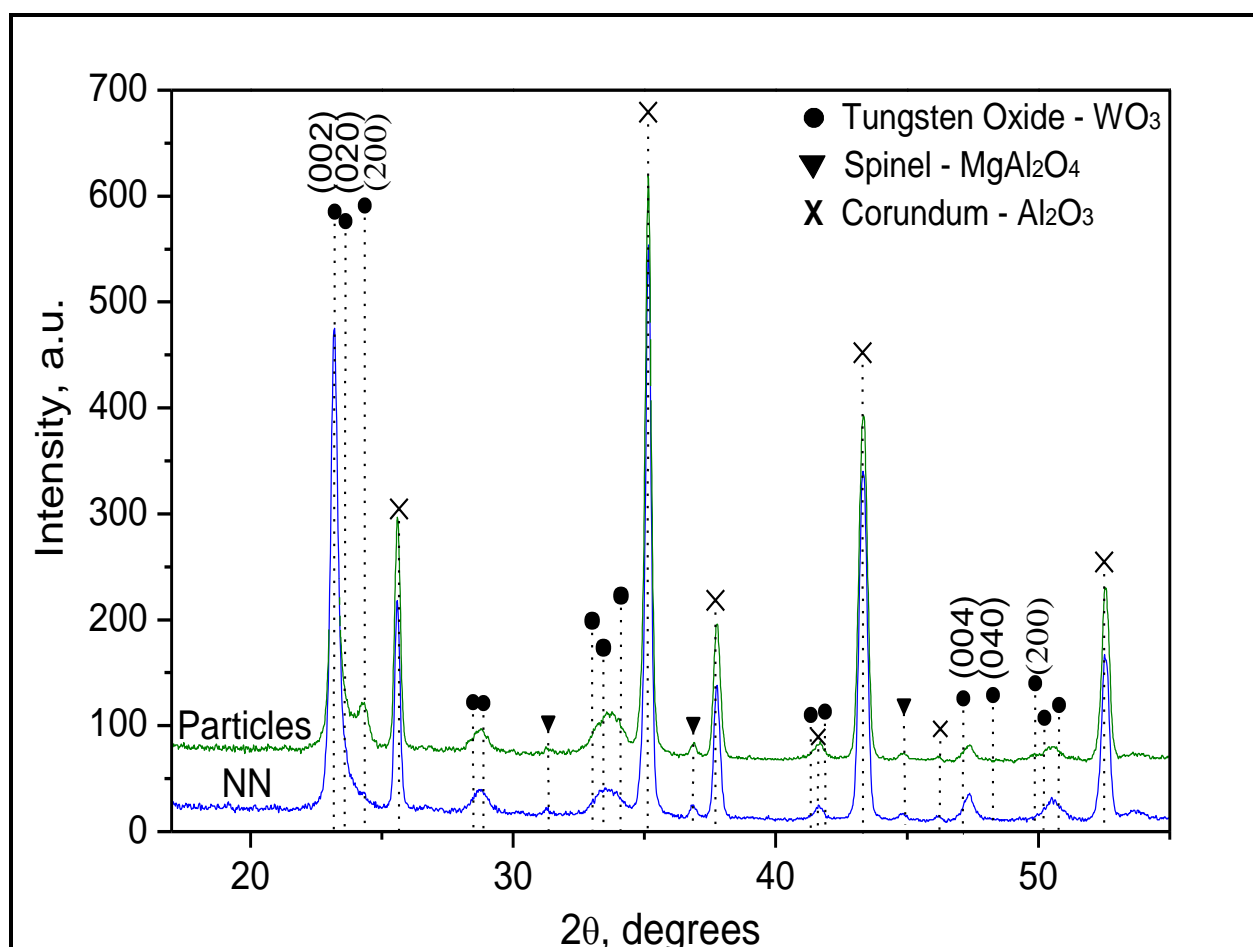


Figure IV.9: X-ray patterns of the polycrystalline (P) and nanoneedle (NN) WO₃-based films

3.2. Gas sensing characterization

In order to compare the WO₃ morphology and study its effect on the gas sensor performance, three types of gas sensor devices were fabricated using the mixture of acetone and toluene as the solvent. The gas sensors were assembled following the procedure steps described in point 3.1 of the experimental part. The active sensing materials based on intrinsic WO₃ polycrystalline structure, intrinsic WO₃ nanoneedles and Au-functionalised WO₃ nanoneedles *via* r.f. magnetron sputtering, were deposited onto the alumina gas sensor substrates. The response of the WO₃ to various gases was analyzed in the range of 100°C to 300°C operating temperatures.

3.2.1. Sensor response - reducing gases

The electrical resistance changes of the WO₃ gas sensors, composed of polycrystalline structure, nanoneedles and Au/WO₃ nanoneedles, were examined under several reducing environments. All tested samples demonstrated important resistance changes to EtOH and H₂. However, the gas sensors were not sensitive to CO, H₂S and C₆H₆. Higher sensor responses under exposure of EtOH were observed at 250 °C and 300 °C, for 1.5 ppm and 20 ppm concentrations, respectively. The typical sensor responses to EtOH are show in Figure IV.10.a. On the contrary, higher sensor responses for 1000 ppm of H₂ were observed at 150 °C, which is much lower operating temperature. In Figure IV.10.b are shown typical responses to H₂.

It was found, that the Au/WO₃ nanoneedle sensing films showed better sensitivities at the optimum sensor operating temperature, demonstrating that the sputtered Au nanoparticles play an active role in the reaction process at the surface of the film. However, at higher concentrations (20 ppm) and operating temperature (300 °C) a different behaviour was observed for EtOH, whereas Au/WO₃ nanoneedles showed no improvement of the gas sensing properties.

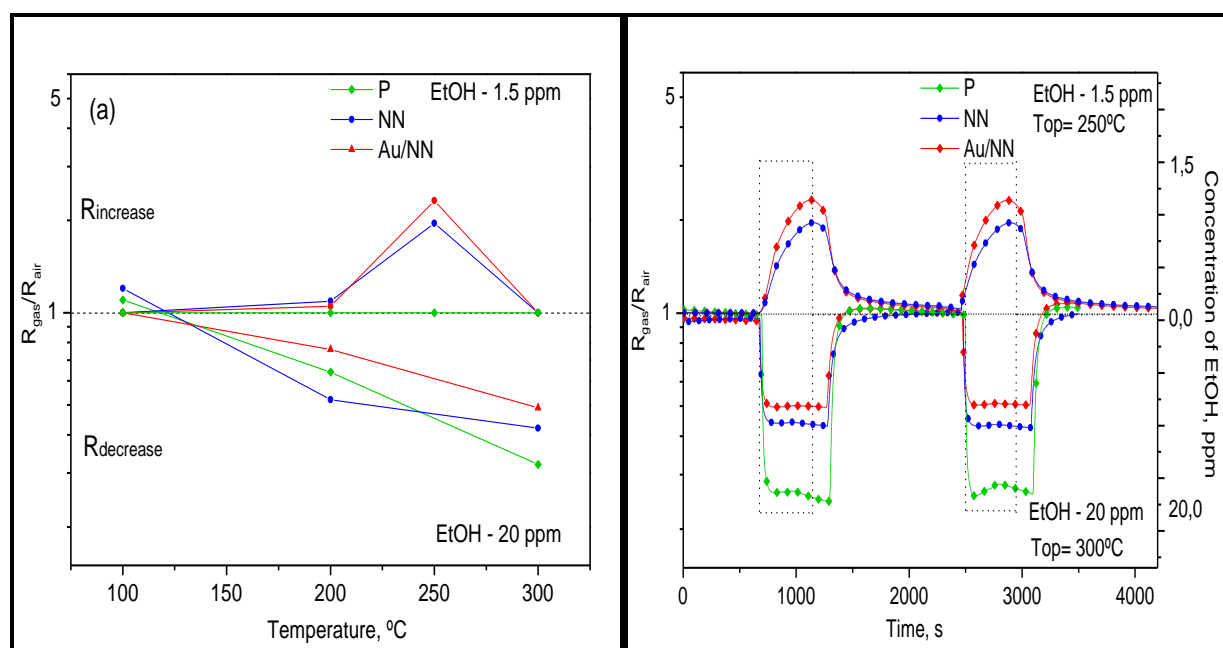


Figure IV.10.a: The temperature dependence and the higher sensor response obtained towards EtOH using WO₃ gas sensors based on polycrystalline (P), nanoneedle-like (NN) and Au-sputtered nanoneedle-like (Au/NN) structures

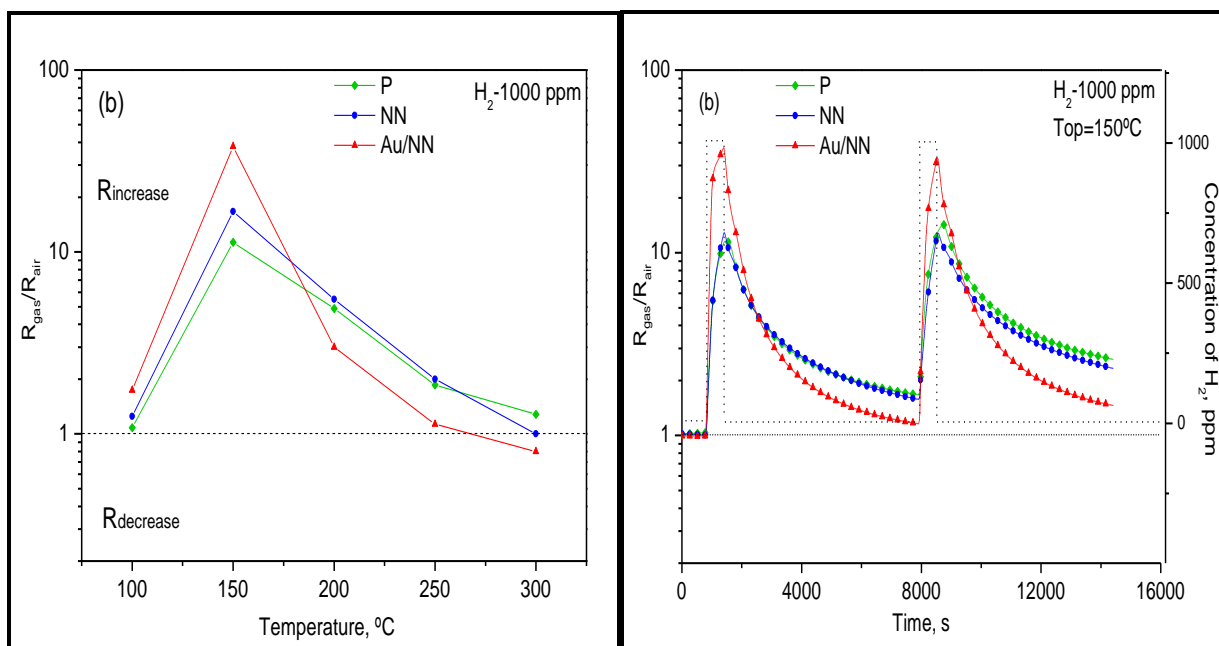


Figure IV.10.b: The temperature dependence and the higher sensor response obtained towards H_2 using WO_3 gas sensors based on polycrystalline (P), nanoneedle-like (NN) and Au-sputtered nanoneedle-like (Au/NN) structures

Normally, n-type semiconductors such as WO_3 would show decrease in their resistance when exposed to reducing gases and an increase of the resistance in the presence of oxidising gases. However, the experiments showed that sensing layers based on intrinsic WO_3 nanoneedles and Au-functionalised WO_3 nanoneedles, increase in electrical resistance when exposed to a lower concentration of EtOH (i.e. 1,5 ppm) and H_2 and decrease in electrical resistance when exposed to a higher EtOH (i.e. 20 ppm) concentration, turning the conductivity from p-type to n-type, once the concentration is increased. This effect could be attributed to the formation of an inversion layer, which results in a transition from n-type to p-type conduction [198, 199], which was also observed in WO_3 nanorods [200] and TeO_2 nanowire-based [201] gas sensors upon exposure to EtOH. Comparing to the bulk materials, it is possible that the effect occurs more easily in nanostructured materials, due to the comparable dimensions of the mean free path of the carriers and the diameter and/or thickness of the nanostructured materials. The formation of an inversion layer and the changes in the conduction type of the gas sensing film could be induced either by certain kind of reductive ambient, the use of additives on the surface or various types of surface reactions under different conditions, for instance humidity and temperature. In the case of EtOH, the formation of an inversion layer is related to the fact that the reaction

mechanism of EtOH at the metal-oxide surface may belong to a class of acceptor or donor reaction [202]. In our experiments we believed that a kind of acceptor reaction occurs at low EtOH concentrations. This resulted in resistance changes only in the nanoneedle-based films due to the higher surface-to-volume ratio and better utility factor of these structures comparing with the polycrystalline-based films. In contrast, when exposed to higher concentration of EtOH a donor class reaction occurs. This in turn shows a typical decrease of the film resistance both in nanoneedle and polycrystalline-based films. In the case of H₂, the formation of an inversion layer could be linked with a more complex phenomena probably related to the rates of the adsorption and recombination of H₂ at the WO₃ surface [202].

3.2.2. Sensor response - oxidizing gases

The WO₃ gas sensors were also examined in an oxidizing environment. Figure IV.11 displays the temperature dependence of the sensor response, when exposed to 1 ppm of NO₂. The higher sensor responses to NO₂ were observed at 150 °C, both for WO₃ nanoneedles or Au/WO₃ nanoneedle films. However, longer recovery times were measured for NO₂ at this temperature, compared to the recovery times for EtOH and H₂ exposure. It was noted that the variation in the gas sensor responses depended on the WO₃ morphology. Slightly better responses were achieved for the polycrystalline-based gas sensors when compared to the intrinsic nanoneedle-based ones. The Au-functionalised *via* r.f. sputtering WO₃ nanoneedle structures showed better responses to NO₂ compared to the non-functionalised WO₃ nanoneedles.

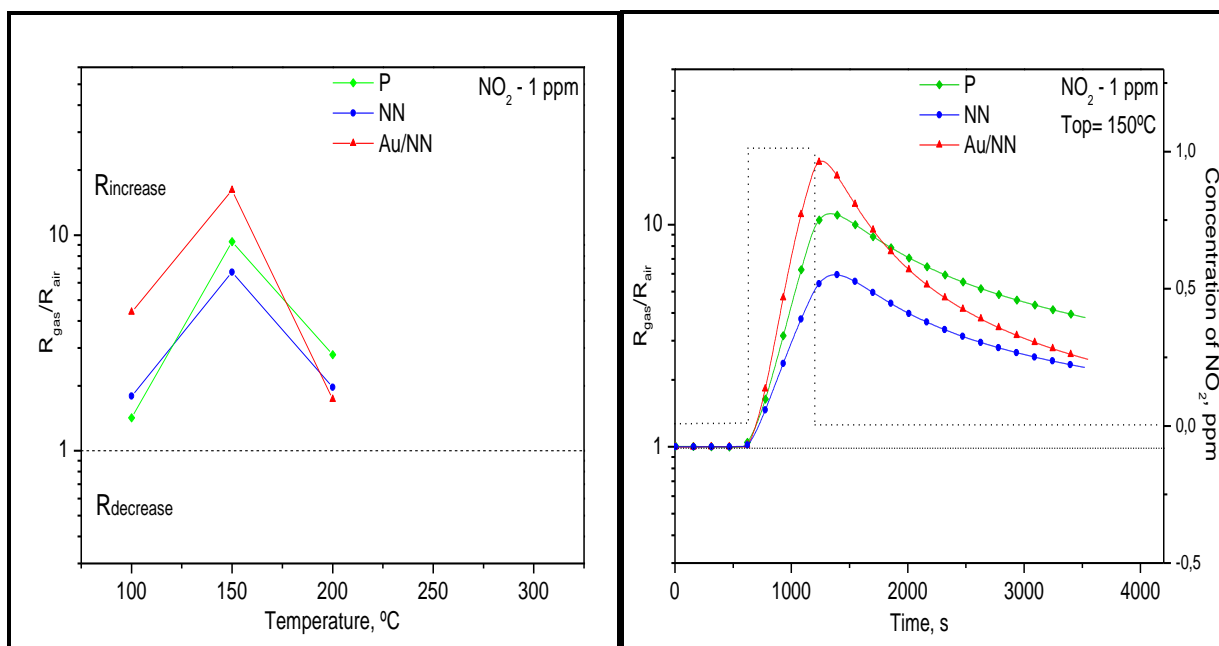


Figure IV.11: The temperature dependence and higher sensors response obtained towards NO₂ using WO₃ gas sensors based on polycrystalline (P), nanoneedle-like (NN) and Au-sputtered nanoneedle-like (Au/NN) structures

During the experiments, each gas sensor has been exposed to the analysed gas concentration for a period of 10 min. After passing the whole period of exposure to the particular toxic gas, the resistance of the alumina gas sensors did not reach the steady state and the analysed gas was switched off. This indicated that the response and the recovery times for all alumina gas sensors were found to be slower for lower operating temperatures, while a slight improvement was observed when the gas sensors were operating at higher operating temperatures. This probably occurs because of the increase of the reaction velocity at the higher operating temperatures. As the adsorption and desorption rates depend exponentially on the temperature, the dynamic properties of the gas sensors, such as response and recovery times are highly temperature dependent [203].

3.2.3. Stability

The sensor baseline resistance changes were recorded in air over the twelve weeks of the experiment. In Figure IV.12 are presented the sensing layer resistance changes in air for the alumina-based gas sensors. It was found that after twelve weeks

of measurements, the changes in the baseline resistance were negligible for all of the tested samples, indicating a good stability.

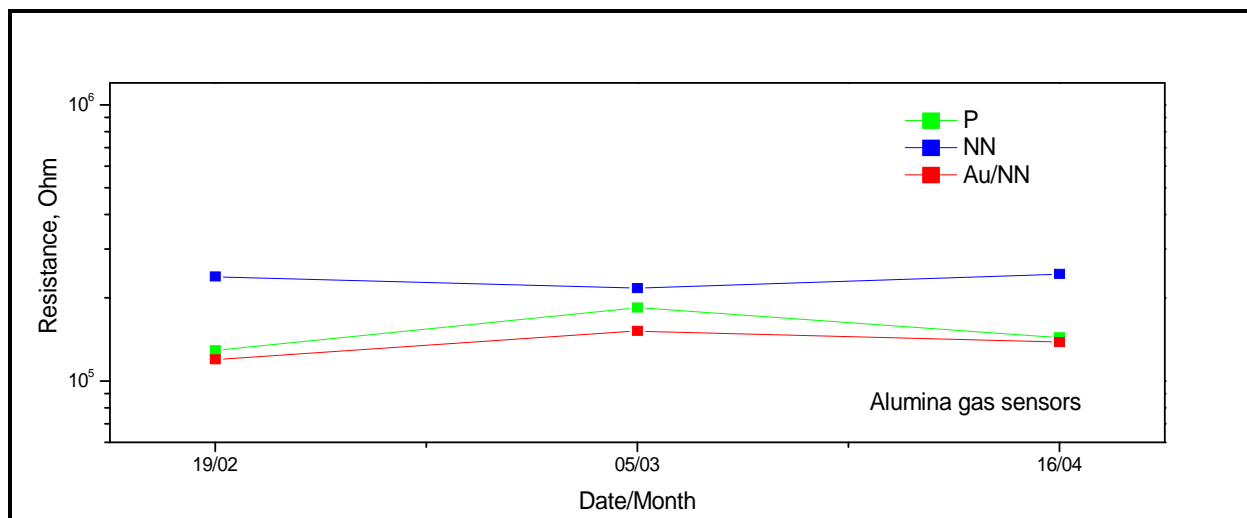


Figure IV.12: Baseline resistance of the gas sensing WO₃ layers in air over twelve weeks

In this section of the study of a particular interest is that the results observed for 20 ppm of EtOH, H₂ and NO₂ showed few differences on the response of polycrystalline and WO₃ nanoneedle-based gas sensor. These results seem to be to some extent related to the smaller crystallite size of the polycrystalline-based samples and the wider gap of the electrodes, which are normally used with polycrystalline films in the traditional devices. Previously, it was demonstrated that the shorter gap between the electrodes favours a mat-like network for nanowires and improve the semiconductor-semiconductor junction between the nanostructures [204-206]. Therefore, it is suggested that there is the need for the special electrode design for the adequate exploitation of the nanoneedle-like structures in the commercial gas sensing devices. These results were used as the start up point for further investigation of the ideal gas sensor substrate arrangement for the nanoneedle-like structure growth in-situ *via* AACVD method.

Furthermore, it was demonstrated that the Au-functionalisation *via* r.f. sputtering of the WO₃ nanoneedles in some cases could improve the gas sensing properties. However, the Au-functionalisation *via* r.f. sputtering was found to be time consuming and an expensive process, where the functionalisation was achieved in the second

step. These findings led us to a possible solution for one step simultaneous growth of WO₃ nanoneedles functionalised with Au-nanoparticles by using the co-deposition *via* AACVD method, presented in the next section.

4. Characterization of gas sensors based on Au-functionalised WO₃ nanoneedle-like films

The co-deposition *via* AACVD method was used for the simultaneous growth of Au nanoparticles and WO₃ nanoneedles, where the Au nanoparticles were inserted on the surface of the WO₃ nanoneedles in one single step. In order to insert Au nanoparticles on the surface of the WO₃ nanoneedles, a precise control of the precursor supersaturation during the co-deposition process is required. This is to prevent formation of non-adherent powders or polycrystalline thin films. In this context, the choice of precursors and the control of the degree of homogenous and heterogeneous gas-phase reactions are crucial. The gold precursor should decompose at the lower temperature than the main metal-oxide precursor by manipulating the reaction conditions of the deposition of nanostructured metal-oxide. Therefore, this ensures that the gold precursor undergoes homogenous nucleation in the gas phase to form Au nanoparticles, whereas the main metal-oxide precursor must undergo some degree of heterogeneous reaction on the substrate surface. The substrate temperature required for deposition of the Au-functionalised WO₃ nanoneedle-based layers were found to be around 350 °C. For comparison, a deposition temperature of 500 °C is required to deposit WO₃ nanoneedles from [W(OPh)₆] alone on the identical substrates, which was mentioned in our previous study [164, 207].

In our previous study [52] it was found that the lower deposition temperatures were required for the formation of quasi-one dimensional structures observed during the co-deposition of tungsten oxide with Au nanoparticles. Hence, it was suggested that the presence of the co-deposited gold precursor could have influenced the optimal deposition temperature for nanoneedle growth. However, recent results reported in [164] showed that the use of methanol as the solvent encourage the growth of nanostructured material at lower temperatures, suggesting that methanol could act as the reactive 'precursor' and not simply as the 'carrier' solvent.

4.1. Film analysis

4.1.1. Morphology

The surface morphology analysis of the Au co-deposited WO₃ nanostructures, deposited at 350 °C on alumina substrate, confirmed the presence of a high density of non-aligned nanoneedles, similar to the ones observed in the non-functionalised films deposited from the mixture of acetone and toluene (Figure IV.6). ESEM image of the observed WO₃ nanostructure is presented in Figure IV.13.

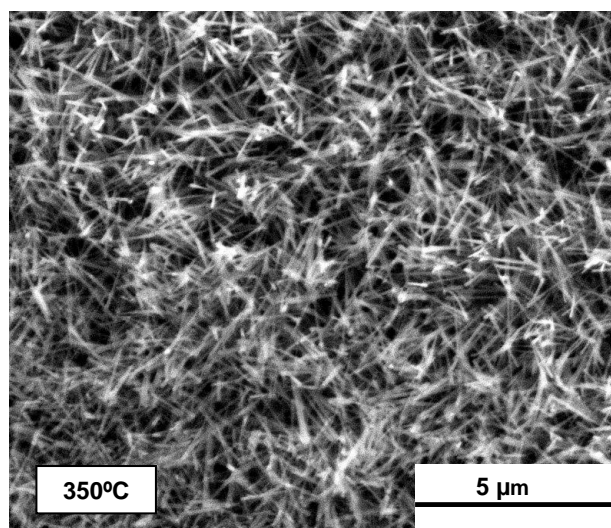


Figure IV.13: ESEM image of Au/WO₃ nanoneedles deposited *via* AACVD onto alumina gas sensor substrate at 350 °C

The TEM image of the WO₃ nanoneedles functionalised with Au nanoparticles in-situ *via* AACVD revealed traces of Au nanoparticles around the nanoneedle surface (Figure IV.14). Furthermore, the HRTEM analysis of WO₃ nanoneedles functionalised with Au nanoparticles was carried out, showing that the WO₃ nanoneedles are single crystalline. Clear lattice fringes can be observed in the two insets in Figure IV.15. The inset (Figure IV.15.a), shows an interplanar spacing of 0.35 – 0.37 nm consistent with an internal order of the WO₃ nanoneedles in the [001] ($0.5d = 0.3650$ nm) or [020] ($0.5d = 0.3770$ nm) directions. The surface of the nanoneedles was homogeneously covered with well-dispersed quasi-spherical Au nanoparticles with diameter between

9-25 nm. The inset (Figure IV.15.b), shows a typical high resolution image of Au nanoparticles, where one could note the family of planes with lattice spacing of 2.4 Å, corresponding to (111) planes.

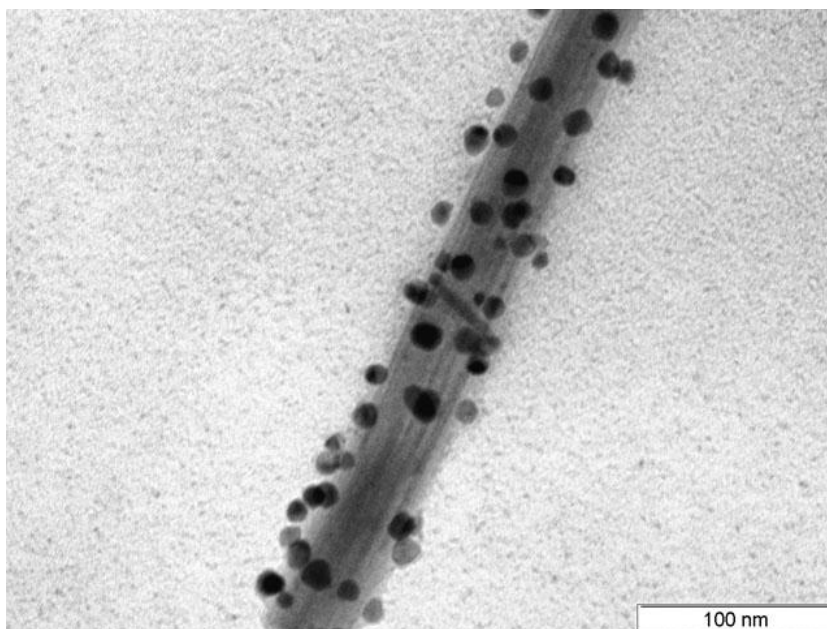


Figure IV.14: TEM images of the Au-functionalised in-situ *via* AACVD WO₃ nanoneedle

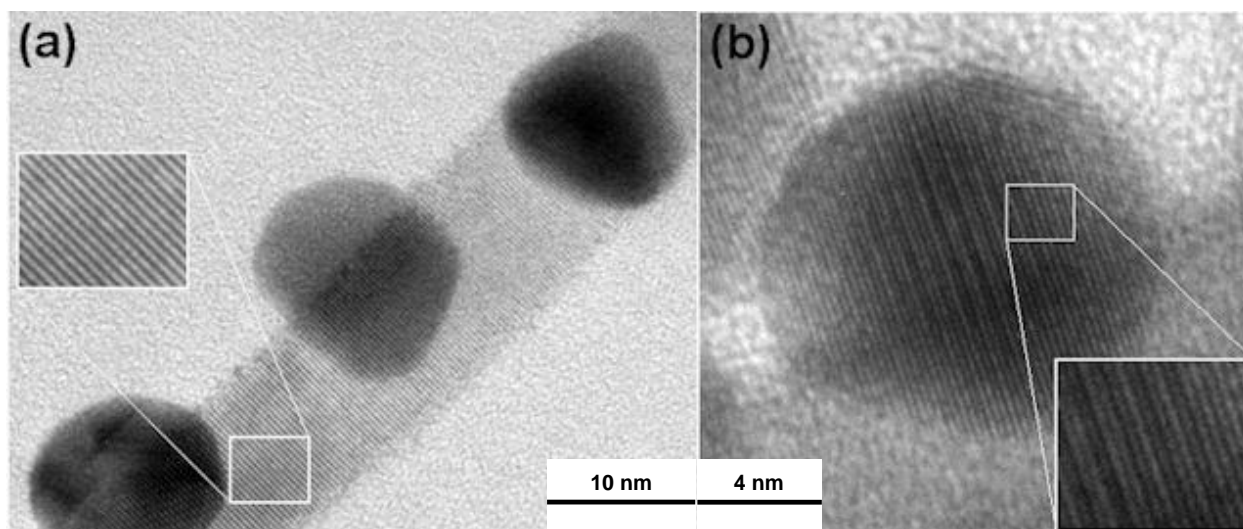


Figure IV.15: TEM images of WO₃. The insets show the crystalline structure of both WO₃ nanoneedle (a) and Au nanoparticle (b) [52]

4.1.2. Chemical composition

The chemical composition of the hybrid structures was determined by XPS. The W 4f and W 5p_{3/2} core level spectra were recorded using XPS on a standard WO₃ powder sample and on the co-deposited Au nanoparticles and WO₃ nanoneedles (Au/WO₃) grown on silicon substrates (Figure IV.16.a).

Examination of the W 4f and W 5p_{3/2} core level XPS spectrum of Au/WO₃ samples compared to a WO₃ thin film standard showed no difference in the peak positions, indicating only a weak interaction between the WO₃ nanoneedles and the co-deposited Au nanoparticles.

The peak broadening observed in the Au/WO₃ sample is associated with the presence of surface defects in the WO₃ nanoneedles which became quantitatively important in the XPS spectrum due to the higher surface area of the WO₃ nanoneedles compared to the WO₃ thin film standard [102].

Examination of the Au 4f core level XPS spectra showed that the deposited Au nanoparticles were metallic, again indicating only a weak electronic interaction with the WO₃ nanoneedles. In Figure IV.16.b, is shown the comparison of the Au core level spectrum recorded on the sample and on Au crystal.

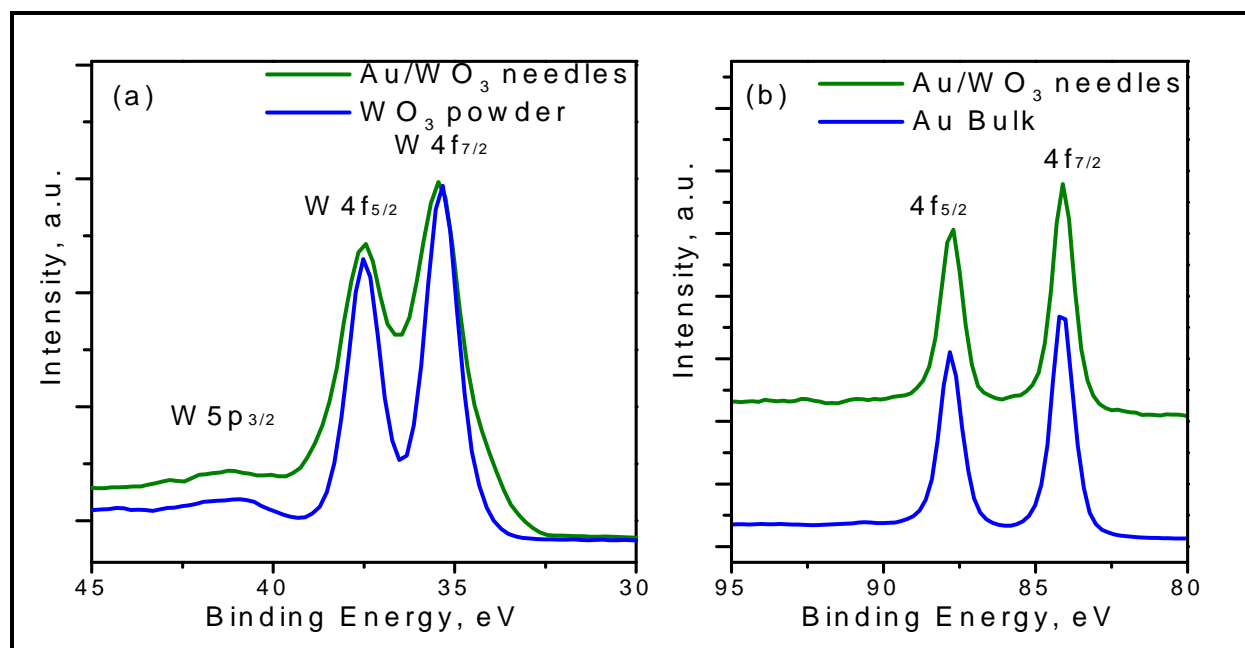


Figure IV.16: W 4f core levels for WO₃ powder and Au-functionalised WO₃ nanoneedles (a) and Au 4f core level recorded on the sample functionalised with gold and the gold crystal (b) [52]

4.1.3. XRD analysis

XRD analysis confirmed the presence of the monoclinic phase of WO₃ described with the P2₁/n space group, ICDD card no. 72-0677 and lattice parameters $a = 7.30600 \text{ \AA}$, $b = 7.54000 \text{ \AA}$, $c = 7.69200 \text{ \AA}$ and $\beta = 90.881^\circ$. Analysis of the XRD patterns found the lattice constants to be $a = 7.4112(44) \text{ \AA}$, $b = 7.7234(53) \text{ \AA}$, $c = 7.7909(26) \text{ \AA}$ and $\beta = 91.1641(43)^\circ$, with preferred orientation in the [001] direction. The obtained results have shown that the structure and the preferred orientation were similar to the results obtained for the intrinsic nanoneedle-like structures deposited previously (section 3, point 3.1.2). The XRD patterns are shown in Figure IV.17. The diffraction peak at $38.1841^\circ 2\theta$ was assigned to the (111) plane of Au. Similarly to the previous samples the remaining peaks were assigned to Al₂O₃ (corundum) and MgAl₂O₄ (spinel) from the alumina gas sensor substrates.

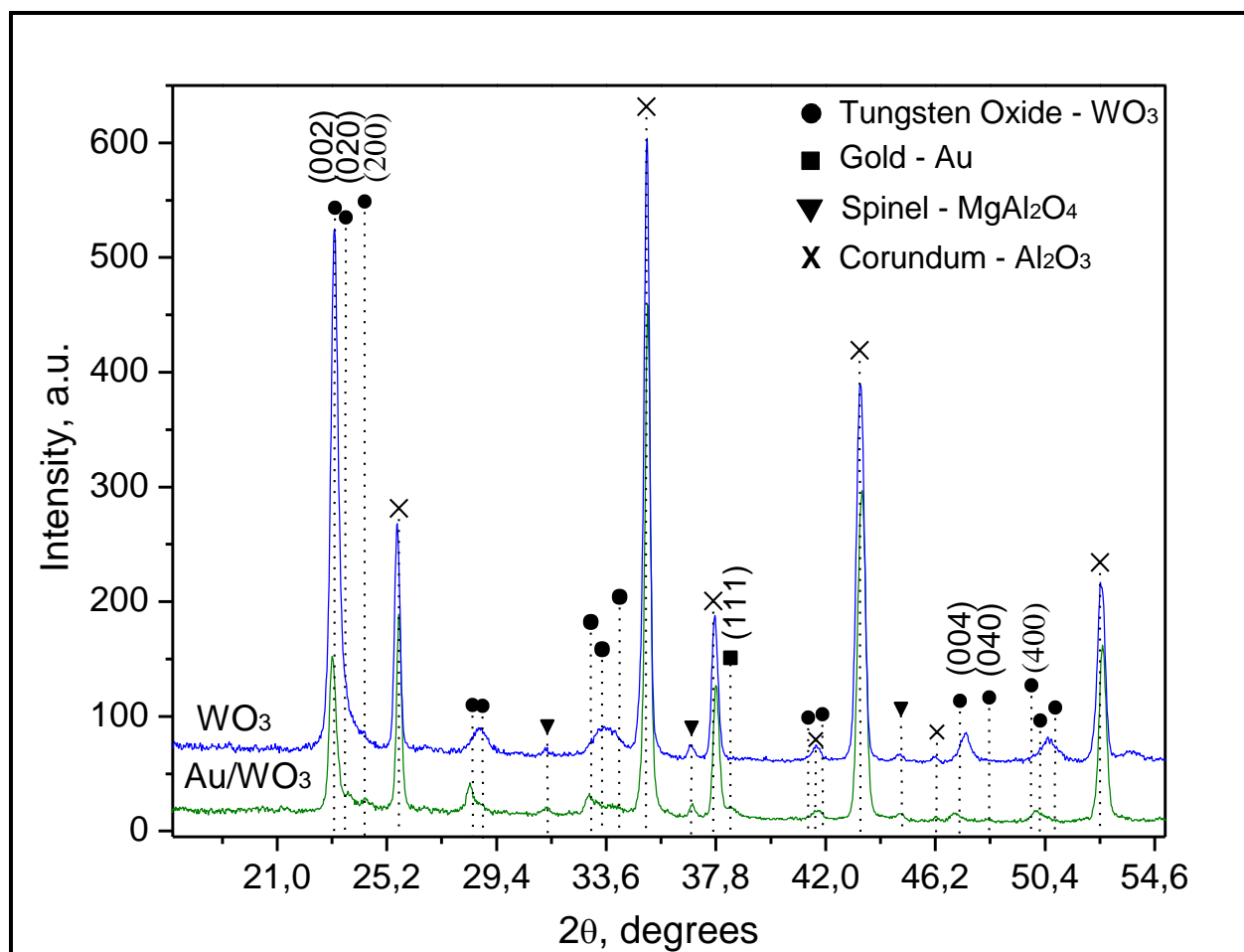


Figure IV.17: XRD pattern of Au/WO₃ nanoneedles deposited via AACVD compared with non-functionalised WO₃ nanoneedles [52]

4.2. Gas sensing characterization

The gas sensing characterization was carried out by monitoring the resistance change of the Au/WO₃ samples during the exposure to the trace concentrations of the target gases. Several sensor operating temperatures, in the range from 150 °C to 350 °C with the 50 °C incremental step were tested.

4.2.1. Sensor response

The resistance changes of the Au/WO₃ samples during the exposure to the traces of several reducing environments were examined. All tested samples demonstrated high resistance changes to EtOH. However, the sensors again were not sensitive to CO, H₂S and C₆H₆ and had shown no important response changes when exposed to H₂. Higher sensor response to 1.5 ppm of EtOH was achieved at an operating temperature of 250 °C. A typical resistance change (or sensor response) for these conditions are displayed in Figure IV.18.

The Au/WO₃ samples gave higher sensor response ($S = 12$) to lower concentrations (1.5 ppm) of EtOH. When comparing with our previous study (section 3), the measured sensor responses were much lower. AACVD deposited intrinsic WO₃ nanoneedles had sensor response ($S = 2$) to EtOH, for the same concentrations and functionalisation of the WO₃ nanoneedles by sputtering with Au, provided no increase in the sensor response. AACVD co-deposition of Au nanoparticles functionalised WO₃ nanoneedles provided a six-fold increase in the sensitivity of the WO₃ nanoneedles towards lower (1.5 ppm) concentrations of EtOH compared with either AACVD deposited intrinsic WO₃ nanoneedles or WO₃ nanoneedles decorated with sputtered Au by ex-situ technique.

The Au nanoparticles encourage reactions at the surface of the metal-oxide and alter the Fermi energy of the system through the metal/semiconductor interface, therefore enhancing sensitivity over non-functionalised WO₃ nanoneedles. However, when comparing the two doping strategies used in this doctoral study, it was found that lower dispersion and agglomeration of Au nanoparticles in the sputtered samples was observed. Therefore, the enhanced sensitivity of the AACVD co-deposited samples is

ascribed to the smaller size and the higher dispersion of the Au nanoparticles, as both factors are known to promote sensitivity [79, 208].

Similarly to our previous study (section 3), Au/WO₃ samples have shown an increase in the electrical resistance when exposed to lower concentrations of EtOH (Figure IV.18), whereas WO₃ gas sensors normally show a reduction in resistance.

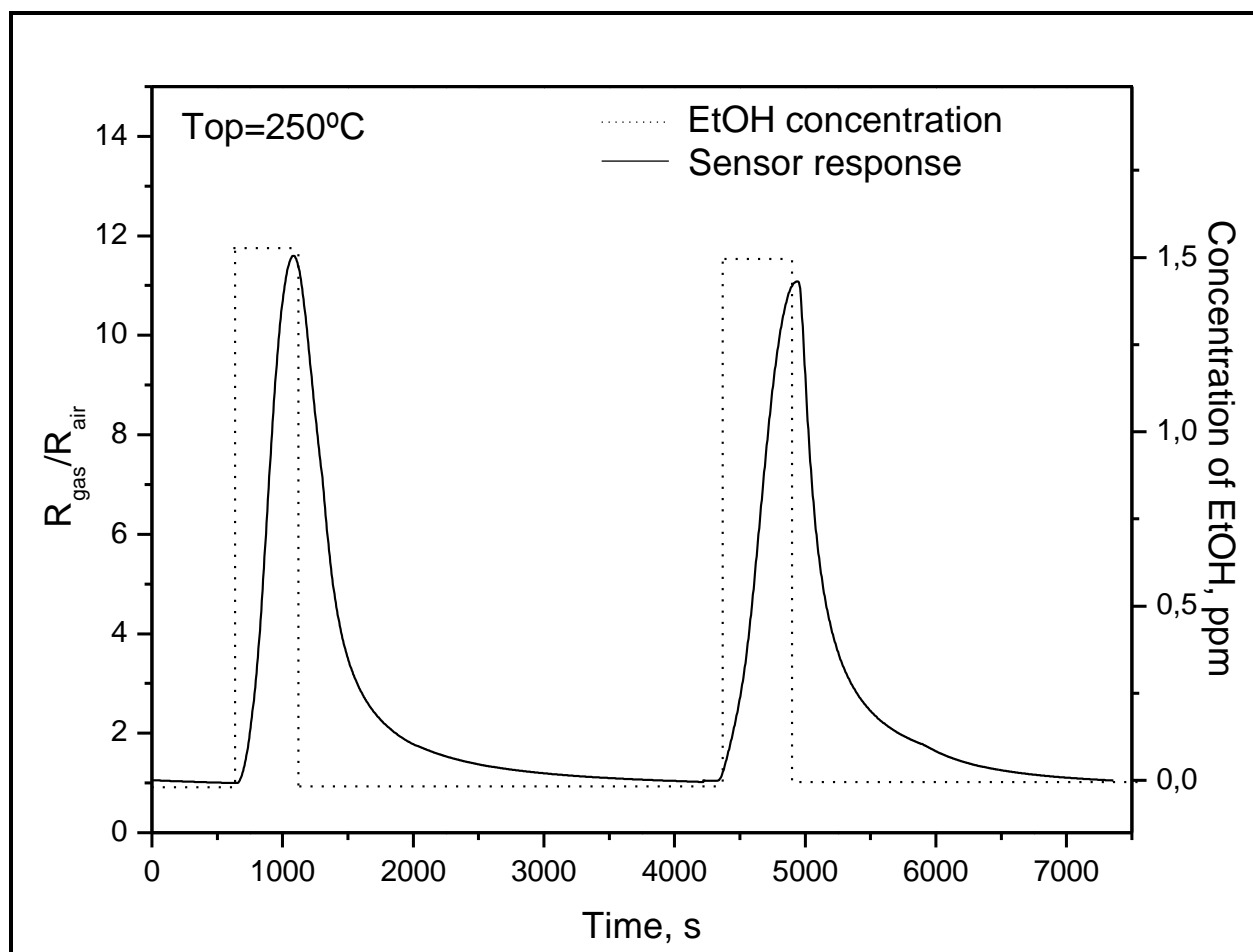


Figure IV.18: Typical gas sensor response to 1.5 ppm EtOH at 250 °C operating temperature [52]

4.2.2. Stability

Similarly to the sensors tested in section 3, after the gas sensing experiments that were running for a month at temperatures of up to 350 °C and in several toxic environments (NO₂, CO, C₆H₆), the Au/WO₃ samples were examined again using ESEM and TEM techniques. The results have shown no changes in the dispersion and

the size of the Au nanoparticles when comparing to the initial morphology of the WO₃ nanoneedle samples. This indicates a good stability of the obtained structures and the potential use of these materials for gas sensor applications.

5. Micro-machined gas sensors with nanostructured WO₃ films

In the previous stage (section 3) of our study it was verified that nanostructured WO₃ films deposited *via* in-situ AACVD method onto traditional alumina gas sensor substrates can be used as an active sensing material for gas sensor applications. The results suggested the need of a different substrate and/or electrode arrangement to enhance the performance of nanostructured WO₃ gas sensor. Hence, in this section AACVD deposition of intrinsic WO₃ nanostructures was performed on microhotplate gas sensor substrates [188] using a silicon shadow mask for the protection of the contacts. The microhotplate gas sensor substrate was composed of inter-digitated electrodes with a shorter gap (~50 μm) compared to the alumina substrate (~200 μm) used in section 3. Three deposition temperatures (350 °C, 450 °C and 500 °C) were used to grow the structures in order to obtain polycrystalline films, non-aligned and quasi-aligned nanoneedle structures.

5.1. Film analysis

5.1.1. Morphology

ESEM analysis of the WO₃ nanostructure deposited at three different deposition temperatures on microhotplate gas sensor substrate was carried out. The result confirmed the presence of thin non-aligned and quasi-aligned WO₃ nanoneedles in films deposited at 450 °C and 500 °C respectively, whereas the samples deposited at 350 °C have shown porous polycrystalline films with mean diameter of the grains of approximately 300 nm.

It was found that the nature of the substrate allows growth of WO₃ nanoneedles even at the lower deposition temperature (450 °C). According to our first study

(section 3), WO₃ nanoneedles were observed at 500 °C or higher deposition temperatures, whereas WO₃ nanotubes were formed at 450 °C. The possible reason for this behaviour could be the change in the initial polycrystalline layer formation mechanism due to the nature of the gas sensor substrate used. Thus, due to the less rugged surface of the silicon substrate used, the initial nucleation of the nanostructured layer could have formed thinner and smaller nanoneedles at the lower temperatures. The ESEM images of the observed WO₃ nanostructures are presented in Figure IV.19.

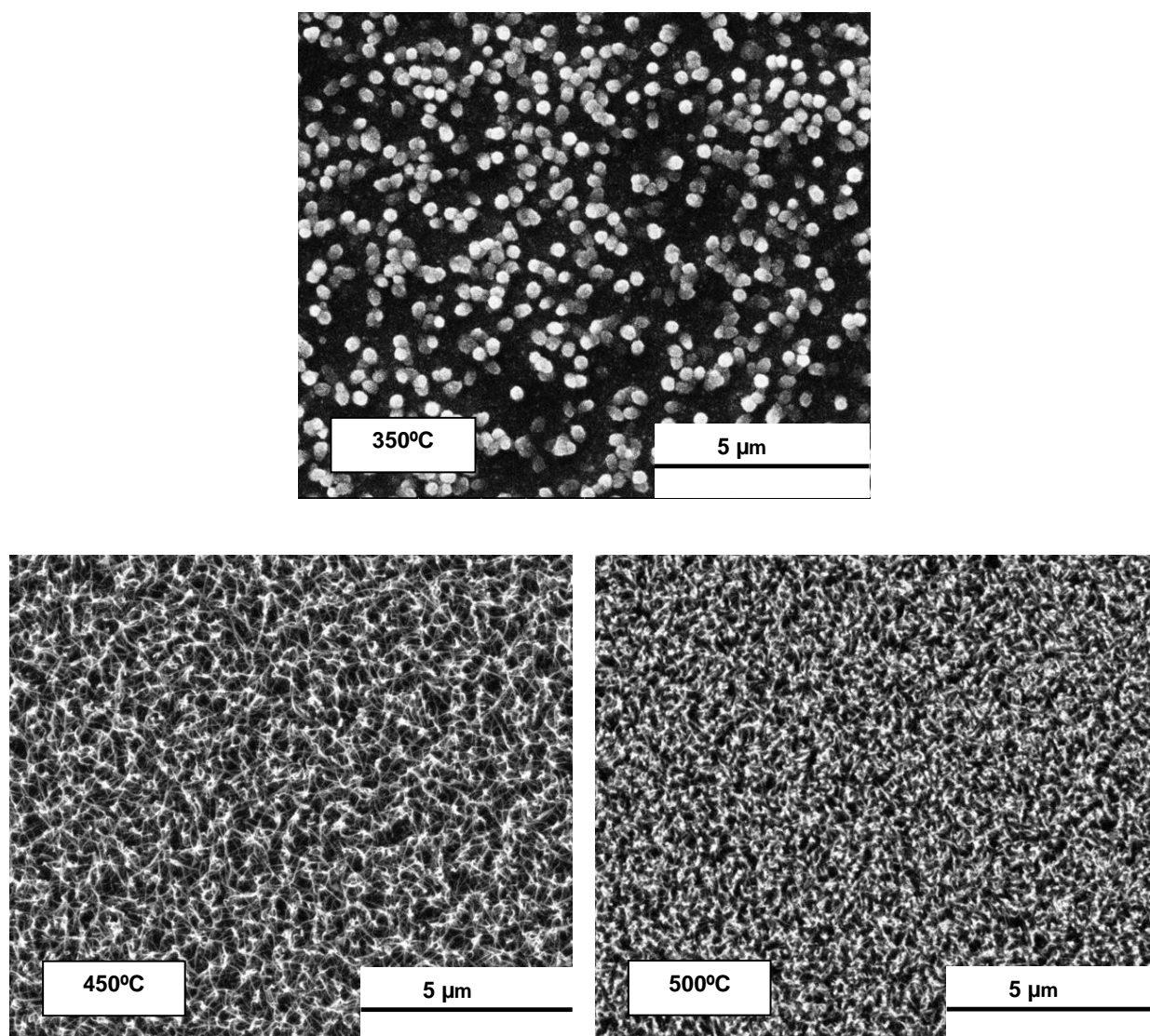


Figure IV.19: ESEM image of WO₃ nanostructures deposited *via* AACVD onto microhotplate gas sensor substrate at 350 °C (polycrystalline film), 450 °C (non-aligned nanoneedles) and 500 °C (quasi-aligned nanoneedles)

5.1.2. XRD analysis

The phase and crystallinity of the as-deposited tungsten oxide layers on the microhotplate gas sensor substrates were investigated using XRD. The layers were grown from the AACVD reaction of [W(OPh)₆] dissolved in a mixture of acetone and toluene at 350 °C, 450 °C and 500 °C.

In all analyzed samples XRD analysis confirmed the presence of the monoclinic phase of WO₃ described with the P2₁/n space group, ICDD card no. 72-0677 and lattice parameters $a = 7.30600 \text{ \AA}$, $b = 7.54000 \text{ \AA}$, $c = 7.69200 \text{ \AA}$ and $\beta = 90.881^\circ$. The XRD patterns are shown in Figure IV.20. The size of the crystallite was determined from the XRD patterns and it was estimated to be around 19.05(50) nm in the polycrystalline-composed films deposited at 350 °C and 17.15(80) nm and 18.49(85) nm in the nanoneedle-composed films, deposited at 450 °C and 500 °C respectively. The results for the crystalline size calculation for the WO₃ films deposited onto microhotplate gas sensor substrates were found to be smaller than the results obtained for the WO₃ films deposited onto alumina substrates.

The direction of preferred orientation for samples based on non-aligned (450 °C/WO₃) and quasi-aligned (500 °C/WO₃) nanoneedle-like structures was the same: [001]. The WO₃ polycrystalline-based sample deposited at 350 °C, presents a preferred orientation in [100].

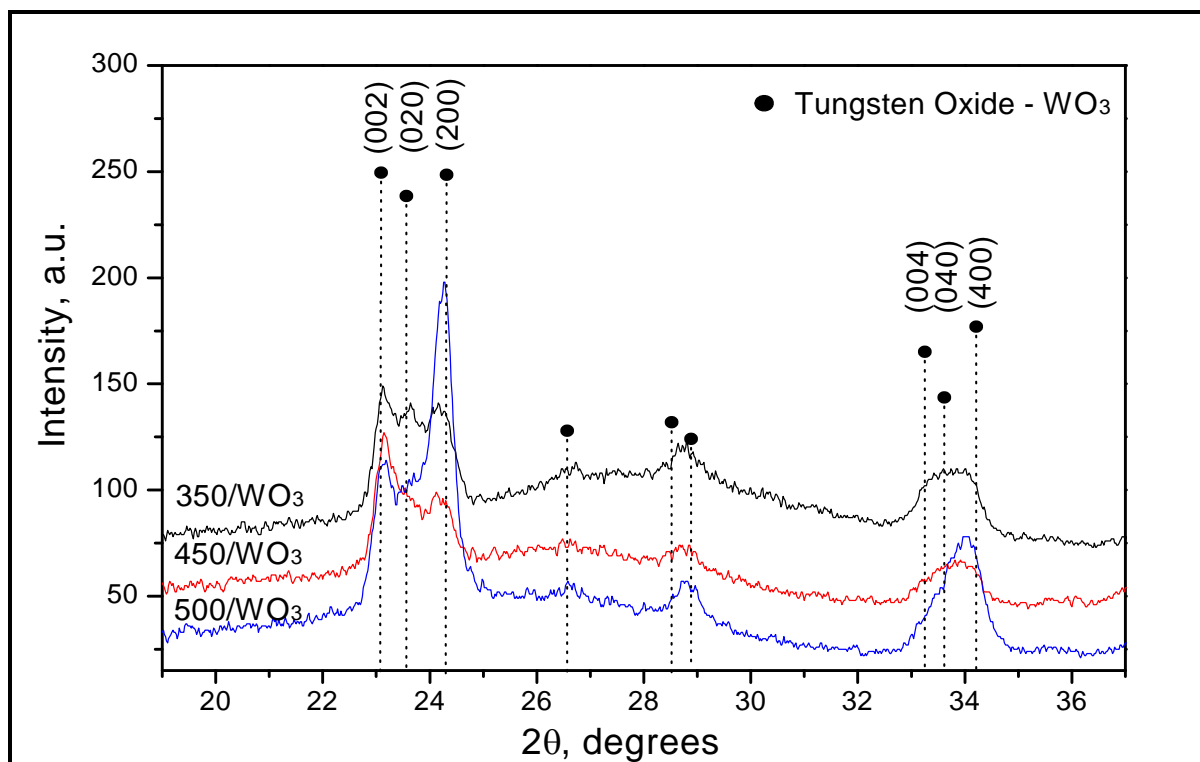


Figure IV.20: X-ray patterns of the WO₃-based films deposited at 350 °C, 450 °C and 500 °C

5.2. Gas sensing characterization

The gas sensor characterization study was conducted for the three types of WO₃ layers deposited onto the microhotplate substrates. The WO₃ films of the samples were based on the polycrystalline structure deposited at 350 °C, non-aligned nanoneedles deposited at 450 °C and quasi-aligned nanoneedles deposited at 500 °C. The experiment studied the gas sensor's response to different target gases and the influence of the operating temperature examined in the range from 100 °C to 300 °C.

5.2.1. Sensor response - reducing gases

The response of the WO₃ gas sensors was measured when exposed to different reducing target gases and various concentrations. The devices responded to all toxic gases tested. The mean value of the sensor response measurements shown below are the average of five repetitions (± 0.3 standard error). It was found that the gas sensor devices based on 450 °C/WO₃ (i.e. non-aligned nanoneedles) had shown higher gas sensor response for all tested gases comparing to the other two samples.

The structures deposited at 500 °C/WO₃ (i.e. quasi-aligned nanoneedles) were found to be less sensitive comparing with 450 °C/WO₃ nanoneedle ones, but still had shown an improvement of the sensor response comparing with polycrystalline structure deposited at 350 °C/WO₃. These results suggested that the non-aligned nanoneedle-like structures that were formed at 450 °C deposition temperature could have more advantages for gas sensing applications. Moreover, the obtained gas sensor responses proved that the technological process used, leads to more sensitive metal-oxide gas sensors, comparing with our previous study (section 3) for sensing WO₃ nanoneedle-based layers deposited onto alumina gas sensor substrate.

The microhotplate WO₃ gas sensors had shown gas sensing response ($S = 4.36$) to H₂S at the lower (150 °C) operating temperature. Moreover, CO and C₆H₆ gases were detectable in lower concentrations. Toxic gases like CO, H₂S and C₆H₆ were not detected in our previous studies for WO₃ nanostructured gas sensors deposited onto alumina substrates. The typical gas sensor responses at their optimal operating temperatures to the exposure of H₂S (Figure IV.21.a), CO (Figure IV.21.b) and C₆H₆ (Figure IV.21.c) are presented in Figure IV.21.

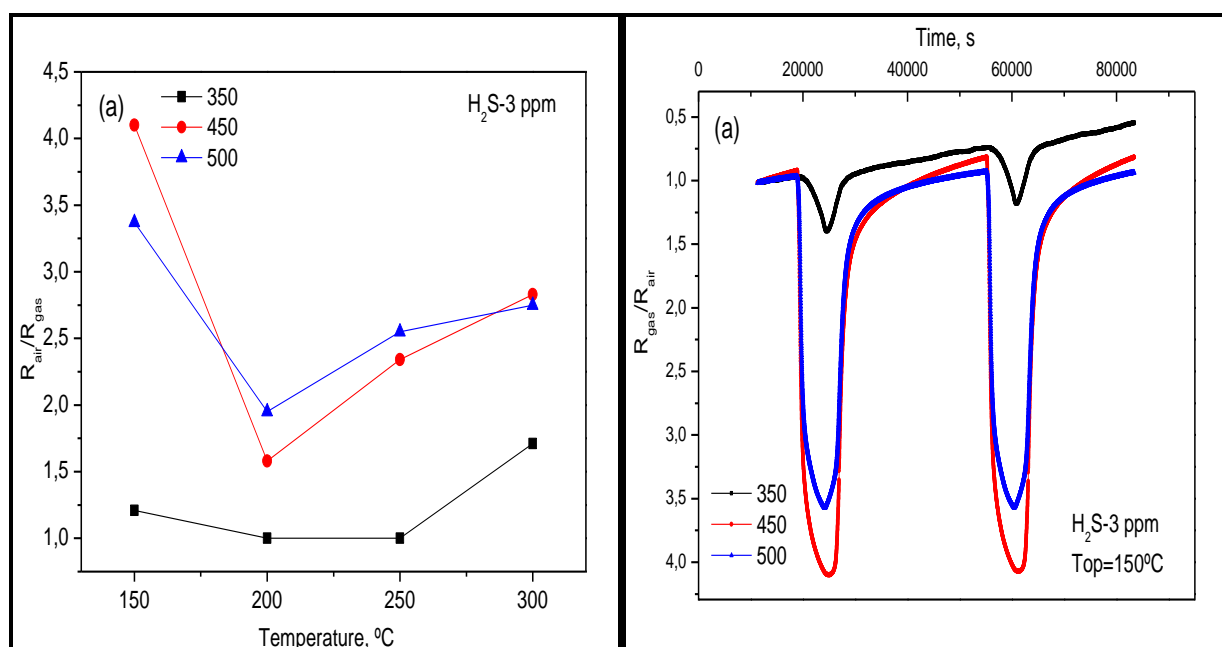


Figure IV.21.a: The temperature dependence (mean values) and maximum sensor's response (over 5 measurements) to H₂S for WO₃ gas sensors deposited at 350 °C, 450 °C and 500 °C onto microhotplate substrate

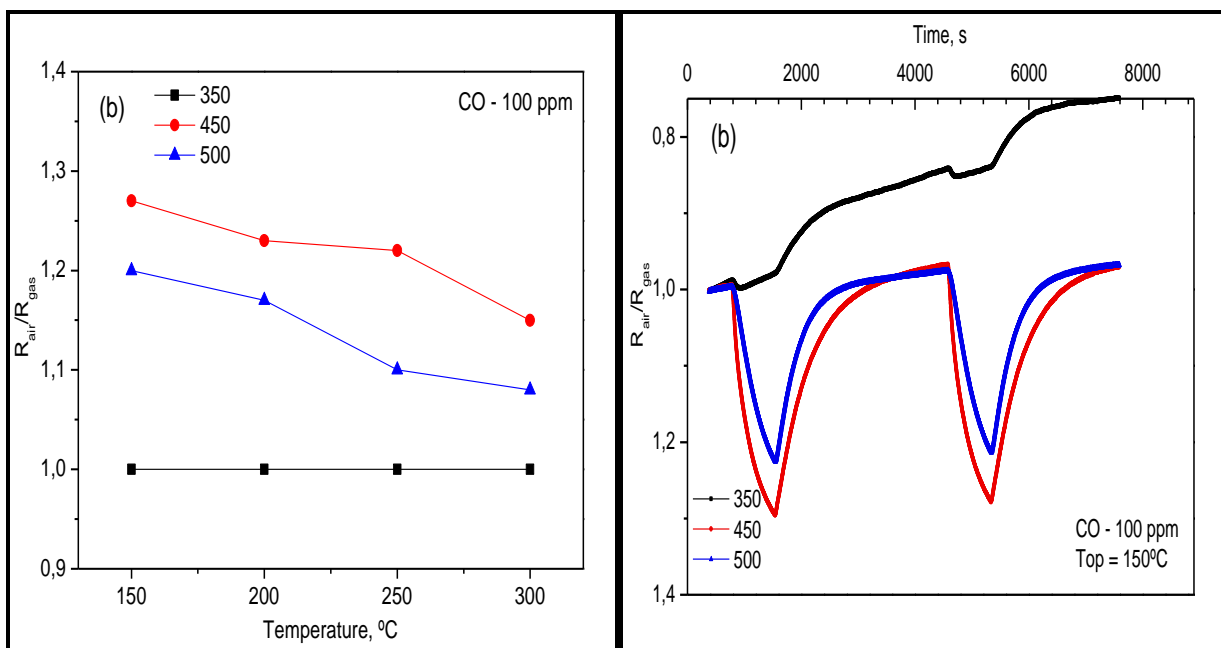


Figure IV.21.b: The temperature dependence (mean values) and maximum sensor's response (over 5 measurements) to CO for WO₃ gas sensors deposited at 350 °C, 450 °C and 500 °C onto microhotplate substrate

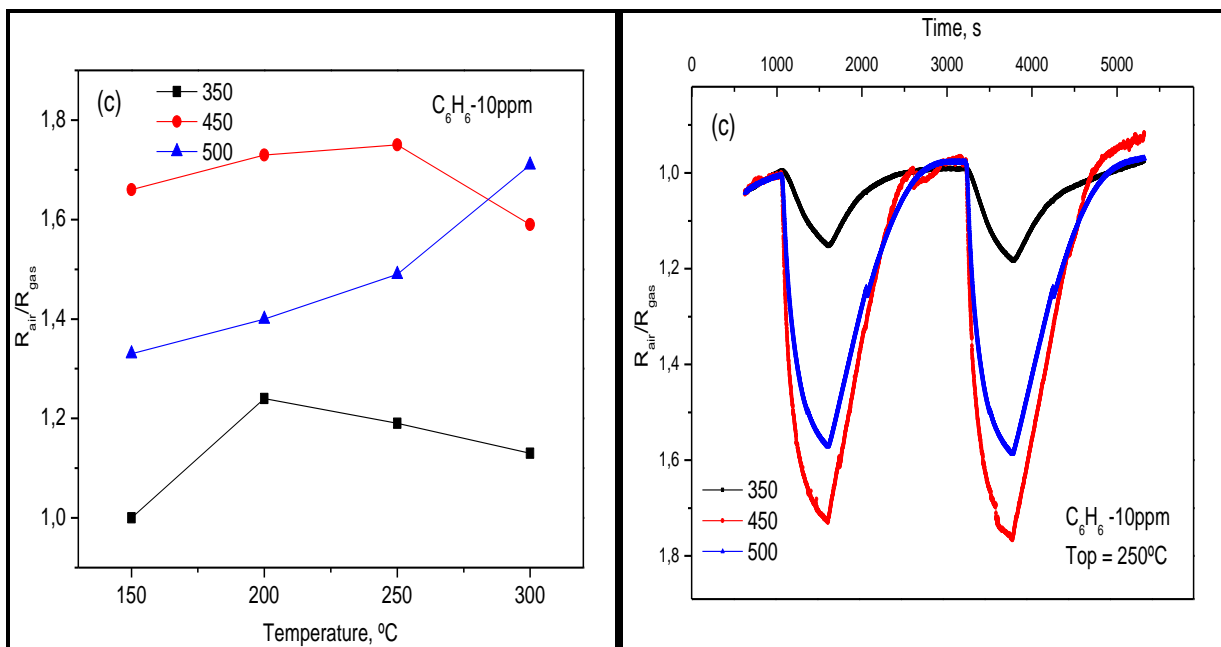


Figure IV.21.c: The temperature dependence (mean values) and maximum sensor's response (over 5 measurements) to C₆H₆ for WO₃ gas sensors deposited at 350 °C, 450 °C and 500 °C onto microhotplate substrate

In this study, the WO₃ gas sensors based on microhotplate substrate have shown normal response behaviour to reducing gases such as EtOH and H₂, i.e. they have reduced resistance when exposed to the mentioned gases. The gas sensing results obtained for H₂ were found to be lower comparing with the results obtained for alumina WO₃ gas sensors. However, at their optimum operating temperature (150 °C), the alumina WO₃ gas sensors have shown very slow response/recovery times. After achieving the deposition onto microhotplate substrate, the response/recovery times were improved for WO₃ gas sensors. Subsequently, the measured response time for 1000 ppm of H₂ at 150 °C was twice faster and the recovery time four times faster.

The microhotplate WO₃ gas sensors have shown their best response towards 1000 ppm of H₂ at 200 °C, where the sensor response coincided with our previous study (Figure IV.10.b) for gas sensors deposited onto alumina substrate. At this temperature, the measured response time was around 30% faster, while the recovery time was almost unchanged.

The microhotplate WO₃ gas sensors were sensitive to EtOH and the gas sensing response was found to be almost at the same levels when compared to the intrinsic and Au-sputtered WO₃ nanoneedle-based alumina gas sensors (Figure IV.10.a). The higher sensor response was measured at 250 °C operating temperature for both microhotplate and alumina-based gas sensors. On the other hand, the microhotplate WO₃ gas sensors were less sensitive comparing with the co-deposited Au-functionalised WO₃ nanoneedles onto alumina gas sensor substrate. This result confirmed once again that the in-situ functionalisation *via* AACVD with noble metal nanoparucules improves the gas sensing properties of the metal-oxide-based gas sensors. The typical gas sensor response to the exposure of EtOH (Figure IV.22.a) and H₂ (Figure IV.22.b) are shown below.

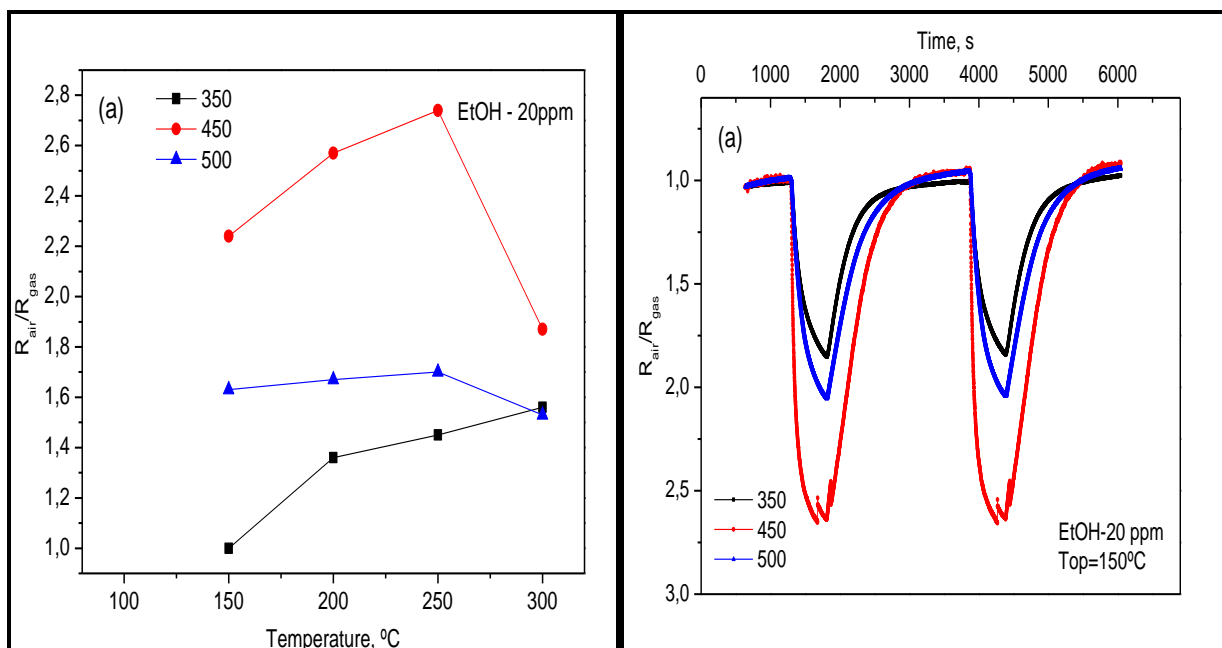


Figure IV.22.a: The temperature dependence (mean values) and maximum sensor's response (over 5 measurements) to EtOH for WO₃ gas sensors deposited at 350 °C, 450 °C and 500 °C onto microhotplate substrate

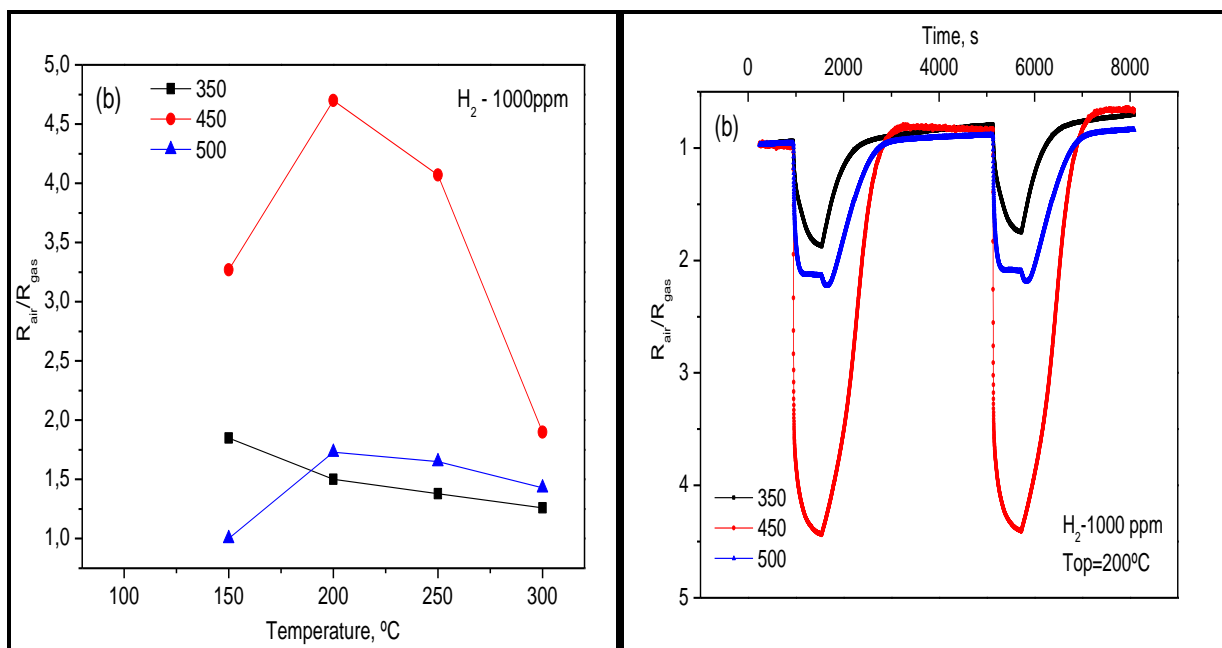


Figure IV.22.b: The temperature dependence (mean values) and maximum sensor's response (over 5 measurements) to H₂ for WO₃ gas sensors deposited at 350 °C, 450 °C and 500 °C onto microhotplate substrate

5.2.2. Sensor response - oxidizing gases

Similarly, it was examined the WO₃ gas sensors based on microhotplate substrate, when exposed to an oxidizing gas. The 450 °C/WO₃ films (i.e non-aligned nanoneedles) shown increased sensitivity to NO₂ gas and their gas sensor response was approximately ($S = 22.17$) or 3 times higher comparing with the intrinsic alumina WO₃ nanoneedle gas sensors (Figure IV.11). Higher gas sensor response to 1 ppm of NO₂ was achieved at the lower (100 °C) operating temperature, comparing with the 150 °C optimal operating temperature found for alumina WO₃ gas sensor. However, the microhotplate gas sensors based on non-aligned nanoneedles (450 °C/WO₃) had shown slower response and recovery times at this operating temperature, similarly to the alumina WO₃ nanoneedle gas sensors.

In Figure IV.23 it is displayed the temperature dependence of the microhotplate WO₃ gas sensor response, when exposed to 1 ppm of NO₂. The higher sensor response to NO₂ was observed at 100 °C, for devices based on non-aligned nanoneedle-like structure, deposited at 450 °C. However, the samples deposited at 500 °C and based on quasi-aligned WO₃ nanoneedle-like structure were less sensitive. On the other hand, the samples deposited at 350 °C and based on WO₃ polycrystalline structure have shown absence of gas sensor response for 1 ppm of NO₂ gas.

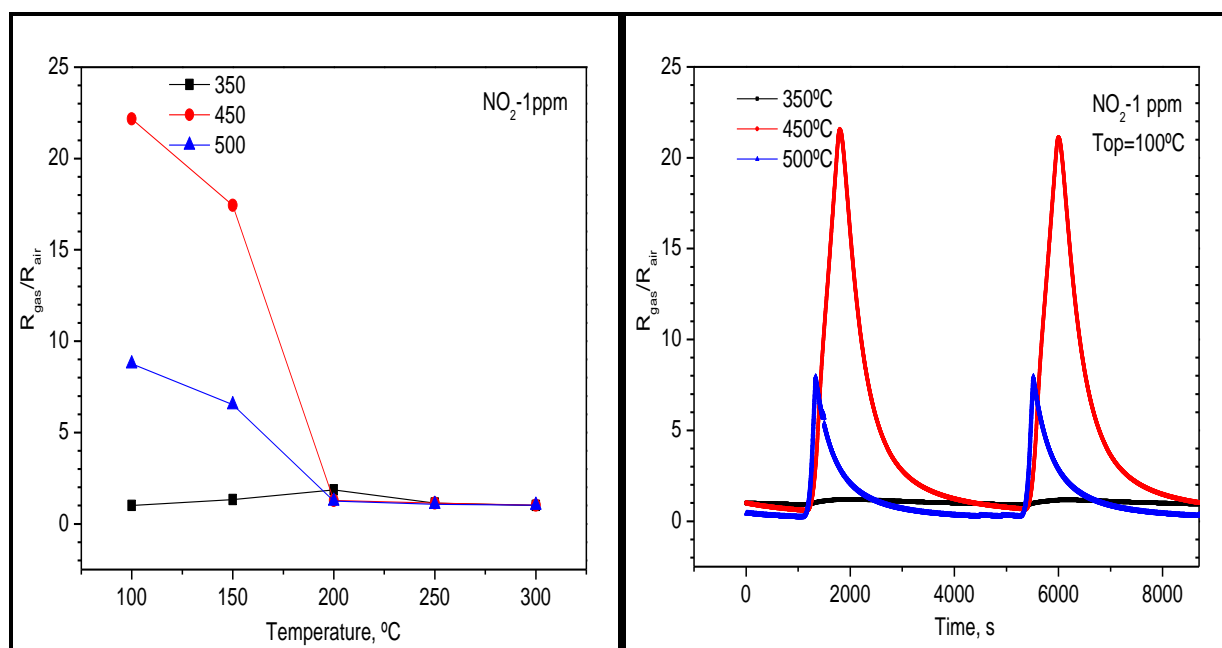


Figure IV.23: The temperature dependence (mean values) and maximum sensor's response (over 5 measurements) to NO₂ for WO₃ gas sensors deposited at 350 °C, 450 °C and 500 °C onto microhotplate substrate

Similarly to our previous study (section 3), the response and the recovery times were found to decrease when the operating temperature is increased due to the increase of the reaction velocity at the higher operating temperatures. The difference in the response and the recovery times for all the samples were not very significant, showing a slightly better time scale for the 450 °C/WO₃ nanoneedles. It was observed that the response and the recovery times were improved for gas sensors deposited onto microhotplate substrate at higher operating temperature, compared with alumina WO₃ gas sensors. For example, at 200 °C and 300 °C operating temperatures the response and the recovery times for NO₂ decreased twice. In the case of EtOH at higher operating temperatures slightly better response and recovery times were observed for alumina WO₃ gas sensors.

5.2.3. Stability

The sensor baseline resistance changes were recorded in air over the two week period. In Figure IV.24 are presented the resistance changes of the sensing layer in air for the microhotplate-based gas sensors. It was found that after the two week period of the gas characterization study, the changes in the baseline resistance were negligible for all the tested samples.

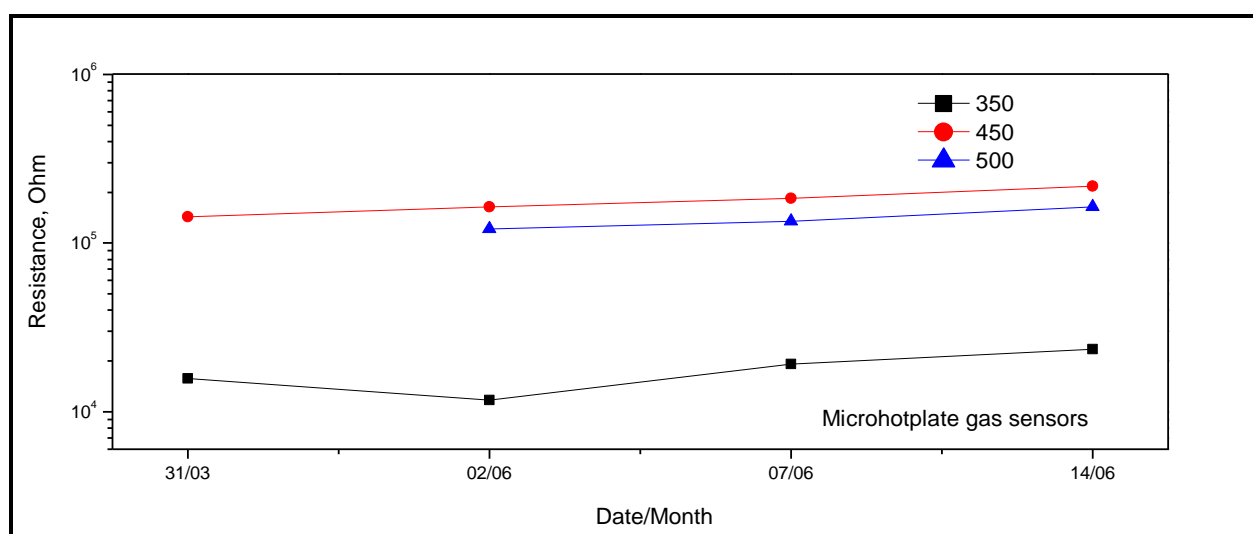


Figure IV.24: Baseline resistance of the gas sensing WO₃ layers in air over two weeks

In this study the AACVD method was used for direct deposition of WO₃ polycrystalline and nanoneedle-like structures and has proven its capability for application in the silicon technology by improving the gas sensing properties. The improved gas sensor substrate design, as well as the initial nucleation of the nanostructured layer due to the nature of the substrate surface, were found to enhance the gas sensing properties, indicating the importance of these parameters.

6. Summary

A self-catalysed direct vapour-solid mechanism was used to grow nanostructured films, where the metal vapour condenses and oxidizes directly, acting as the self-catalyst for nanoneedle growth. The results for AACVD deposition of tungsten oxide from [W(OPh)₆] dissolved in different solvents demonstrated that it is possible to selectively deposit polycrystalline or nanoneedle-like structures simply by adjusting the solvent and deposition temperature of the AACVD reaction. It was demonstrated that, the formation of the nanostructured features evolves with the increasing of the deposition temperature, while the form of the nanostructures were dependent on whether acetone, toluene or their mixture is used as the solvent. In this doctoral study it was demonstrated, that AACVD method allows deposition of nanostructured metal-oxide films and their easy integration on the gas sensor substrates by the in-situ deposition.

The three groups of WO₃ gas sensor devices, fabricated via AACVD were tested. Each of the groups is described in detail below.

The first group, studies three types of gas sensors based on: WO₃ polycrystalline film, WO₃ nanoneedle-like structure directly deposited *via* AACVD method onto classical alumina gas sensor substrates at 350 °C and 500 °C respectively, and Au-functionalised WO₃ nanoneedles achieved in the second step *via* r.f. sputtering method. We used the acetone and toluene mixture as the solvent, due to the better coverage and adhesion to the substrate, which was determined in our previous study.

The obtained gas sensing results for alumina-based gas sensor revealed a higher sensitivity of WO₃ nanostructures to NO₂ and it was observed the gas sensor response at lower concentration (1.5 ppm) of EtOH and at 1000 ppm of H₂. However,

the gas sensors were not sensitive to CO, H₂S and C₆H₆ gases. The Au-functionalised WO₃ nanoneedles (*via* r.f. sputtering) revealed better gas sensor response compared with the non-functionalised structures towards NO₂, EtOH and H₂ gases.

ESEM and XRD analysis of the films, after the gas sensing experiments, showed that the morphology and the structure of the samples were unchanged, indicating a good stability of the structures.

The second group, studies gas sensors based on Au nanoparticles functionalised WO₃ nanoneedles deposited in-situ *via* co-deposition by AACVD method. These sensing layers were directly deposited onto alumina gas sensor substrates in one single step. The gas sensors had shown a higher sensitivity to lower concentrations (1.5 ppm) of EtOH and provided a six-fold increase in the gas sensor response. These results, suggest that the AACVD method could provide a simple and flexible way to directly deposit nanostructured materials functionalised with metal nanoparticles onto defined surfaces for use in the catalysis and gas sensing.

Finally, the third group of gas sensors studies the three types of WO₃ films directly deposited onto microhotplate substrates *via* AACVD method. This demonstrated the compatibility of the AACVD method with the silicon technology by achieving a successful deposition process onto the microhotplate substrates. During the deposition process, in order to protect the contacts and the non-sensing areas, a shadow mask was used. The WO₃ films were based on polycrystalline structure deposited at 350 °C and nanoneedle-like structure deposited at 450 °C and 500 °C. The fabricated gas sensor had shown a higher sensitivity at lower concentrations (1 ppm) of NO₂ and had also shown detection of H₂S, CO and C₆H₆, whereas such toxic gases were not detected in our previous studies of WO₃ nanostructured gas sensor deposited onto alumina substrates. Moreover, the comparison of the response and the recovery times for microhotplate and alumina WO₃ gas sensors, results in an improvement of these times for the microhotplate gas sensor. These results confirm our suggestion that the shorter gap between the electrodes (~ 50µm and ~ 200µm for microhotplate and alumina gas sensor substrates respectively), as well as the initial nucleation of the nanostructured layer due to the nature of the gas sensor substrate may enhance the gas sensitivity. It was observed that the gas sensor responses for the microhotplate-based gas sensors to NO₂ were higher than for the gas sensors based on the alumina substrate.

In general, during the gas characterization study it was noticed that the gas sensors based both on alumina and microhotplate gas sensor substrates have shown absence or relatively low response to reducing gases at lower operating temperatures. At the same time, the gas sensor response to oxidising gases, such as NO₂, was higher at 100 °C and 150 °C operating temperatures. These results show the low cross sensitivity of all the fabricated WO₃ gas sensors to reducing gases, such as CO, H₂S and C₆H₆, at lower operating temperatures. On the other hand, by increasing the operating temperatures, higher responses were observed for EtOH between 250 °C and 300 °C, while the responses for the other tested gases were relatively low.

UNIVERSITAT ROVIRA I VIRGLI
FABRICATION AND GAS SENSING PROPERTIES OF PURE AND AU-FUNCTIONALISED W03 NANONEEDLE-LIKE STRUCTURES,
SYNTHESISED VIA AEROSOL ASSISTED CHEMICAL VAPOUR DEPOSITION METHOD
Toni Stoycheva
DL:T-1803-2011

**Fabrication and characterization of
intrinsic tin oxide (SnO₂)-based gas sensors
deposited *via* AACVD method**

UNIVERSITAT ROVIRA I VIRGLI
FABRICATION AND GAS SENSING PROPERTIES OF PURE AND AU-FUNCTIONALISED W03 NANONEEDLE-LIKE STRUCTURES,
SYNTHESISED VIA AEROSOL ASSISTED CHEMICAL VAPOUR DEPOSITION METHOD
Toni Stoycheva
DL:T-1803-2011

V. Fabrication and characterization of intrinsic tin oxide (SnO₂)-based gas sensors deposited *via* AACVD method

1. Introduction

A wide variety of metal-oxide gas sensors exhibit sensitivity towards oxidizing and reducing gases, changing their resistance when exposed to them. One of the first and still most frequently used metal-oxide materials for gas sensing applications is SnO₂. In 1962 Seiyama et.al [209] for the first time proposed the use of tin oxide semiconductors for detection of flammable gases. SnO₂ semiconductor sensors can be used for detection of reducing gases such as H₂, CO, hydrocarbons and other flammable gases [78, 210, 211], as well as oxidising gases such as NO₂ and other toxic gases [212, 213]. SnO₂ is an n-type semiconductor with a natural non-stoichiometry characteristic that easily adsorbs oxygen on its surface, which increases its resistance. When reducing species are adsorbed instead of oxygen, there is a drop in the resistance. SnO₂ has been widely studied for a wide range of applications and reviewed in various works [63, 214, 215].

SnO₂ nanostructures have been produced by many deposition techniques suitable for gas sensor applications [216]. However, Chemical Vapour Deposition (CVD) methods are probably the most attractive among them, where a nanostructure growth *via* the gas phase can be directly deposited onto the solid substrates for the immediate device applications. Additionally, Aerosol Assisted CVD (AACVD) as a variant of the conventional CVD provides more flexibility in the process control and improves the compatibility of the gas sensor fabrication process. Previously, SnO₂ films were deposited by AACVD method from tin complexes used as precursors and have shown dense films composed by spherical grains [167, 217]. In [167], authors deposited pure and Cu-doped SnO₂ thin films at 400 °C, using SnCl₂·2H₂O as a precursor, dissolved in ethanol. The films consisted of uniformed spherical grains with an average size of 55 nm and showed high response to 50 ppm of H₂S at 25 °C. Ying Liu et al. [217] reported the SnO₂ deposition at 850 °C from a tin(II) 2-ethylhexanoate [CH₃(CH₂)₃CH(C₂H₅)CO₂]₂Sn dissolved in ethanol. The films consisted of particles with an average size of 30 nm in diameter and manifested higher responses to 500 ppm of EtOH. These results suggest that nanostructured SnO₂ films could be formed using

similar tin precursors and adjusting certain parameters of AACVD deposition, such as the concentration of a solution or the aerosol generation. Moreover, recent works have demonstrated that the deposition of nanostructured SnO₂ was successfully implemented *via* aerosol routes [193, 218, 219].

This chapter discusses the results of the film analysis, sensor fabrication and gas sensing findings for the SnO₂ active layers, grown *via* AACVD method, using the two new tin complexes, namely [Sn(18-Cr-6)Cl₄] and [Sn(H₂O)2Cl₄](18-Cr-6), as the precursors. We describe the study of deposition conditions used for the direct SnO₂ film growth *via* AACVD method is. The obtained film morphology was determined by AFM analysis and has shown polycrystalline films, where at certain deposition conditions nanostructured features were observed. Finally, SnO₂ sensing active layers were grown *via* AACVD at 400 °C onto alumina substrates. The gas sensors characterization study was conducted by applying the experimental conditions described in point 4 of the experimental part.

2. Film analysis

2.1. Morphology

The surface morphology analysis of the SnO₂ layers was examined by AFM technique. These SnO₂ layers deposited *via* AACVD from the tin complexes I and II, with presumable structure [Sn(18-Cr-6)Cl₄] and [Sn(H₂O)2Cl₄](18-Cr-6), respectively, were observed. Due to the higher roughness of the alumina gas sensor substrates, they were not suitable for AFM analysis. For this reason, the SnO₂ films were grown on the silicon wafers and used for detailed study of the morphology of the obtained tin oxide layers. The AFM analysis revealed that the as-deposited films have closely packed polycrystalline films with particle size and geometry different for each complex and deposition temperature. The AFM results obtained for both tin complexes deposited at three different deposition temperatures are shown in Figure V.1. It was found, that particle size rises from 8 nm to 43 nm as the deposition temperature increases. Summary of the experiment conditions together with the obtained results is presented in Table V.1. Apart from the coalescence at higher temperatures, the

particles were found to change their shape as a function of deposition temperature. In the case of a tin complex I, used as a precursor, the particles acquired an unusual, oval and elongated shape at 400 °C, which was less pronounced at 550°C. This grains-like orientated morphology was not reported previously for the SnO₂ films grown *via* AACVD method.

By comparing particle sizes presented in Table V.1, it is clear that both precursors resulted in roughly the same SnO₂ particle size, taking into account the experimental error. However, one can notice that slightly smaller particles are observed at 250 °C and 400 °C for a tin complex I, while at 500 °C smaller particles were found for a tin complex II, comparing with tin complex I.

Table V.1: Summary of the experimental conditions and average particle size observed on a silicon substrate by AFM [220]

Precursor	Deposition temperature, °C	SnO ₂ mean particle size, nm
Tin complex I [Sn(18-Cr-6)Cl ₄]	250	6 – 11
	400	18 – 36
	550	28 – 52
Tin complex II [Sn(H ₂ O)2Cl ₄](18-Cr-6)	250	8 – 16
	400	20 – 42
	550	23 – 48

The obtained AFM results were used to determine the SnO₂ morphology regarding the deposition temperature and precursor used. According to this, the deposition temperature of 400 °C was chosen for sensor fabrication due to the unusual particle geometry found in a tin complex I.

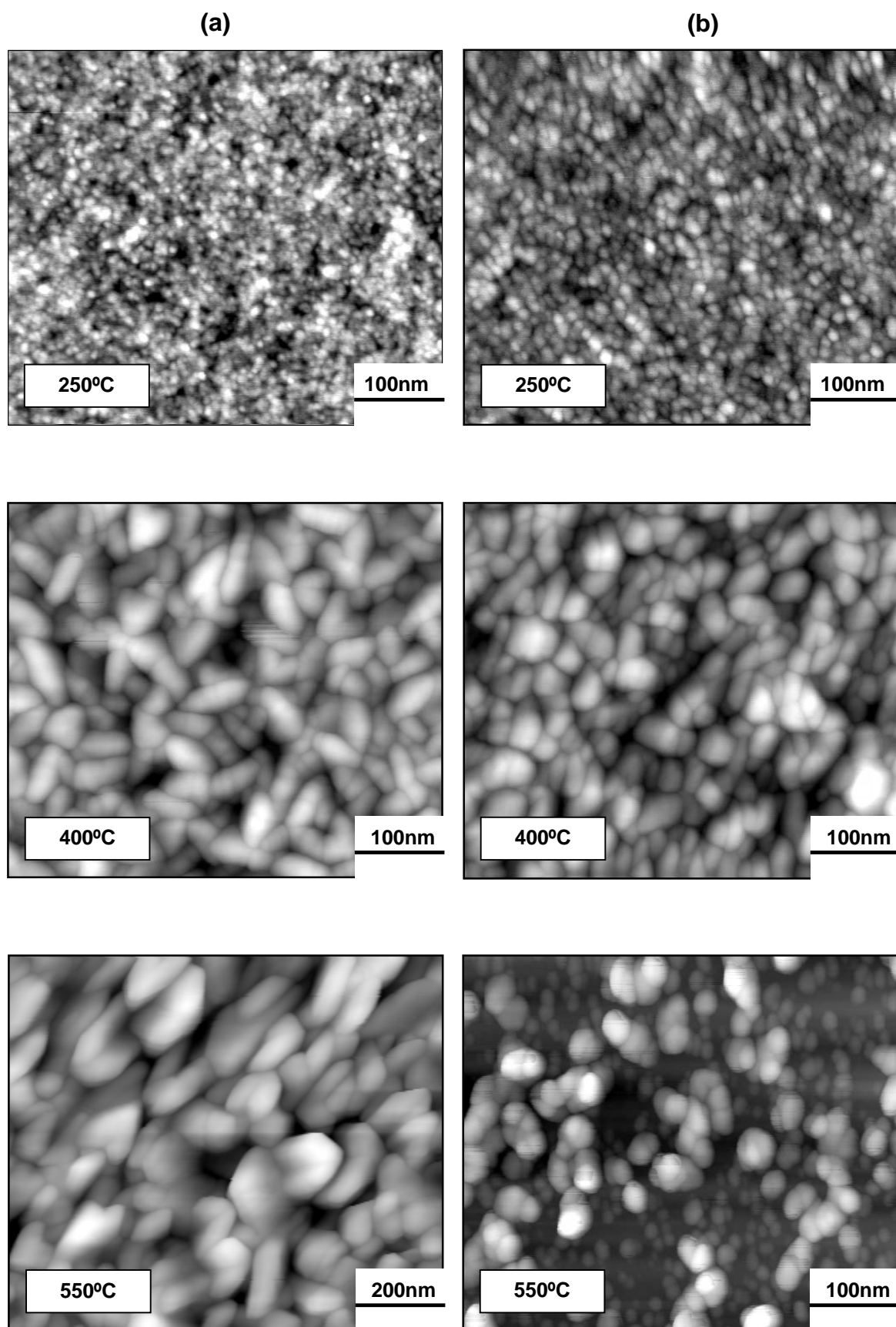


Figure V.1: AFM of tin oxide films deposited *via* AACVD at 250 °C, 400 °C and 500 °C, using tin complex I (a) and tin complex II (b) [220]

2.2. XRD analysis

The films grown on silicon wafers and alumina gas sensor substrates were analyzed by XRD method. The XRD of the as-deposited samples at 400 °C, either on alumina or silicon substrates, showed that tetragonal phase of SnO₂ with P4/mnm space group (ICDD card no. 041-1445 and lattice parameters $a = 4.73820 \text{ \AA}$ and $c = 3.18710 \text{ \AA}$), was formed from both precursors, regardless of the substrate employed. The XRD patterns obtained for the films deposited onto alumina substrate are shown in Figure V.2. The peaks assigned to Corundum (Al₂O₃) and Spinel (MgAl₂O₄) were originated from the alumina substrate. Crystalline size calculations were determined from the XRD diffractogram and revealed values of 28.3(5) nm and 16.0(4) nm for the films synthesised from a tin complex I and a tin complex II, respectively. The XRD analysis of the same samples that were annealed at 400 °C for 2 h, have shown similar results, indicating a stable structure.

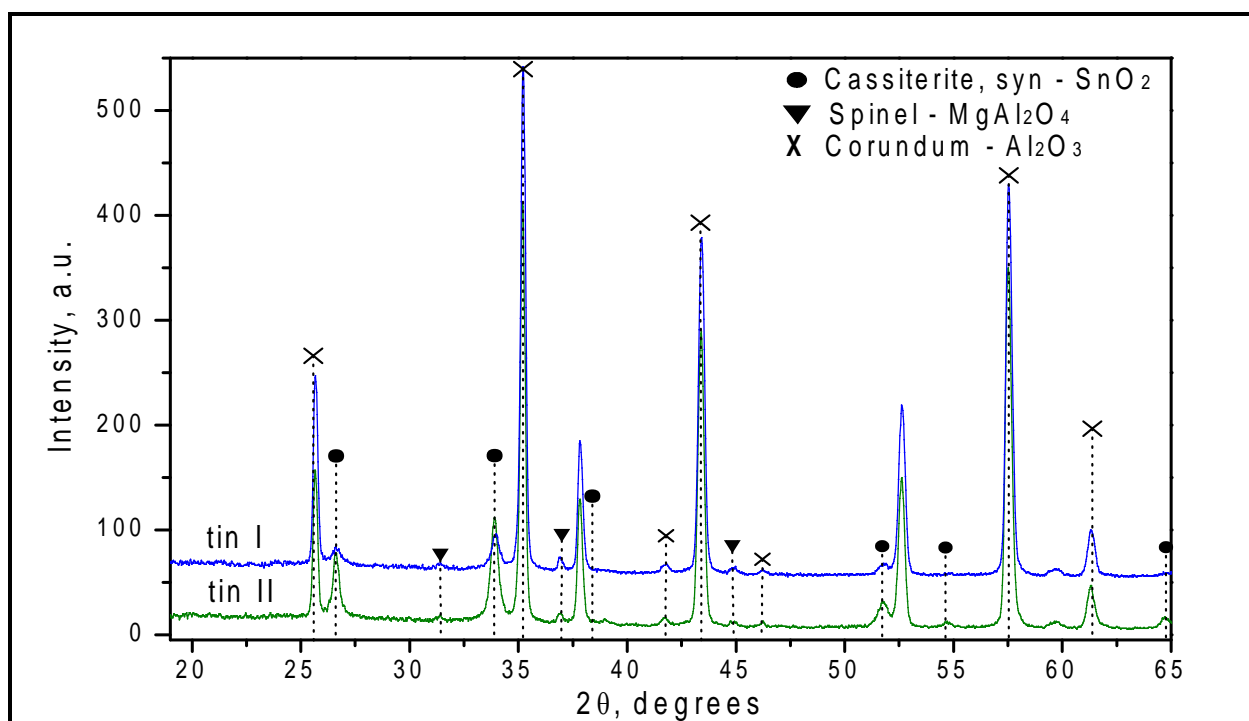


Figure V.2: X-ray pattern of tin oxide layers deposited by the AACVD at 400 °C, using a tin complex I and a tin complex II [220]

3. Gas sensing characterization

Two types of tin oxide gas sensing films were deposited at 400 °C using a tin complex I and a tin complex II, as the precursors. The sensors were tested towards the exposure of several gases (NO₂, EtOH, H₂S, C₆H₆) in synthetic air at three different operating temperatures 200°C, 250°C and 300°C.

3.1. Sensor response

The obtained gas sensing results for SnO₂-based alumina gas sensors have shown resistance changes to NO₂ gas. However, the gas sensors were not sensitive to EtOH, H₂S and C₆H₆ gases. The typical sensor responses are shown in Figure V.3 and their maximum values are summarised in Table V.2. It was observed, that the sensor response to the exposure of NO₂ gas increases with the increase of the operating temperature, showing the higher value at 300 °C.

Table V.2: Summary of the maximum sensor response at each operating temperature [220]

Precursor used	Sensing material	Operating temperature	Sensor response
		T, °C	NO ₂ , 10 ppm
Tin complex I [Sn(18-Cr-6)Cl ₄]	SnO ₂	200	1.29
		250	1.53
		300	1.70
Tin complex II [Sn(H ₂ O) ₂ Cl ₄](18-Cr-6)	SnO ₂	200	1
		250	1
		300	1.32

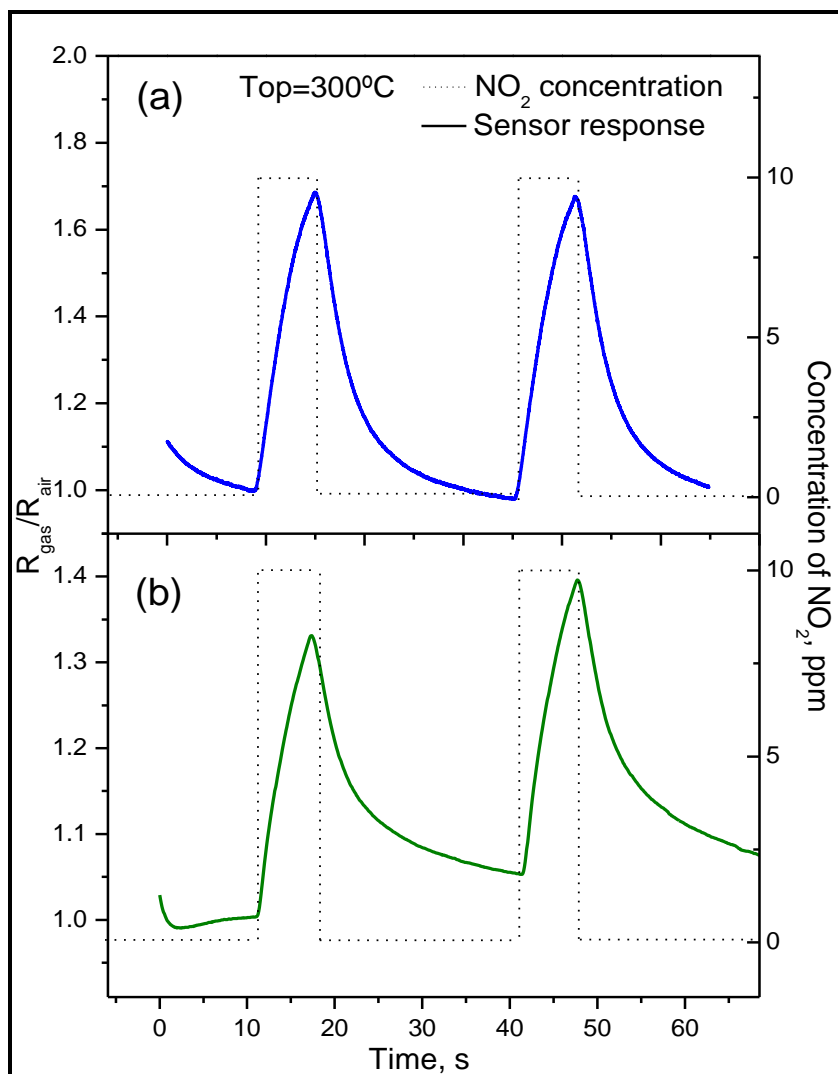


Figure V.3: Sensor response to 10 ppm NO_2 in air at 300 °C (sensor operating temperature) for the gas sensor deposited from tin complex I (a) and tin complex II (b). Both SnO_2 materials were deposited at 400 °C [220]

3.2. Stability

The sensor baseline resistance changes were recorded in air over three weeks of the experiments. In Figure V.4 are presented the resistance changes of the SnO_2 sensing layer in air, based on the alumina gas sensor substrates. It was found that during the period of the gas characterization study, the changes in the baseline resistance of the SnO_2 sensing layers deposited from tin complex II were negligible, indicating a good sensor stability. On the other hand, the resistance changes of the SnO_2 sensing layers deposited from the tin complex I were more pronounced during the first week. For both tin complexes, the XRD analysis of the films after the gas sensing

experiments, showed that the structure of the samples was unchanged, indicating a good stability of the structures.

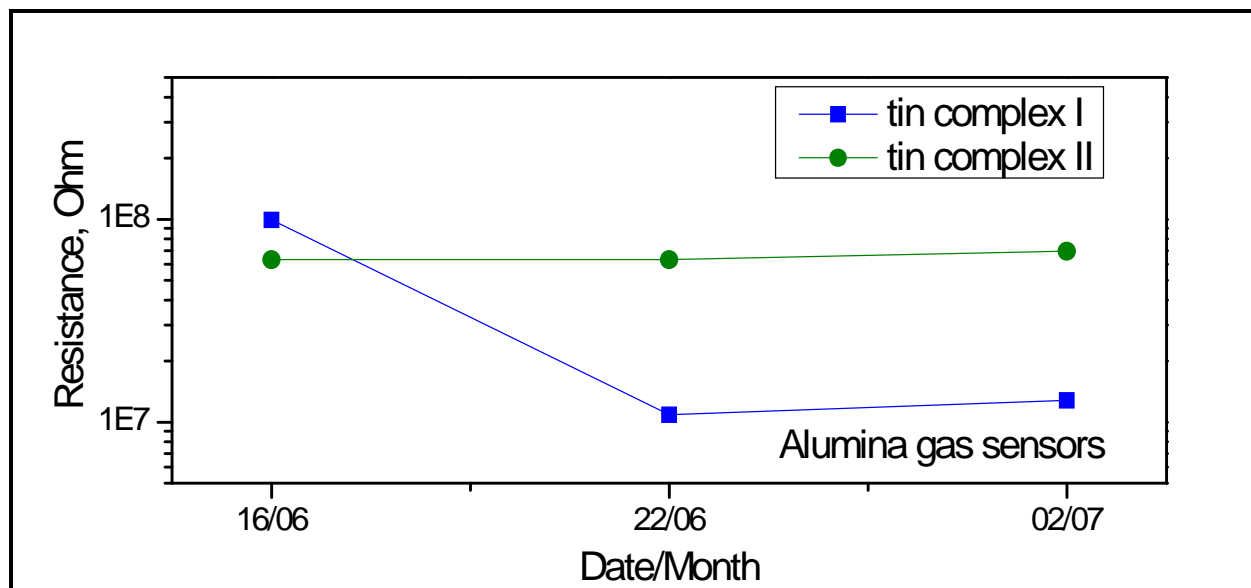


Figure IV.4: Baseline resistance changes of the gas sensing SnO₂ layers in air over three weeks

4. Summary

In this research it was found that apart from the optimization of technical parameters of the deposition (temperature, flow, solvents, substrate etc.), the selection of the precursor plays a key role in design of the deposited material properties. Similarly, it was shown [221] that the precursor solution modifies significantly the chemical nature of the molecule participating in the film development, hence the nature of the growth structure. Various precursors were reported to be used for SnO₂ synthesis, and it is unanimous that the precursor nature and its interaction with the solvent determine the particle shape and size – the most important parameters for gas sensor applications [222].

Morphology as well as sensing properties of the deposited *via* AACVD SnO₂ films have shown to be dependent on the structure and the composition of tin complexes used as SnO₂ precursors. Using the two new tin precursors it was demonstrated the possibility to grow SnO₂ layers directly onto the gas sensor substrate.

The results have shown that the new tin complex I with the presumable structure $[\text{Sn}(18\text{-Cr-6})\text{Cl}_4]$ gave unusually elongated shape of the deposited particles of SnO_2 , contradicting the results obtained from the structure from the new tin complex II - $[\text{Sn}(\text{H}_2\text{O})_2\text{Cl}_4](18\text{-Cr-6})$, where spherical particles were observed.

In our experiments, it has been found that the film deposited using a tin complex I as SnO_2 precursor, manifests slightly higher response to 10 ppm of NO_2 gas and twice shorter recovery time, comparing with the films deposited using a tin complex II. Furthermore, it was noticed that the SnO_2 gas sensor based on the alumina gas sensor substrates have shown absence of response to reducing gases such as EtOH, H_2S and C_6H_6 , while at the same time, showing gas sensor response to NO_2 .

These results show the low cross sensitivity of the fabricated SnO_2 gas sensor to reducing gases. One can note, that the sensor resistance (Figure V.2) recovers completely before reaching the initial value, 20 min after the NO_2 concentration was switched off. These preliminary gas testing results, suggest that the elongated shape of the particles and their unusual orientation may increase the specific surface area, utility factor (accessibility of the inner oxide layers to the target gas [222]), as well as the nature of the ratio of the different crystal facets exposed to the tested gas as it was remarked in [223].

In fact, several reports have shown the performance of gas sensors is strongly linked to the shape and the size of the sensing active film, displaying a positive influence on the sensitivity, stability, response/recovery times, and to some extent on the humidity effects, when the size is decreased [224]. A quantitative comparison of the sensor outputs, obtained from both the literature and from our results, is complicated since the sensor performance also depends on parameters such as the film thickness, the electrode configuration and the working temperature control.

UNIVERSITAT ROVIRA I VIRGLI
FABRICATION AND GAS SENSING PROPERTIES OF PURE AND AU-FUNCTIONALISED W03 NANONEEDLE-LIKE STRUCTURES,
SYNTHESISED VIA AEROSOL ASSISTED CHEMICAL VAPOUR DEPOSITION METHOD
Toni Stoycheva
DL:T-1803-2011

Conclusions

UNIVERSITAT ROVIRA I VIRGLI
FABRICATION AND GAS SENSING PROPERTIES OF PURE AND AU-FUNCTIONALISED W03 NANONEEDLE-LIKE STRUCTURES,
SYNTHESISED VIA AEROSOL ASSISTED CHEMICAL VAPOUR DEPOSITION METHOD
Toni Stoycheva
DL:T-1803-2011

VI. Conclusions

In this doctoral thesis the AACVD method was applied for the deposition of high-quality tungsten oxide (WO₃) nanostructured thin films. AACVD method is an extremely competitive and promising technique for gas sensors applications. The findings described herein demonstrate that AACVD method could use precursors, which are soluble in a solvent, and result in a production of a good quality films, whose morphology and the structure are dependent on experimental parameters. The presented work has dealt with the investigation of material properties of the intrinsic and Au-functionalised WO₃ films and their gas sensing application. This study has also described the surface functionalisation of WO₃ nanoneedles with gold nanoparticles. By applying ex-situ (r.f. sputtering) and in-situ (AACVD co-deposition) deposition techniques, the WO₃ nanoneedles were modified and enhancement of the gas sensing properties was observed. Additionally, tin oxide (SnO₂) thin films, synthesised from two new tin precursors, were deposited *via* AACVD method, confirming the suitability of the method to grow this popular metal-oxide for gas sensing applications. A summary of the findings of this thesis is listed below:

1. The material properties of the WO₃ films deposited *via* AACVD method, were investigated in the first part of our study. AACVD method was successfully applied for the direct growth of WO₃ nanoneedles on gas sensor substrates with the typical thickness of the films being in the range of ~7000 to 12000 nm. The nanoneedles were densely packed, non-aligned and vertically grown on top of the substrate with the typical width in the range of ~12 to 35 nm. We have successfully set up the deposition system and determined the deposition conditions for WO₃ nanoneedle growth. It was found that it is possible to selectively deposit polycrystalline or nanoneedle-like structures by simply adjusting the solvent and the deposition temperature of the AACVD reaction. The optimal deposition temperature was found to be 500 °C for WO₃ nanoneedle-like structure and 350 °C for WO₃ polycrystalline structure, when the mixture of the acetone and toluene is used as a solvent. This was used as the basis for successful deposition of sensing active films directly onto the gas sensor substrates.

2. Applying co-deposition *via* AACVD technique, the Au-functionalised nanostructured WO₃ was directly grown onto the gas sensor substrate. The fabrication of Au-functionalised WO₃ nanoneedles *via* AACVD co-deposition combined two syntheses together in one single process, which led in effect to a higher sensor response in co-deposited AACVD films for the investigated precursor. The distributed Au nanoparticles on the surface of WO₃ nanoneedles have shown the average diameters of ~10 nm. To the best of our knowledge, co-deposition *via* AACVD method was successfully used, for the first time to functionalise nanostructured metal-oxides for gas sensing applications.
3. In this study gas sensors based on a traditional alumina and microhotplate substrates have been fabricated. The successfully fabricated alumina gas sensing devices based on WO₃ polycrystalline and nanoneedle-like structures were grown at 350 °C and 500 °C deposition temperature, respectively. The AACVD method was successfully applied for the direct growth of WO₃ nanostructures onto microhotplate substrate using a shadow mask for the protection of the contacts and the non-sensing areas. The fabrication of microhotplate devices based on WO₃ was achieved at 350 °C, 450 °C and 500 °C. This in turn demonstrated that this technique is compatible with the silicon gas sensor technology.
4. The effect of Au nanoparticles on the gas sensor's response was measured and presented in this thesis. The test results revealed that the addition of Au nanoparticles to the WO₃ nanoneedles has increased the sensor's response towards the tested gases (i.e. EtOH). It was therefore demonstrated that the Au-functionalisation has an enhancing effect on the gas sensing properties of WO₃ nanoneedles. The effective functionalisation with Au nanoparticles was conducted for sensing films based on WO₃ nanoneedles using the ex-situ (r.f. sputtering) and the in-situ (co-deposition *via* AACVD) techniques. It was found that the in-situ Au-functionalisation *via* AACVD of the WO₃ nanoneedles, provides gas sensor devices with enhanced sensing properties comparing with the ex-situ Au-functionalised and intrinsic WO₃ nanoneedles. The higher sensor response ($S = 12$) was observed at 250 °C operating temperature for lower

concentrations of EtOH (1.5 ppm), which represents a six-fold increase in the sensor's response of the WO₃ nanoneedles.

5. The AACVD has proven to be an inexpensive and relatively simple implementation technique, that has various advantages and it represents a promising deposition method for the mass gas sensor production. Thus, this deposition technique may have a significant impact on the future gas sensor fabrication and will undoubtedly be used for the investigation of the nanostructured metal-oxides.
6. Finally, it was suggested that the improvement of the electrode design for the adequate exploitation of various nanostructures in commercial gas sensing devices is needed. This study concluded that the gap between the electrodes, in the gas sensor design, should be proportionate to the nanoneedle's length, thus providing an easier integration and possible linear orientation of the nanoneedles, that in turn would bring an improvement to the gas sensing properties.

UNIVERSITAT ROVIRA I VIRGLI
FABRICATION AND GAS SENSING PROPERTIES OF PURE AND AU-FUNCTIONALISED W03 NANONEEDLE-LIKE STRUCTURES,
SYNTHESISED VIA AEROSOL ASSISTED CHEMICAL VAPOUR DEPOSITION METHOD
Toni Stoycheva
DL:T-1803-2011

Bibliography

UNIVERSITAT ROVIRA I VIRGLI

FABRICATION AND GAS SENSING PROPERTIES OF PURE AND AU-FUNCTIONALISED W03 NANONEEDLE-LIKE STRUCTURES,
SYNTHESISED VIA AEROSOL ASSISTED CHEMICAL VAPOUR DEPOSITION METHOD

Toni Stoycheva

DL:T-1803-2011

VII. Bibliography

- [1] P. J. Shaver, "Activated tungsten oxide gas detectors," *Applied Physics Letters*, vol. 11, pp. 255-8, 1967.
- [2] Y.-K. Chung, *et al.*, "Gas sensing properties of WO₃ thick film for NO₂ gas dependent on process condition," *Sensors and Actuators B: Chemical*, vol. 60, pp. 49-56, 1999.
- [3] S. C. Moulzolf, *et al.*, "Stoichiometry and microstructure effects on tungsten oxide chemiresistive films," *Sensors and Actuators B: Chemical*, vol. 77, pp. 375-382, 2001.
- [4] M. Penza, *et al.*, "Tungsten trioxide (WO₃) sputtered thin films for a NO_x gas sensor," *Sensors and Actuators B: Chemical*, vol. 50, pp. 9-18, 1998.
- [5] M. Stankova, *et al.*, "Sensitivity and selectivity improvement of rf sputtered WO₃ microhotplate gas sensors," *Sensors and Actuators B: Chemical*, vol. 113, pp. 241-248, 2006.
- [6] C. G. Granqvist, "Electrochromic tungsten oxide films: Review of progress 1993-1998," *Solar Energy Materials & Solar Cells* vol. 60, pp. 201-262, 2000.
- [7] N. I. Fernandes, *et al.*, "Thermo and photochromic properties of Na₂O-WO₃-SbPO₄ glasses," *Solid State Ionics*, vol. 181, pp. 1125-1130, 2010.
- [8] R. Binions, *et al.*, "Doped and un-doped vanadium dioxide thin films prepared by atmospheric pressure chemical vapour deposition from vanadyl acetylacetonate and tungsten hexachloride: the effects of thickness and crystallographic orientation on thermochromic properties," *Journal of Materials Chemistry*, vol. 17, pp. 4652-4660, 2007.
- [9] H. Hashimoto, *et al.*, "Growth and evaporation of tungsten oxide crystals," *Journal of the Physical Society of Japan*, vol. 15, pp. 1006-1014, 1960.
- [10] ChemicalEncyclopedia. *Tungsten oxide*. Available: <http://www.xumuk.ru/encyklopedia/814.html>
- [11] *Chemical and physical information - Tungsten*. Available: <http://www.atsdr.cdc.gov/ToxProfiles/tp186-c4.pdf>
- [12] M. A. Butler, "Photoelectrolysis and physical properties of semiconducting electrode WO₃," *Journal of Applied Physics*, vol. 48, pp. 1914-1920, 1977.
- [13] E. Lassner and W.-D. Schubert, *Tungsten: properties, chemistry, technology of the element, alloys, and chemical compounds*: Plenum Publishers, New York, 1999.
- [14] N. Taguchi, "Gas detecting device," US No. 3631436 Patent, 1971.
- [15] Y. Shimizu and M. Egashira, "Basic aspects and challenges of semiconductor gas sensors," *Mrs Bulletin*, vol. 24, pp. 18-24, Jun 1999.
- [16] L. Y. Kupriyanov, *Semiconductor sensors in physico-chemical studies*: Elsevier, 1996.
- [17] FigaroEngineering. *Operating principle of semiconductor type gas sensors*. Available: <http://www.figaro.co.jp/en/item2.html>
- [18] D. E. Williams, *et al.*, "Modelling the response of a tungsten oxide semiconductor as a gas sensor for the measurement of ozone," *Measurement Science & Technology*, vol. 13, pp. 923-931, Jun 2002.
- [19] S. M. Kanan, *et al.*, "Semiconducting metal oxide based sensors for selective gas pollutant detection," *Sensors*, pp. 8158-8196, 2009.
- [20] *Solid-state gas sensors*. Available: <http://www.intlsensor.com/pdf/solidstate.pdf>
- [21] J.-I. Yang, *et al.*, "Influence of binders on the sensing and electrical characteristics of WO₃-based gas sensors," *Sensors and Actuators B: Chemical*, vol. 60, pp. 71-77, 1999.
- [22] H. Meixner and U. Lampe, "Metal oxide sensors," *Sensors and Actuators B: Chemical*, vol. 33, pp. 198-202, 1996.
- [23] J. Shieh, *et al.*, "WO₃ and W---Ti---O thin-film gas sensors prepared by sol-gel dip-coating," *Sensors and Actuators B: Chemical*, vol. 86, pp. 75-80, 2002.
- [24] T. Siciliano, *et al.*, "WO₃ gas sensors prepared by thermal oxidization of tungsten," *Sensors and Actuators B: Chemical*, vol. 133, pp. 321-326, 2008.
- [25] C.-J. Jin, *et al.*, "Dependence of NO₂ gas sensitivity of WO₃ sputtered films on film density," *Thin Solid Films*, vol. 474, pp. 255-260, 2005.

- [26] I. M. Szilágyi, *et al.*, "Gas sensing selectivity of hexagonal and monoclinic WO₃ to H₂S," *Solid State Sciences*, vol. 12, pp. 1857-1860, 2010.
- [27] L. F. Reyes, *et al.*, "Gas sensor response of pure and activated WO₃ nanoparticle films made by advanced reactive gas deposition," *Sensors and Actuators B: Chemical*, vol. 117, pp. 128-134, 2006.
- [28] C. Zhang, *et al.*, "Sensing properties of atmospheric plasma-sprayed WO₃ coating for sub-ppm NO₂ detection," *Sensors and Actuators B: Chemical*, vol. 144, pp. 280-288, 2010.
- [29] Y.-G. Choi, *et al.*, "Wet process-based fabrication of WO₃ thin film for NO₂ detection," *Sensors and Actuators B: Chemical*, vol. 101, pp. 107-111, 2004.
- [30] H. Kawasaki, *et al.*, "Properties of metal doped tungsten oxide thin films for NO_x gas sensors grown by PLD method combined with sputtering process," *Sensors and Actuators B: Chemical*, vol. 100, pp. 266-269, 2004.
- [31] C. Matei Ghimbeu, *et al.*, "Detection of H₂S, SO₂, and NO₂ using electrostatic sprayed tungsten oxide films," *Materials Science in Semiconductor Processing*, vol. 13, pp. 1-8, 2010.
- [32] Z. Liu, *et al.*, "Facile synthesis and NO₂ gas sensing of tungsten oxide nanorods assembled microspheres," *Sensors and Actuators B: Chemical*, vol. 140, pp. 514-519, 2009.
- [33] A. A. Tomchenko, *et al.*, "WO₃ thick-film gas sensors," *Sensors and Actuators B: Chemical*, vol. 46, pp. 8-14, 1998.
- [34] J. Tamaki, *et al.*, "Detection of dilute nitrogen dioxide and thickness effect of tungsten oxide thin film sensors," *Sensors and Actuators B: Chemical*, vol. 95, pp. 111-115, 2003.
- [35] I. Jiménez, *et al.*, "Crystalline structure, defects and gas sensor response to NO₂ and H₂S of tungsten trioxide nanopowders," *Sensors and Actuators B: Chemical*, vol. 93, pp. 475-485, 2003.
- [36] G. Xie, *et al.*, "Gas sensing characteristics of WO₃ vacuum deposited thin films," *Sensors and Actuators B: Chemical*, vol. 123, pp. 909-914, 2007.
- [37] A. Ponzoni, *et al.*, "Structural and gas-sensing characterization of tungsten oxide nanorods and nanoparticles," *Sensors and Actuators B: Chemical*, vol. In Press, Corrected Proof, 2010.
- [38] Y. Qin, *et al.*, "Effect of annealing on microstructure and NO₂-sensing properties of tungsten oxide nanowires synthesized by solvothermal method," *Sensors and Actuators B: Chemical*, vol. In Press, Accepted Manuscript.
- [39] Y. Qin, *et al.*, "Microstructure characterization and NO₂-sensing properties of tungsten oxide nanostructures," *Sensors and Actuators B: Chemical*, vol. 150, pp. 339-345, 2010.
- [40] A. Yan, *et al.*, "Synthesis, formation mechanism and sensing properties of WO₃ hydrate nanowire netted-spheres," *Materials Research Bulletin*, vol. 45, pp. 1541-1547, 2010.
- [41] J. L. Solis, *et al.*, "Semiconductor gas sensors based on nanostructured tungsten oxide," *Thin Solid Films*, vol. 391, pp. 255-260, 2001.
- [42] M. Stankova, *et al.*, "Detection of SO₂ and H₂S in CO₂ stream by means of WO₃-based micro-hotplate sensors," *Sensors and Actuators B: Chemical*, vol. 102, pp. 219-225, 2004.
- [43] J. L. Solis, *et al.*, "Nanocrystalline tungsten oxide thick-films with high sensitivity to H₂S at room temperature," *Sensors and Actuators B: Chemical*, vol. 77, pp. 316-321, 2001.
- [44] R. Ionescu, *et al.*, "Ethanol and H₂S gas detection in air and in reducing and oxidising ambience: application of pattern recognition to analyse the output from temperature-modulated nanoparticulate WO₃ gas sensors," *Sensors and Actuators B: Chemical*, vol. 104, pp. 124-131, 2005.
- [45] L. J. LeGore, *et al.*, "The optimization of a tungsten trioxide film for application in a surface acoustic wave gas sensor," *Sensors and Actuators B: Chemical*, vol. 35, pp. 164-169, 1996.
- [46] L. F. Zhu, *et al.*, "Self-heated hydrogen gas sensors based on Pt-coated W₁₈O₄₉ nanowire networks with high sensitivity, good selectivity and low power consumption," *Sensors and Actuators B: Chemical*, vol. In Press, Corrected Proof.

- [47] C. S. Rout, *et al.*, "H₂S sensors based on tungsten oxide nanostructures," *Sensors and Actuators B: Chemical*, vol. 128, pp. 488-493, 2008.
- [48] M. Decarli, *et al.*, "Integration of a technique for the deposition of nanostructured films with MEMS-based microfabrication technologies: Application to micro gas sensors," *Microelectronic Engineering*, vol. 86, pp. 1247-1249, 2009.
- [49] K. Galatsis, *et al.*, "Comparison of single and binary oxide MoO₃, TiO₂ and WO₃ sol-gel gas sensors," *Sensors and Actuators B: Chemical*, vol. 83, pp. 276-280, 2002.
- [50] M. Stankova, *et al.*, "Influence of the annealing and operating temperatures on the gas-sensing properties of rf sputtered WO₃ thin-film sensors," *Sensors and Actuators B: Chemical*, vol. 105, pp. 271-277, 2005.
- [51] M. Sriyudthsak and S. Supothina, "Humidity-insensitive and low oxygen dependence tungsten oxide gas sensors," *Sensors and Actuators B: Chemical*, vol. 113, pp. 265-271, 2006.
- [52] S. Vallejos, *et al.*, "Au nanoparticle-functionalised WO₃ nanoneedles and their application in high sensitivity gas sensor devices," *Chemical Communications*, vol. 47, pp. 565-567, 2011.
- [53] Y. S. Kim, "Thermal treatment effects on the material and gas-sensing properties of room-temperature tungsten oxide nanorod sensors," *Sensors and Actuators B: Chemical*, vol. 137, pp. 297-304, 2009.
- [54] N. V. Hieu, *et al.*, "Preparing large-scale WO₃ nanowire-like structure for high sensitivity NH₃ gas sensor through a simple route," *Current Applied Physics*, vol. In Press, Corrected Proof.
- [55] T. D. Senguttuvan, *et al.*, "Gas sensing properties of nanocrystalline tungsten oxide synthesized by acid precipitation method," *Sensors and Actuators B: Chemical*, vol. 150, pp. 384-388, 2010.
- [56] R. Triantafyllopoulou, *et al.*, "Nanostructured oxides on porous silicon microhotplates for NH₃ sensing," *Microelectronic Engineering*, vol. 85, pp. 1116-1119, 2008.
- [57] Y. M. Zhao and Y. Q. Zhu, "Room temperature ammonia sensing properties of W₁₈O₄₉ nanowires," *Sensors and Actuators B: Chemical*, vol. 137, pp. 27-31, 2009.
- [58] L. F. Zhu, *et al.*, "Study of physical and chemical processes of H₂ sensing of Pt-coated WO₃ nanowire films," *The Journal of Physical Chemistry C*, vol. 114, pp. 15504-15509, 2010.
- [59] C. Zhang, *et al.*, "Highly sensitive hydrogen sensors based on co-sputtered platinum-activated tungsten oxide films," *International Journal of Hydrogen Energy*, vol. 36, pp. 1107-1114, 2011.
- [60] A. Boudiba, *et al.*, "Preparation of highly selective, sensitive and stable hydrogen sensors based on Pd-doped tungsten trioxide," *Procedia Engineering*, vol. 5, pp. 180-183, 2010.
- [61] M. Bendahan, *et al.*, "Characterization of ozone sensors based on WO₃ reactively sputtered films: influence of O₂ concentration in the sputtering gas, and working temperature," *Sensors and Actuators B: Chemical*, vol. 100, pp. 320-324, 2004.
- [62] C. Cantalini, *et al.*, "Investigation on the O₃ sensitivity properties of WO₃ thin films prepared by sol-gel, thermal evaporation and r.f. sputtering techniques," *Sensors and Actuators B: Chemical*, vol. 64, pp. 182-188, 2000.
- [63] C. Wang, *et al.*, "Metal oxide gas sensors: Sensitivity and influencing factors," *Sensors*, vol. 10, pp. 2088-2106, 2010.
- [64] P. Ivanov, *et al.*, "On the effects of the materials and the noble metal additives to NO₂ detection," *Sensors and Actuators B: Chemical*, vol. 118, pp. 311-317, 2006.
- [65] V. Khatko, *et al.*, "Gas sensing properties of WO₃ thin films deposited by rf sputtering," *Sensors and Actuators B: Chemical*, vol. 126, pp. 400-405, 2007.
- [66] F. Mitsugi, *et al.*, "Pulsed laser deposited WO₃ thin films for gas sensor," *Surface and Coatings Technology*, vol. 169-170, pp. 553-556, 2003.
- [67] K. L. Choy, "Vapor processing of nanostructured materials," in *Handbook of Nanostructured Materials and Nanotechnology*, N. Hari Singh, *et al.*, Eds., ed Burlington: Academic Press, pp. 533-577, 2000.

- [68] S. Ashraf, *et al.*, "Aerosol assisted chemical vapour deposition of WO₃ thin films from tungsten hexacarbonyl and their gas sensing properties," *Journal of Materials Chemistry*, vol. 17, pp. 3708-3713, 2007.
- [69] S. Ashraf, *et al.*, "The APCVD of tungsten oxide thin films from reaction of WCl₆ with ethanol and results on their gas-sensing properties," *Polyhedron*, vol. 26, pp. 1493-1498, 2007.
- [70] K. J. Choi and H. W. Jang, "One-dimensional oxide nanostructures as gas-sensing materials: review and issues," *Sensors*, vol. 10, pp. 4083-4099, Apr 2010.
- [71] E. Comini, *et al.*, "Quasi-one dimensional metal oxide semiconductors: Preparation, characterization and application as chemical sensors," *Progress in Materials Science*, vol. 54, pp. 1-67, 2009.
- [72] C. C. Koch, *Nanostructured materials: processing, properties, and applications*: William Andrew Pub., 2007.
- [73] J. P. Reithmaier, *et al.*, *Nanostructured materials for advanced technological applications*: Springer, 2009.
- [74] S. Barth, *et al.*, "Synthesis and applications of one-dimensional semiconductors," *Progress in Materials Science*, vol. 55, pp. 563-627, 2010.
- [75] X.-J. Huang and Y.-K. Choi, "Chemical sensors based on nanostructured materials," *Sensors and Actuators B: Chemical*, vol. 122, pp. 659-671, 2007.
- [76] A. Liu, "Towards development of chemosensors and biosensors with metal-oxide-based nanowires or nanotubes," *Biosensors and Bioelectronics*, vol. 24, pp. 167-177, 2008.
- [77] G. Bläser, *et al.*, "Nanostructured semiconductor gas sensors to overcome sensitivity limitations due to percolation effects," *Physica A: Statistical Mechanics and its Applications*, vol. 266, pp. 218-223, 1999.
- [78] N. Yamazoe, "New approaches for improving semiconductor gas sensors," *Sensors and Actuators B: Chemical*, vol. 5, pp. 7-19, 1991.
- [79] A. Kolmakov, *et al.*, "Functionalizing nanowires with catalytic nanoparticles for gas sensing application," *Journal of Nanoscience and Nanotechnology*, vol. 8, pp. 111-121, Jan 2008.
- [80] J. S. Williams, "Ion implantation of semiconductors," *Materials Science and Engineering A*, vol. 253, pp. 8-15, 1998.
- [81] R. G. Palgrave and I. P. Parkin, "Aerosol assisted chemical vapor deposition using nanoparticle precursors: A route to nanocomposite thin films," *Journal of the American Chemical Society*, vol. 128, pp. 1587-1597, Feb 2006.
- [82] Q. Xiang, *et al.*, "Au nanoparticle modified WO₃ nanorods with their enhanced properties for photocatalysis and gas sensing," *Journal of Physical Chemistry C*, vol. 114, pp. 2049-2055, Feb 2010.
- [83] B. Zhang, *et al.*, "Synthesis of single-crystalline potassium-doped tungsten oxide nanosheets as high-sensitive gas sensors," *Journal of Alloys and Compounds*, vol. 439, pp. 55-58, Jul 2007.
- [84] N. S. Ramgir, *et al.*, "A room temperature nitric oxide sensor actualized from Ru-doped SnO₂ nanowires," *Sensors and Actuators B: Chemical*, vol. 107, pp. 708-715, 2005.
- [85] Y. Shen, *et al.*, "Microstructure and H₂ gas sensing properties of undoped and Pd-doped SnO₂ nanowires," *Sensors and Actuators B: Chemical*, vol. 135, pp. 524-529, 2009.
- [86] L. Liu, *et al.*, "Improved H₂ sensing properties of Co-doped SnO₂ nanofibers," *Sensors and Actuators B: Chemical*, vol. 150, pp. 806-810, 2010.
- [87] J. M. Baik, *et al.*, "Tin-oxide-nanowire-based electronic nose using heterogeneous catalysis as a functionalization strategy," *Acs Nano*, vol. 4, pp. 3117-3122, Jun 2010.
- [88] R. K. Joshi, *et al.*, "Au decorated zinc oxide nanowires for CO sensing," *Journal of Physical Chemistry C*, vol. 113, pp. 16199-16202, Sep 2009.
- [89] X. H. Liu, *et al.*, "Amino acid-assisted one-pot assembly of Au, Pt nanoparticles onto one-dimensional ZnO microrods," *Nanoscale*, vol. 2, pp. 1178-1184, 2010.
- [90] G. K. Mor, *et al.*, *A room-temperature TiO₂-nanotube hydrogen sensor able to self-clean photoactively from environmental contamination* vol. 19. Warrendale: Materials Research Society, 2004.

- [91] G. Cao, "Nanostructures and nanomaterials: Synthesis, properties and applications," *London, UK: Imperial College Press*, 2004.
- [92] E. I. Givargizov and A. M. Melnikova, "Growth of crystals," *Plenum Publishers, New York*, vol. 21, 1987.
- [93] Y. N. Xia, *et al.*, "One-dimensional nanostructures: Synthesis, characterization, and applications," *Advanced Materials*, vol. 15, pp. 353-389, Mar 2003.
- [94] D. Mijatovic, *et al.*, "Technologies for nanofluidic systems: top-down vs. bottom-up-a review," *Lab on a Chip*, vol. 5, pp. 492-500, 2005.
- [95] R. S. Wagner and W. C. Ellis, "Vapor-liquid solid mechanism of single crystal growth " *Applied Physics Letters*, vol. 4, pp. 89-90, 1964.
- [96] K. W. Kolasinski, "Catalytic growth of nanowires: Vapor-liquid-solid, vapor-solid-solid, solution-liquid-solid and solid-liquid-solid growth," *Current Opinion in Solid State and Materials Science*, vol. 10, pp. 182-191, 2006.
- [97] G. W. Sears, "A growth mechanism for mercury whiskers," *Acta Metallurgica*, vol. 3, pp. 361-366, 1955.
- [98] D. Calestani, *et al.*, "Low temperature thermal evaporation growth of aligned ZnO nanorods on ZnO film: a growth mechanism promoted by Zn nanoclusters on polar surfaces," *CrystEngComm*, vol. 13, pp. 1707-1712, 2011.
- [99] J. Thangala, *et al.*, "Large-scale, Hot-Filament-Assisted synthesis of tungsten oxide and related transition metal oxide nanowires," *Small*, vol. 3, pp. 890-896, 2007.
- [100] S. Sharma and M. K. Sunkara, "Direct synthesis of gallium oxide tubes, nanowires and nanopaintbrushes," *Journal of the American Chemical Society*, vol. 124, pp. 12288-12293, 2002.
- [101] S. Vaddiraju, *et al.*, "Mechanisms of 1D crystal growth in reactive vapor transport: Indium nitride nanowires," *Nano Letters*, vol. 5, pp. 1625-1631, 2005.
- [102] J. Huang and Q. Wan, "Gas sensors based on semiconducting metal oxide one-dimensional nanostructures," *Sensors*, vol. 9, pp. 9903-9924, 2009.
- [103] N. S. Ramgir, *et al.*, "Nanowire-based sensors," *Small*, vol. 6, pp. 1705-1722, 2010.
- [104] A. Tischner, *et al.*, "Tin oxide nanocrystalline films and nanowires for gas sensing applications," *Microelectronic Engineering*, vol. 86, pp. 1258-1261, 2008.
- [105] S. Santra, *et al.*, "CMOS alcohol sensor employing ZnO nanowire sensing films," in *Olfaction and Electronic Nose, Proceedings*. vol. 1137, M. Pardo and G. Sberveglieri, Eds., ed Melville: Amer Inst Physics, pp. 119-122, 2009.
- [106] J. Q. Xu, *et al.*, "Uniform ZnO nanorods can be used to improve the response of ZnO gas sensor," *Materials Science and Engineering B-Advanced Functional Solid-State Materials*, vol. 150, pp. 55-60, Apr 2008.
- [107] N. K. Singh, *et al.*, "Optical and room temperature sensing properties of highly oxygen deficient flower-like ZnO nanostructures," *Applied Surface Science*, vol. 257, pp. 1544-1549, 2010.
- [108] J. Park and J. Y. Oh, "Highly-sensitive NO₂ detection of ZnO nanorods grown by a sonochemical process," *Journal of the Korean Physical Society*, vol. 55, pp. 1119-1122, Sep 2009.
- [109] T. Krishnakumar, *et al.*, "CO gas sensing of ZnO nanostructures synthesized by an assisted microwave wet chemical route," *Sensors and Actuators B: Chemical*, vol. 143, pp. 198-204, 2009.
- [110] E. Comini, *et al.*, "Stable and highly sensitive gas sensors based on semiconducting oxide nanobelts," *Applied Physics Letters*, vol. 81, pp. 1869-1871, Sep 2002.
- [111] F. Hernández-Ramírez, *et al.*, "High response and stability in CO and humidity measures using a single SnO₂ nanowire," *Sensors and Actuators B: Chemical*, vol. 121, pp. 3-17, 2007.
- [112] M. R. Yang, *et al.*, "Synthesis and study of the SnO₂ nanowires growth," *Sensors and Actuators B-Chemical*, vol. 122, pp. 269-273, Mar 2007.
- [113] Z. Zhan, *et al.*, "Flame aerosol reactor synthesis of nanostructured SnO₂ thin films: High gas-sensing properties by control of morphology," *Sensors and Actuators B: Chemical*, vol. 150, pp. 609-615, 2010.

- [114] L. Francioso, *et al.*, "TiO₂ nanowires array fabrication and gas sensing properties," *Sensors and Actuators B: Chemical*, vol. 130, pp. 70-76, 2008.
- [115] I. D. Kim, *et al.*, "Ultrasensitive chemiresistors based on electrospun TiO₂ nanofibers," *Nano Letters*, vol. 6, pp. 2009-2013, Sep 2006.
- [116] E. Li, *et al.*, "Indium oxide with novel morphology: Synthesis and application in C₂H₅OH gas sensing," *Crystal Growth & Design*, vol. 9, pp. 2146-2151, May 2009.
- [117] N. Du, *et al.*, "Porous indium oxide nanotubes: Layer-by-layer assembly on carbon-nanotube templates and application for room-temperature NH₃ gas sensors," *Advanced Materials*, vol. 19, pp. 1641-1645, Jun 2007.
- [118] D. H. Zhang, *et al.*, "Push the limit of metal oxide nanowire chemical sensing: selective detection of NO₂ down to ppb levels," in *Nanosensing: Materials and Devices*. vol. 5593, M. S. Islam and A. K. Dutta, Eds., ed Bellingham: Spie-Int Soc Optical Engineering, pp. 207-214, 2004.
- [119] G. Shaw, *et al.*, "Control of semiconducting oxide gas-sensor microstructure by application of an electric field during aerosol-assisted chemical vapour deposition," *Journal of Materials Chemistry*, vol. 15, pp. 149-154, 2005.
- [120] K. M. Sawicka, *et al.*, "Metal oxide nanowires for use in chemical sensing applications," *Sensor Letters*, vol. 3, pp. 31-35, Mar 2005.
- [121] M. Breedon, *et al.*, "Synthesis of nanostructured tungsten oxide thin films: A simple, controllable, inexpensive, aqueous sol-gel method," *Crystal Growth & Design*, vol. 10, pp. 430-439, 2009.
- [122] Y. S. Kim, *et al.*, "Room-temperature semiconductor gas sensor based on nonstoichiometric tungsten oxide nanorod film," *Applied Physics Letters*, vol. 86, May 2005.
- [123] Y. Li, *et al.*, "Ethanol sensing properties of tungsten oxide nanorods prepared by microwave hydrothermal method," *Ceramics International*, vol. 36, pp. 1917-1920, 2010.
- [124] Y. S. Kim, "Thermal treatment effects on the material and gas-sensing properties of room-temperature tungsten oxide nanorod sensors," *Sensors and Actuators B-Chemical*, vol. 137, pp. 297-304, Mar 2009.
- [125] D. L. Chen, *et al.*, "The enhanced alcohol-sensing response of ultrathin WO₃ nanoplates," *Nanotechnology*, vol. 21, Jan 2010.
- [126] N. V. Hieu, *et al.*, "Preparing large-scale WO₃ nanowire-like structure for high sensitivity NH₃ gas sensor through a simple route," *Current Applied Physics*, vol. 11, pp. 657-661, 2011.
- [127] Y. M. Zhao and Y. Q. Zhu, "Room temperature ammonia sensing properties of W₁₈O₄₉ nanowires," *Sensors and Actuators B: Chemical*, vol. 137, pp. 27-31, 2009.
- [128] E. Comini, *et al.*, "Gas sensing properties of MoO₃ nanorods to CO and CH₃OH," *Chemical Physics Letters*, vol. 407, pp. 368-371, May 2005.
- [129] A. M. Taurino, *et al.*, "Synthesis, electrical characterization, and gas sensing properties of molybdenum oxide nanorods," *Applied Physics Letters*, vol. 88, p. 152111, 2006.
- [130] T. W. Chao, *et al.*, "Quartz crystal microbalance sensor based on nanostructured IrO₂," *Sensors and Actuators B: Chemical*, vol. 122, pp. 95-100, 2007.
- [131] Z. Liu, *et al.*, "O₂ and CO sensing of Ga₂O₃ multiple nanowire gas sensors," *Sensors and Actuators B: Chemical*, vol. 129, pp. 666-670, 2008.
- [132] V. V. Sysoev, *et al.*, "Percolating SnO₂ nanowire network as a stable gas sensor: Direct comparison of long-term performance versus SnO₂ nanoparticle films," *Sensors and Actuators B: Chemical*, vol. 139, pp. 699-703, 2009.
- [133] Q. O. Wang, *et al.*, "A parallel solid-state NMR and sensor property study on flower-like nanostructured SnO₂," *Journal of Physical Chemistry C*, vol. 114, pp. 22671-22676, Dec 2010.
- [134] M.-H. Seo, *et al.*, "Detection of organic gases using TiO₂ nanotube-based gas sensors," *Procedia Chemistry*, vol. 1, pp. 192-195, 2009.
- [135] I. Raible, *et al.*, "V₂O₅ nanofibres: novel gas sensors with extremely high sensitivity and selectivity to amines," *Sensors and Actuators B: Chemical*, vol. 106, pp. 730-735, 2005.
- [136] R. F. Bunshah, *Handbook of deposition technologies for films and coatings: science, technology, and applications*: Noyes Publications, 1994.

- [137] K. L. Choy, "Chemical vapour deposition of coatings," *Progress in Materials Science*, vol. 48, pp. 57-170, 2003.
- [138] G. Wahl, *et al.*, "CVD processes for coatings and surface modifications," *Surface and Coatings Technology*, vol. 100-101, pp. 132-141, 1998.
- [139] H. O. Pierson, *Handbook of chemical vapor deposition (CVD): principles, technology, and applications*: Noyes Publications/William Andrew Pub., 1999.
- [140] A. C. Dillon, *et al.*, "Hot-wire chemical vapor synthesis for a variety of nano-materials with novel applications," *Thin Solid Films*, vol. 501, pp. 216-220, 2006.
- [141] A. Forleo, *et al.*, "Fabrication at wafer level of miniaturized gas sensors based on SnO₂ nanorods deposited by PECVD and gas sensing characteristics," *Sensors and Actuators B: Chemical*, vol. In Press, Corrected Proof.
- [142] H. Huang, *et al.*, "Plasma treatment of SnO₂ nanocolumn arrays deposited by liquid injection plasma-enhanced chemical vapor deposition for gas sensors," *Sensors and Actuators B: Chemical*, vol. 138, pp. 201-206, 2009.
- [143] W. Yin, *et al.*, "In situ growth of SnO₂ nanowires on the surface of Au-coated Sn grains using water-assisted chemical vapor deposition," *Chemical Physics Letters*, vol. 471, pp. 11-16, 2009.
- [144] Y. C. Lee, *et al.*, "Semiconductor gas sensor based on Pd-doped SnO₂ nanorod thin films," *Sensors and Actuators B: Chemical*, vol. 132, pp. 239-242, 2008.
- [145] F. S.-S. Chien, *et al.*, "Fast-response ozone sensor with ZnO nanorods grown by chemical vapor deposition," *Sensors and Actuators B: Chemical*, vol. 144, pp. 120-125, 2010.
- [146] N. Han, *et al.*, "Photoluminescence investigation on the gas sensing property of ZnO nanorods prepared by plasma-enhanced CVD method," *Sensors and Actuators B: Chemical*, vol. 145, pp. 114-119, 2010.
- [147] K. Zheng, *et al.*, "The properties of ethanol gas sensor based on Ti doped ZnO nanotetrapods," *Materials Science and Engineering: B*, vol. 166, pp. 104-107, 2010.
- [148] D. Barreca, *et al.*, "1D ZnO nano-assemblies by Plasma-CVD as chemical sensors for flammable and toxic gases," *Sensors and Actuators B: Chemical*, vol. 149, pp. 1-7, 2010.
- [149] D. Barreca, *et al.*, "Chemical vapor deposition of copper oxide films and entangled quasi-1D nanoarchitectures as innovative gas sensors," *Sensors and Actuators B: Chemical*, vol. 141, pp. 270-275, 2009.
- [150] A. Qurashi, *et al.*, "Catalyst supported growth of In₂O₃ nanostructures and their hydrogen gas sensing properties," *Sensors and Actuators B: Chemical*, vol. 147, pp. 48-54, 2010.
- [151] F. Demami, *et al.*, "Silicon nanowires synthesis for chemical sensor applications," *Procedia Engineering*, vol. 5, pp. 351-354, 2010.
- [152] J. Akedo and M. Lebedev, "Microstructure and electrical properties of lead zirconate titanate (Pb(Zr₅₂/Ti₄₈)O₃) thick films deposited by aerosol deposition method," *Japanese Journal of Applied Physics, Part 1: Regular Papers and Short Notes and Review Papers*, vol. 38, pp. 5397-5401, 1999.
- [153] J. B. Mooney and S. B. Radding, "Spray pyrolysis processing," *Annual Review of Materials Science*, vol. 12, pp. 81-101, 1982.
- [154] G. Blandenet, *et al.*, "Thin layers deposited by the pyrosol process," *Thin Solid Films*, vol. 77, pp. 81-90, 1981.
- [155] S. C. Zhang, *et al.*, "YBa₂Cu₃O_{7-x} Superconductor powder synthesis by spray pyrolysis of organic acid solutions," *Journal of Aerosol Science*, vol. 22, pp. 585-599, 1991.
- [156] R. Strobel and S. E. Pratsinis, "Flame aerosol synthesis of smart nanostructured materials," *Journal of Materials Chemistry*, vol. 17, pp. 4743-4756, 2007.
- [157] L. G. Hubert-Pfalzgraf and H. Guillon, "Trends in precursor design for conventional and aerosol-assisted CVD of high-Tc superconductors," *Applied Organometallic Chemistry*, vol. 12, pp. 221-236, 1998.
- [158] X. H. Hou and K. L. Choy, "Processing and applications of aerosol-assisted chemical vapor deposition," *Chemical Vapor Deposition*, vol. 12, pp. 583-596, 2006.

- [159] C.S. Blackman, *et al.*, "Templated growth of tungsten oxide micro/nanostructures using aerosol assisted chemical vapour deposition," *Materials Letters*, vol. 62, pp. 4582-4584, 15 December 2008.
- [160] J.-L. Todoli and J.-M. Mermet, "Pneumatic Nebulizer Design," in *Liquid Sample Introduction in ICP Spectrometry*, ed Amsterdam: Elsevier, pp. 17-76, 2008.
- [161] C. H. Chen, *et al.*, "Unique porous LiCoO₂ thin layers prepared by electrostatic spray deposition," *Journal of Materials Science*, vol. 31, pp. 5437-5442, 1996.
- [162] K. L. Choy and B. Su, "Growth behavior and microstructure of CdS thin films deposited by an electrostatic spray assisted vapor deposition (ESAVD) process," *Thin Solid Films*, vol. 388, pp. 9-14, 2001.
- [163] T. T. Kodas, *et al.*, *Aerosol processing of materials*: Wiley-VCH, 1999.
- [164] S. Vallejos, *et al.*, "AACVD control parameters for selective deposition of tungsten oxide nanostructures " *Journal of Nanoscience and Nanotechnology*, in press.
- [165] Sobia Ashraf, *et al.*, "Aerosol assisted chemical vapour deposition of WO₃ thin films from tungsten hexacarbonyl and their gas sensing properties," *Journal of Materials Chemistry*, vol. 17, pp. 3708-3713, 2007.
- [166] S. Ashraf, *et al.*, "Aerosol-assisted chemical vapour deposition of WO₃ thin films using polyoxometallate precursors and their gas sensing properties," *Journal of Materials Chemistry*, vol. 17, pp. 1063-1070, 2007.
- [167] Jun Zhao, *et al.*, "Tin oxide thin films prepared by aerosol-assisted chemical vapor deposition and the characteristics on gas detection " *Sensors and Actuators B: Chemical*, vol. 145, pp. 788-793, 19 March 2010.
- [168] L. Mädler, *et al.*, "Direct formation of highly porous gas-sensing films by in situ thermophoretic deposition of flame-made Pt/SnO₂ nanoparticles," *Sensors and Actuators B: Chemical*, vol. 114, pp. 283-295, 2006.
- [169] M. Hussain, *et al.*, "High efficiency ZnO nano sensor, fabrication and characterization," *Journal of the Iranian Chemical Society*, vol. 7, pp. S59-S69, 2010.
- [170] S. O'Brien, *et al.*, "Zinc oxide thin films: Characterization and potential applications," *Thin Solid Films*, vol. 518, pp. 4515-4519, 2010.
- [171] K. Sahner, *et al.*, "Assessment of the novel aerosol deposition method for room temperature preparation of metal oxide gas sensor films," *Sensors and Actuators B: Chemical*, vol. 139, pp. 394-399, 2009.
- [172] M. H. Siadati, *et al.*, "CVD of CeO₂-doped Y₂O₃-stabilized zirconia onto dense and porous substrates," *Chemical Vapor Deposition*, vol. 3, pp. 311-317, 1997.
- [173] P. Althainz, *et al.*, "The influence of morphology on the response of iron-oxide gas sensors," *Sensors and Actuators B: Chemical*, vol. 25, pp. 448-450, 1995.
- [174] W. B. Cross, *et al.*, "Tungsten Oxide Coatings from the Aerosol-Assisted Chemical Vapor Deposition of W(OAr)₆ (Ar = C₆H₅, C₆H₄F-4, C₆H₃F₂-3,4); Photocatalytically Active -WO₃ Films," *Chemistry of Materials*, vol. 15, pp. 2786-2796, 2003.
- [175] W. B. Cross, "Chemical Vapour Deposition of Tungsten Oxide Thin Films from Single-Source Precursors," University College of London, London, 2002.
- [176] A. Antsyshkina, *et al.*, "Synthesis and structure of tin tetrachloride adducts with crown ether: Crystal structure of [Sn(H₂O)₂Cl₄].18C6 and [Sn(H₂O)₂Cl₄].18C6.2H₂O," *Russian Journal of Inorganic Chemistry*, vol. 56, pp. 530-538, 2011.
- [177] P. Eaton, *et al.*, *Atomic Force Microscopy*: OXFORD University Press, 2010.
- [178] M. D. Graef, *Introduction to conventional transmission electron microscopy*. Cambridge University Press, 2003.
- [179] C. Suryanarayana and M. G. Norton, *X-Ray diffraction: a practical approach* Plenum Press, New York, 1998.
- [180] P. Scherrer, "Estimation of the size and internal structure of colloidal particles by means of r.ovrddot.ontgen rays," *Nachr. Ges. Wiss. Göttingen*, pp. 96-100, 1918.
- [181] H. Rietveld, "A profile refinement method for nuclear and magnetic structures," *Journal of Applied Crystallography*, vol. 2, pp. 65-71, 1969.
- [182] TOPAS, "General Profile and Structure Analysis Software for Powder Diffraction Data," V3.1, Bruker AXS GmbH ed. Karlsruhe, Germany.

- [183] A. March, "Mathematical theory on regulation according to the particle shape i affine deformation," *Zeitschrift Fur Kristallographie*, vol. 81, pp. 285-297, Feb 1932.
- [184] V. I. Nefedov, *X-ray photoelectron spectroscopy of solid surfaces*: VSP BV, 1988.
- [185] A. C. McLaren, *Transmission electron microscopy of minerals and rocks*: Cambridge University Press, 1991.
- [186] P. Ivanov, *et al.*, "A route toward more selective and less humidity sensitive screen-printed SnO₂ and WO₃ gas sensitive layers," *Sensors and Actuators B: Chemical*, vol. 100, pp. 221-227, Jun 1 2004.
- [187] I. Simon, *et al.*, "Micromachined metal oxide gas sensors: opportunities to improve sensor performance," *Sensors and Actuators B: Chemical*, vol. 73, pp. 1-26, 2001.
- [188] R. Inglés, *et al.*, "Electro-thermal simulation and characterization of preconcentration membranes," *Sensors and Actuators A: Physical*, vol. In Press, Corrected Proof.
- [189] R. Inglés, "Modelization, simulation and design of micro-electro-mechanicized systems (mems) preconcentrators for gas sensing," Departament d'Enginyeria Electrònica, Elèctrica i Automàtica, Universitat Rovira i Virgili, Tarragona, 2010.
- [190] W. B. Cross and I. P. Parkin, "Aerosol assisted chemical vapour deposition of tungsten oxide films from polyoxotungstate precursors: active photocatalysts," *Chemical Communications*, pp. 1696-1697, 2003.
- [191] Y. Zhao, *et al.*, "Flower-like tungsten oxide particles: Synthesis, characterization and dimethyl methylphosphonate sensing properties," *Analytica Chimica Acta*, vol. 675, pp. 36-41, 2010.
- [192] S. Wang, *et al.*, "Formation and growth mechanism of tungsten oxide microtubules," *Chemical Physics Letters*, vol. 427, pp. 350-355, 2006.
- [193] Y. Liu and M. Liu, "Growth of aligned square-shaped SnO₂ tube arrays," *Advanced Functional Materials*, vol. 15, pp. 57-62, 2005.
- [194] Y. Wu, *et al.*, "Growth of hexagonal tungsten trioxide tubes," *Journal of Crystal Growth*, vol. 292, pp. 143-148, 2006.
- [195] J. S. Jeong, *et al.*, "Single-crystalline ZnO microtubes formed by coalescence of ZnO nanowires using a simple metal-vapor deposition method," *Chemistry of Materials*, vol. 17, pp. 2752-2756, 2005.
- [196] I. Gràcia, *et al.*, "Results on the reliability of silicon micromachined structures for semiconductor gas sensors," *Sensors and Actuators B: Chemical*, vol. 77, pp. 409-415, 2001.
- [197] S. T. Ho, *et al.*, "Catalyst-free selective-area growth of vertically aligned zinc oxide nanowires," *Chemical Physics Letters*, vol. 463, pp. 141-144, 2008.
- [198] A. Gurlo, *et al.*, "An n- to p-type conductivity transition induced by oxygen adsorption on alpha-Fe₂O₃," *Applied Physics Letters*, vol. 85, pp. 2280-2282, 2004.
- [199] A. Gurlo, *et al.*, "A p- to n-transition on [alpha]-Fe₂O₃-based thick film sensors studied by conductance and work function change measurements," *Sensors and Actuators B: Chemical*, vol. 102, pp. 291-298, 2004.
- [200] Y. S. Kim, *et al.*, "Room-temperature semiconductor gas sensor based on nonstoichiometric tungsten oxide nanorod film," *Applied Physics Letters*, vol. 86, pp. 213105-3, 2005.
- [201] T. Siciliano, *et al.*, "Transition from n- to p-type electrical conductivity induced by ethanol adsorption on [alpha]-tellurium dioxide nanowires," *Sensors and Actuators B: Chemical*, vol. 138, pp. 207-213, 2009.
- [202] T. Wolkenstein, *Electronic processes on semiconductor surfaces during chemisorption*. New York: Consultants Bureau, pp 216-221, 1991.
- [203] D. K. Aswal and S. K. Gupta, *Science and technology of chemiresistor gas sensors*: Nova Science Publishers, 2007.
- [204] Y. J. Choi, *et al.*, "Novel fabrication of an SnO₂ nanowire gas sensor with high sensitivity," *Nanotechnology*, vol. 19, Mar 2008.
- [205] V. Alberto and *et al.*, "Direct integration of metal oxide nanowires into an effective gas sensing device," *Nanotechnology*, vol. 21, p. 145502, 2010.
- [206] B. Deb, *et al.*, "Gas sensing behaviour of mat-like networked tungsten oxide nanowire thin films," *Nanotechnology*, vol. 18, Jul 2007.

- [207] T. Stoycheva, *et al.*, "Characterization and gas sensing properties of intrinsic and Au-doped WO₃ nanostructures deposited by AACVD technique," *Procedia Engineering*, vol. 5, pp. 131-134, 2010.
- [208] B. R. Cuenya, "Synthesis and catalytic properties of metal nanoparticles: Size, shape, support, composition, and oxidation state effects," *Thin Solid Films*, vol. 518, pp. 3127-3150, 2010.
- [209] T. Seiyama, *et al.*, "A new detector for gaseous components using semiconductive thin films," *Analytical Chemistry*, vol. 34, pp. 1502-1503, 1962.
- [210] F. Lu, *et al.*, "Nanosized tin oxide as the novel material with simultaneous detection towards CO, H₂ and CH₄," *Sensors and Actuators B: Chemical*, vol. 66, pp. 225-227, 2000.
- [211] D. Kohl, "Surface processes in the detection of reducing gases with SnO₂-based devices," *Sensors and Actuators*, vol. 18, pp. 71-113, 1989.
- [212] W. Göpel and K. D. Schierbaum, "SnO₂ sensors: current status and future prospects," *Sensors and Actuators: B. Chemical*, vol. 26, pp. 1-12, 1995.
- [213] M. C. Horrillo, *et al.*, "Influence of the deposition conditions of SnO₂ thin films by reactive sputtering on the sensitivity to urban pollutants," *Sensors and Actuators B: Chemical*, vol. 45, pp. 193-198, 1997.
- [214] S. Seal and S. Shukla, "Nanocrystalline SnO gas sensors in view of surface reactions and modifications," *JOM Journal of the Minerals, Metals and Materials Society*, vol. 54, pp. 35-38, 2002.
- [215] G. F. Fine, *et al.*, "Metal oxide semi-conductor gas sensors in environmental monitoring," *Sensors*, vol. 10, pp. 5469-5502, 2010.
- [216] V. Meille, "Review on methods to deposit catalysts on structured surfaces," *Applied Catalysis A: General*, vol. 315, pp. 1-17, 2006.
- [217] Y. Liu, *et al.*, "A highly sensitive and fast-responding SnO₂ sensor fabricated by combustion chemical vapor deposition," *Chemistry of Materials*, vol. 17, pp. 3997-4000, 2005.
- [218] T. Sahm, *et al.*, "Flame spray synthesis of tin dioxide nanoparticles for gas sensing," *Sensors and Actuators B: Chemical*, vol. 98, pp. 148-153, 2004.
- [219] J. R. Brown, *et al.*, "Response behaviour of tin oxide thin film gas sensors grown by MOCVD," *Sensors and Actuators B: Chemical*, vol. 63, pp. 109-114, 2000.
- [220] T. T. Stoycheva, *et al.*, "Aerosol-Assisted CVD of SnO₂ Thin Films for Gas-Sensor Applications," *Chemical Vapor Deposition*, vol. 17, pp. 247-252, 2011.
- [221] A. Smith, *et al.*, "Relation between solution chemistry and morphology of SnO₂-based thin films deposited by a pyrosol process," *Thin Solid Films*, vol. 266, pp. 20-30, 1995.
- [222] K. C. Molloy, "Precursors for the formation of tin(IV) oxide and related materials," *Journal of Chemical Research*, vol. 2008, pp. 549-554, 2008.
- [223] N. Yamazoe, "Toward innovations of gas sensor technology," *Sensors and Actuators B: Chemical*, vol. 108, pp. 2-14, 2005.
- [224] X. Han, *et al.*, "Synthesis of tin dioxide octahedral nanoparticles with exposed high-energy {221} facets and enhanced gas-sensing properties," *Angewandte Chemie International Edition*, vol. 48, pp. 9180-9183, 2009.
- [225] A. Gurlo, "Nanosensors: Does crystal shape matter?," *Small*, vol. 6, pp. 2077-2079, 2010.